# QUANTIFYING SPATIAL RELATIONSHIPS BETWEEN LANDSCAPE PATTERNS LINKED TO ANTHROPOGENIC DISTURBANCES AND BURULI ULCER DISEASE

By

Lindsay P. Campbell

#### A THESIS

Submitted to
Michigan State University
In partial fulfillment of the requirements
for the degree of

MASTER OF SCIENCE

Geography

2011

#### **ABSTRACT**

## QUANTIFYING SPATIAL RELATIONSHIPS BETWEEN LANDSCAPE PATTERNS LINKED TO ANTHROPOGENIC DISTURBANCES AND BURULI ULCER DISEASE

By

#### Lindsay P. Campbell

Anthropogenic ecosystem disturbances play an important role in the distribution of emerging and re-emerging infectious diseases. Advances in GIS, remote sensing technologies, and spatial statistical methods facilitate the observation and quantification of anthropogenic landscape disturbances, providing the tools necessary to link these disturbances to disease emergence. Investigations into disturbances linked to environmental bacterial infections are an underrepresented research area. One such disease is Buruli ulcer disease (BU), caused by the environmental pathogen *Mycobacterium ulcerans*. The ecological drivers behind pathogen proliferation and transmission to humans are currently unknown. The main objective of this study included using a spatial landscape ecological approach to determine whether land cover patches indicative of anthropogenic landscape disturbances surrounded villages with higher BU rates. Landscape-level results supported study hypotheses that more fragmented landscapes, with more uniform land cover patch shapes, lying within areas more likely to collect water surround villages with higher BU rates, but results were not consistent. Class-level results, analyzing forest, wetland, and a mixed agriculture/forest class, suggested that more aggregated patches with more complex shapes surround villages with higher BU rates. Incorporation of a spatial random effects component accounted for spatial autocorrelation and provided a spatial structure from which to predict BU rates at unsampled locations.

Copyright by

Lindsay P. Campbell

2011

Dedicated to my wonderful and supportive husband, David, and to my parents and sister
who have always believed in me.

#### **ACKNOWLEDGEMENTS**

Foremost, I would like to acknowledge my advisor, Dr. Jiaguo Qi, for his support and guidance throughout my studies. The opportunities he provided to me proved life-changing and laid the foundation to further my academic career.

I would also like to acknowledge the time and effort of my committee members. Dr. Andrew Finley introduced me to the spatial analytical methods central to the formation of this thesis. Dr. M. Eric Benbow introduced me to fieldwork and cultivated all aspects of my research skills. Dr. Richard Merritt offered sage advice and provided excellent opportunities to attend academic conferences where I presented our work.

In addition to my committee members, Dr. Pamela Small acted as a valuable mentor and provided opportunities for international travel. Jenni van Ravensway became a wonderful friend and was an excellent resource throughout this experience. I had the opportunity to meet and to work with several dedicated researchers and graduate students from the U.S, Benin, and Ghana, including Dr. Lance Waller, Dr. Heather Williamson, Dr. Mollie McIntosh, Ryan Kimbirauskas, Dr. Christian Johnson, Dr. Ghishlain Sopoh, Charles Yeboah, and Charles Quaye. I would also like to acknowledge fellow graduate students Chuan Qin, Siam Lawawirowong, Tanita Suepa, Zhang Feng, and Mark DeVisser.

Finally, I would like to express my sincere appreciation for my husband, family, and friends, particularly Cheryl Lyons, who supported me throughout my studies.

## TABLE OF CONTENTS

LIST OF TABLES	
LIST OF EQUATIONS	xiv
INTRODUCTION	1
Chapter 1 LITERATURE REVIEW	4
1.1 Buruli ulcer disease	4
1.2 Symptoms and Treatment	5
1.3 Prevalence and Economic Hardship	8
1.4 Mycobacterium ulcerans	10
1.5 Hypothesized Modes of Transmission	11
1.6 Risk Factors	14
1.7 Landscape Epidemiology/Ecology, GIS, and Remote Sensing	16
1.8 Spatial Autocorrelation	
1.9 Past BU Landscape Studies	
1.10 Objectives	
1.11 Hypotheses	
Chapter 2 MATERIALS AND METHODS	30
2.1 Study Area	
2.2 BU Case Data	32
2.3 Satellite imagery and derivatives	
2.4 Statistical Modeling	
2.5 Landscape-level Configuration Analysis	
2.6 Landscape-level Configuration Analysis Predictor Variables	
2.7 Class-level Configuration Analysis	
2.8 Class-level Configuration Analysis Predictor Variables	
2.9 Spatial GLM	
2.10 Model Verification.	
2.11 Risk Surface	
Chapter 3 RESULTS	58
3.1 Non-Spatial vs. Spatial Model Results	58
3.2 Model Output Interpretation	60
3.3 Landscape-level Configuration Analysis Results	
3.4 Class-level Composition and Configuration Analysis	
3.5 Model Verification.	
3.6 Predictive Surface Model	
Chapter 4 DISCUSSION AND LIMITATIONS	77
4.1 Discussion	
4.2 Limitations	
4.3 Conclusions and Future Directions	88

APPENDICES	9(
Appendix A	91
Appendix B	
Appendix C	
Appendix D	
LITERATURE CITED	15/
LHENATUNE CHED	

## LIST OF TABLES

Table 2-1. Land use and cover classification categories	35
Table 2-2.Initial landscape metrics calculations.	41
Table 2-3. Class-level initial landscape metric candidates	48
Table 3-1. Non-spatial and spatial GLM DIC values.	58
Table 3-2. Non-spatial vs. spatial binomial GLM variable significance.	59
Table 3-3. 1_2k number of patches spatial binomial GLM model summary	61
Table 3-4. Gelman diagnostic 1_2k patch richness density model	61
Table 3-5. 1_6k number of patches spatial binomial GLM model summary	62
Table 3-6. Gelman diagnostic 1_6k numbers of patches model	62
Table 3-7. 2k numbers of patches spatial binomial GLM model summary	63
Table 3-8. Gelman diagnostic 2k number of patches model	63
Table 3-9. 2k patch richness density spatial binomial GLM summary	64
Table 3-10. Gelman diagnostic 2k patch richness density model	64
Table 3-11. 800m wetland class spatial model results	65
Table 3-12. 800m wetland class convergence diagnostic	65
Table 3-13. 800m agriculture/forest class spatial model results	65
Table 3-14. 800m agriculture/forest class convergence diagnostic	66
Table 3-15. 1_2k forest spatial model results	66
Table 3-16. 1_2k forest class convergence diagnostic	67
Table 3-17. 1_2k agriculture/forest spatial model results	67
Table 3-18. 1_2k agriculture/forest class convergence diagnostic	68
Table 3-19.1 6k agriculture/forest spatial model results	69

Table 3-20. 1_6k agriculture/forest class convergence diagnostic	69
Table 3-21. 2k forest class spatial model results	70
Table 3-22. 2k forest class model convergence diagnostic	70
Table 3-23. 2k agriculture/forest class spatial model results	71
Table 3-24. 2k agriculture/forest model convergence diagnostic	71
Table 3-25. Root mean square errors for all spatial binomial GLM training models	72
Table A-1. Landscape-level 400m correlation matrix	92
Table A-2. Landscape-level 500m correlation matrix	93
Table A-3. Landscape-level 600m correlation matrix	94
Table A-4. Landscape-level 700m correlation matrix	95
Table A-5. Landscape-level 800m correlation matrix	96
Table A-6. Landscape-level 900m correlation matrix	97
Table A-7. Landscape-level 1k correlation matrix	98
Table A-8. Landscape-level 1_1k correlation matrix	99
Table A-9. Landscape-level 1_2k correlation matrix	100
Table A-10. Landscape-level 1_3k correlation matrix	101
Table A-11. Landscape-level 1_5k correlation matrix	102
Table A-12. Landscape-level 1_6k correlation matrix	103
Table A-13. Landscape-level 1_7k correlation matrix	104
Table A-14. Landscape-level 1_8k correlation matrix	105
Table A-15. Landscape-level 1_9k correlation matrix	106
Table A-16. Landscape-level 2k correlation matrix	107
Table A-17, 800m forest class correlation matrix	108

Table A-18. 800m wetland class correlation matrix	108
Table A-19. 800m agriculture/forest class correlation matrix	108
Table A-20. 1_2k forest class correlation matrix	109
Table A-21. 1_2k wetland class correlation matrix	109
Table A-22. 1_2k agriculture/forest class correlation matrix	109
Table A-23. 1_6k forest class correlation matrix	110
Table A-24. 1_6k wetland class correlation matrix	110
Table A-25. 1_6k agriculture/forest class correlation matrix	110
Table A-26. 2k forest class correlation matrix.	. 111
Table A-27. 2k wetland class correlation matrix	. 111
Table A-28. 2k agriculture/forest class correlation matrix	. 111
Table C-1. Landscape-level non-spatial binomial GLMs.	127
Table C-2. Landscape-level non-spatial binomial GLMs.	129
Table C-3. Landscape-level non-spatial binomial GLMs.	131
Table C-4. Landscape-level non-spatial binomial GLMs	133
Table C-5. Landscape-level non-spatial binomial GLMs.	135
Table C-6. 800m forest class non-spatial binomial GLMs	137
Table C-7. 800m wetland class non-spatial binomial GLMs	138
Table C-8. 800m agriculture/forest class non-spatial binomial GLMs	139
Table C-9. 1_2k forest class non-spatial binomial GLMs	140
Table C-10. 1_2k wetland class non-spatial binomial GLMs	141
Table C-11. 1_2k agriculture/forest class non-spatial binomial GLMs	142
Table C-12. 1 6k forest class non-spatial binomial GLMs	. 143

Table C-13. 1_6k wetland class non-spatial binomial GLMs	144
Table C-14. 1_6k agriculture/forest class non-spatial binomial GLMs	145
Table C-15. 2k forest class non-spatial binomial GLMs	146
Table C-16. 2k wetland class non-spatial binomial GLMs	147
Table C-17. 2k agriculture/forest class non-spatial binomial GLMs	148
Table D-1. 800m forest class spatial binomial GLM	150
Table D-2. 800m wetland class spatial binomial GLM	150
Table D-3. 800m agriculture/forest class spatial binomial GLM	150
Table D-4. 1_2k forest class spatial binomial GLM	151
Table D-5. 1_2k wetland class spatial binomial GLM	151
Table D-6. 1_2k agriculture/forest class spatial binomial GLM	151
Table D-7. 1_6k forest class spatial binomial GLM	152
Table D-8. 1_6k wetland class spatial binomial GLM	152
Table D-9. 1_6k agriculture/forest spatial binomial GLM	152
Table D-10. 2k forest class spatial binomial GLM	153
Table D-11. 2k wetland class spatial binomial GLM	153
Table D-12. 2k agriculture/forest class spatial binomial GLM	153

## LIST OF FIGURES

Figure 1-1. BU stages. (Images Courtesy of Dr. K. Asiedu and Dr.	6
Figure 1-2. BU Complications (Images Courtesy of the	7
Figure 2-1. Togo and Benin administrative districts included in study area	31
Figure 2-2. Benin 2004 and 2005 BU case data subset	33
Figure 2-3. Land use and land cover classification.	36
Figure 2-4. Concentric buffers example	37
Figure 2-5. Wetness index map.	38
Figure 2-6. Methods and approaches used for final model generation	40
Figure 2-7. Shape index mean surface	44
Figure 2-8. Number of patches surface	45
Figure 2-9. Wetness index average surface	46
Figure 2-10. Patch richness density surface.	47
Figure 2-11. Percent land cover adjacency surface 2k wetland class	50
Figure 2-12. 1_2k agriculture/forest class landscape shape	51
Figure 2-13. New locations and observed locations used to create risk surface	56
Figure 3-1. 1_2k wetland class observed rates, 90% data	73
Figure 3-2. 1_2k wetland class fitted model, 90% data	74
Figure 3-3. 1_2k wetland class spatial random effects	75
Figure 3-4. Predictive BU rates surface across the study domain	76
Figure 4-1. Anthropogenic disturbance within wetland land cover patch	81
Figure B-1. Landscape-level "best model" variable scatterplots	113
Figure B-2. 800m "best model" variable scatterplot	114

Figure B-3. 800m wetland "best model" variable scatterplot	. 115
Figure B-4. 800m agriculture/forest class "best model" variable scatterplot	. 116
Figure B-5. 1_2k forest class "best model" variable scatterplot	. 117
Figure B-6. 1_2k wetland class "best model" variable scatterplot	. 118
Figure B-7. 1_2k agriculture/forest class "best model" variable scatterplot	. 119
Figure B-8. 1_6k forest class "best model" variable scatterplot	. 120
Figure B-9. 1_6k wetland class "best model" variable scatterplot	. 121
Figure B-10. 1_6k agriculture/forest class "best model" variable scatterplot	. 122
Figure B-11. 2k forest class "best model" variable scatterplot	. 123
Figure B-12. 2k wetland class "best model" variable scatterplot	. 124
Figure B-13. 2k agriculture/forest class "best model" variable scatterplot	. 125

## LIST OF EQUATIONS

Equation 2-1	38
Equation 2-2	42
Equation 2-3	43
Equation 2-4	44
Equation 2-5	47
Equation 2-6	49
Equation 2-7	51
Equation 2-8	55

#### INTRODUCTION

Anthropogenic ecosystem disturbances, for example, land use change, human movement, encroachment and wildlife translocation, rapid transport, and climate change play an important role in the distribution of emerging and re-emerging infectious diseases (Wilcox and Gubler, 2005; Patz *et al.*, 2000; Foley *et al.*, 2005; Patz and Confalonieri, 2005; Confalonieri, 2005). These activities have the potential to disrupt natural community assemblages in ecosystems, impacting predator/prey relationships, thereby resulting in an imbalance of population control mechanisms that may have prevented disease pathogens from infecting human populations prior to disturbance (Wilcox and Gubler 2005; Morse 1995).

Land use and land cover (LULC) change at multiple scales are one anthropogenic disturbance linked to disease incidence. Examples include: 1) changes in dry-season irrigation practices at a local scale that created new mosquito-breeding habitats leading to elevated Ross River virus cases in Australia; 2) deforestation of hillsides at a regional scale contributing to nutrient run-off that proliferated macroalgae growth suitable to bacteria responsible for ciguatera fish poisoning; and 3) rainforest degradation at a global scale resulting in new transmission opportunities for simian retroviruses such as HIV/AIDS between human and non-human primates (Cook *et al.*, 2004).

Anthropogenic activities with major impacts on LULC are land degradation, including agriculture intensification and water projects, urbanization, and deforestation (Patz *et al.*, 2008). These activities contribute to habitat fragmentation that can disrupt vector breeding sites and reservoir distributions while creating habitats suitable to ecological edge effects that provide opportunities for niche invasions that promote disease emergence (Patz and Confalonieri, 2005). Further, these activities generate new pathways for humans to interact with environments

undisturbed previously, resulting in reduced proximities to potential vectors, reservoirs, and isolated pathogens (Patz and Confalonieri, 2005; Morse, 1995; Epstein, 2002; Pongsiri *et al.*, 2009).

Landscapes impacted most by widespread anthropogenic ecosystem disturbance are those situated within the tropics, which have experienced the largest ecosystem transformations in history within the last 60 years (Clark *et al.*, 1990). Agriculture intensification is the major driver behind tropical deforestation, and as population growth rates continue to rise, agricultural land is expected to increase by approximately 23% by the year 2050 to meet food and fuel demands (Patz *et al.*, 2008; Hansen *et al.*, 2008). As these regions continue to transition from natural to managed ecosystems, new habitat opportunities suitable to a variety of reservoirs, vectors, and pathogens will continue to surface; therefore, identifying landscape patterns favorable to disease emergence will be a critical first step in human disease prevention.

Advances in GIS and remote sensing technologies, along with spatial statistical methods, facilitate the observation and quantification of anthropogenic landscape disturbances, providing the tools necessary to study location-specific landscape characteristics that might be responsible for disease incidence while enabling spatial modeling capabilities to link these characteristics and to predict disease risk across a landscape (Kitron, 1998). While current research focuses largely on wildlife and vector-borne zoonotic disease emergence, exploring linkages between anthropogenically-disturbed landscapes and human bacterial infections is an underrepresented area of research, although recent results suggest that these disturbances play an important role in spatial distributions of environmental bacteria that pose a human health risk (Goldberg *et al.*, 2008). Quantifying landscape patterns related to bacterial disease emergence is central to the

prediction of present and future public health risk because often the ecological drivers behind these diseases are poorly understood.

One example is Buruli ulcer (BU) disease, caused by the environmental pathogen *Mycobacterium ulcerans*. Although the ecological drivers behind MU growth remain a mystery, dramatic increases in BU cases since the 1980s (Merritt *et al.*, 2005) have been linked empirically and anecdotally to anthropogenic landscape changes; for example, deforestation, habitat fragmentation, aquatic ecosystem disturbances from dam construction and agriculture irrigation, farming practices, and mining activities (Merritt *et al.*, 2010). Although BU is not transferred between persons, the mode or modes of transmission is not determined, and no vaccine exists (Wansbrough-Jones and Phillips, 2006). Therefore, identifying landscape patterns linked to BU incidence will provide a powerful tool for surveillance and prevention while affording opportunities to learn more about the disease system.

## **Chapter 1 LITERATURE REVIEW**

#### 1.1 Buruli ulcer disease

Mycobacterium ulcerans (MU), the causative agent of BU, is an environmental pathogen (Williamson et al., 2008) and the second most common mycobacterium infection in humans after tuberculosis and leprosy (Wansbrough-Jones and Phillips, 2006; Walsh et al. 2008; WHO 2000). BU presents as a necrotizing skin condition that often causes mobility loss and permanent disabilities in patients due to the potential for ulcers to cover large areas of the body. The disease is endemic in over 32 countries worldwide, but occurs predominantly in tropical areas of sub-Saharan Africa and also in more temperate regions; specifically, the Melbourne area of Victoria, Australia (WHO, 2007; Walsh et al., 2008). The World Health Organization (WHO) established the Global Buruli Ulcer Initiative in 1998 with the goals of raising disease awareness, improving treatment access, strengthening surveillance, and providing priority research into disease diagnosis, treatment and prevention (WHO, 2007). BU affects all age groups, but children under the age of 15 are most at risk for the disease (Merritt et al., 2005).

MacCallum and colleagues identified MU as the causal agent of BU in Victoria, Australia in 1948 (MacCallum *et al.*, 1948), although Sir Albert Cook in Africa in 1897 and Kleinshmidt in northeast Congo during the 1920s identified likely BU cases (Johnson *et al.*, 2005). BU has had numerous names worldwide, each representing the region from which cases occurred. In Australia, it was known as Bairnsdale ulcer after the town in which the identification of MU took place and Searls' ulcer after a physician practicing in Bairnsdale during the same era; the infection is named Kumusi in Papua New Guinea and Kakerifu in Zaire (Meyers, 2007). The name Buruli is linked to the former Buruli district in Uganda where a large number of cases

surfaced between 1950 and 1970 (Clancey *et al.*, 1964), and it is the name adopted by the WHO to promote disease awareness (Meyers, 2007).

#### 1.2 Symptoms and Treatment

Three BU disease stages exist: non-ulcerative or pre-ulcerative disease, ulcerative disease, and healing or scarring (Figure 1-1, WHO, 2000). Pre-ulcerative symptoms include painless, raised papules that are usually < 1cm in diameter; painless, mobile nodules beneath the skin; and firm plaques (WHO 2000). Edema and swelling can also occur, but subsides once an ulcer develops (Dobos et al., 1999). An incubation period of approximately three months exists before ulcer eruption, but varies by individual (Horsbough and Meyers, 1997) with as little as two weeks to as long as one year being reported by individuals in contact with endemic regions (Veitch *et al.*, 1997).

The ulcerative disease stage develops when pre-ulcerative symptoms erupt into necrotic skin lesions. Ulcer edges are deeply undermined and necrosis often extends beyond the visible infection (Johnson *et al.*, 1999; Hayman J, 1993). Ulcers are usually painless and continue to enlarge through necrosis of the underlying epidermis surrounding the initial lesion (Huygen *et al.*, 2009). Healing is a slow process that may occur spontaneously, but scarring of affected tissues leads to debilitating conditions. Four methods of laboratory diagnosis exist, including direct smear, culture, Polymerse Chain Reaction (PCR), and histopathology (Walsh *et al.*, 2008).



Figure 1-1. BU stages. (Images Courtesy of Dr. K. Asiedu and Dr. A. Chauty <a href="http://www.who.int/buruli/photos/en/index.html">http://www.who.int/buruli/photos/en/index.html</a>). For interpretation of the references to color in this and all other figures, the reader is referred to the electronic version of this thesis.

Approximately 80% of ulcers present on the limbs or extremities (Walsh *et al.*, 2008), and no significant difference exists between male and female infection rates (Debacker *et al.*, 2004b). A country-wide case study in Ghana found that women and girls were more likely than boys to develop lesions on their arms, but ulcerations on the legs were still dominant in both sexes (Amofah *et al.*, 2002).

Recent treatment advances determined that a combination of Streptomycin-Rifampin antibiotics alone had a high success rate for persons presenting with ulcers < 15 cm in diameter (Chauty *et al.*, 2007), but larger ulcers must be surgically excised along with a large area of surrounding, healthy tissue followed by skin grafting to help prevent disease recurrence, and severe cases require amputation of ulcerated limbs (Sizaire *et al.*, 2006). Although BU eventually subsides on its own, it is not without devastating, long-term negative effects, and disease recurrence rates range between 6.1% and 47% in some endemic regions (Debacker *et al.*, 2005; Amofah *et al.*, 2002).

Although study results suggested that the *M. bovis* bacilli Calmette-Guérin, or BCG, vaccine used commonly to protect against tuberculosis provided partial protection against BU for a six month time period (Portaels *et al.*, 2002), a definitive vaccine does not exist (Huygen *et al.*, 2009). However, the BCG vaccine may prevent more severe infections from developing in

patients (Portaels *et al.*, 2002; Noeske *et al.*, 2004) and may decrease disease duration (Amofah *et al.*, 1993). While these results are promising, contrasting results also exist, suggesting that the BCG vaccination provides no BU protection and may increase infection risk (Nackers *et al.*, 2006). Persons infected with the human immunodeficiency virus (HIV) are not at a higher risk for contracting BU (Raghunathan *et al.*, 2005), but may experience a more severe infection once inoculated (Johnson *et al.*, 1999).

BU complications include mobility loss from surgical treatment and/or scarring of affected tissues. Without adequate physical therapy, patients often experience contracture, or the inability to straighten or flex muscles in affected areas (Hayman 1993). In severe cases, the infection moves into the bone causing osteomyelitis (Johnson et al, 1999). In these cases, the bone develops a "moth-eaten" appearance and severe disability may result (WHO, 2007). Reactive osteitis, or contiguous osteitis, is another BU complication that results from soft tissue destruction above the bone and also creates the potential for mobility loss in patients (WHO, 2007). A recent study in Ghana found that at least 27% of patients experienced a reduced range of motion following treatment and the study suggested that better follow-up care should be a priority to help limit disability from the disease (Figure 1-2, Schunk *et al.*, 2009).



Figure 1-2. BU Complications (Images Courtesy of the National Buruli ulcer Control Programme, Benin, Professor H. Assé, and Dr. K. Asiedu <a href="http://www.who.int/buruli/photos/en/index.html">http://www.who.int/buruli/photos/en/index.html</a>)

#### 1.3 Prevalence and Economic Hardship

BU cases increased steadily and expanded geographically within the past few decades (Merritt *et al.*, 2005). Although elevated disease awareness contributed to higher diagnosis rates, researchers believe an increase in the exposed population also took place (Debacker *et al.*, 2004a). The WHO estimated approximately 24,000 cases were recorded between 1978 and 2006 in Côte d'Ivoire; approximately 7,000 cases were recorded between 1989 and 2006 in Benin; and more than 11,000 cases were recorded since 1993 in Ghana (WHO 2007). Underreporting is a common problem when estimating BU case numbers because many patients do not have access to health care facilities, are misdiagnosed, or live in countries in which BU is not a notifiable disease (WHO 2007).

BU cases increased dramatically in the Melbourne area of Victoria, Australia with only 4 cases reported in 1999 but 61 cases reported in 2006 (Quek *et al.*, 2007) with an outbreak of 83 cases occurring in the city of Point Lonsdale on the Bellarine Peninsula in 2002 (Johnson *et al.*, 2007). Between 1992 and 1995, an outbreak occurred in the city of Cowes located on Phillips Island off the mainland of Australia near Melbourne (Veitch, 1997). Although BU cases were recorded since the 1930s in Melbourne suburbs, previous BU cases on Phillips Island had not been recorded, suggesting that the pathogen expanded its geographic range. BU is also endemic to the Daintree Forest region of Northern Queensland along the eastern coast of Australia, though fewer cases are reported each year than in the Victoria region (Jenkin *et al.*, 2002). Early detection and access to health care, along with fewer overall cases, has prevented BU from becoming a more serious public health problem in Australia, but persons living in developing countries face greater challenges when seeking treatment, and the majority of cases received at medical facilities are in advanced disease stages (WHO, 2000).

Persons presenting with BU often require extensive surgery and hospital stays, creating economic challenges for families of patients (Aujoulat *et al.*, 2003); for example, patient hospital stays average approximately three months in Ghana (Stienstra *et al.*, 2002). The WHO reported in Ghana that the cost of treating a pre-ulcerative nodule in a patient is comparable to 16% of the average total family income for the work-year; the cost of treating a patient requiring amputation is equal to 89% of the average total family income for the work-year; and the average cost of treating a patient in 1994-1996 exceeded the per capita government spending on health care (WHO, 2007). Compounding the problem is income loss due to incapacitation from the disease or from caring for a family member with BU, and families face additional challenges involving prolonged care for members permanently disabled. Fear of surgery, long distances to treatment facilities, and socioeconomic factors contribute to the rural poor being affected most negatively by BU (Raghunathan *et al.*, 2005).

Beyond prohibitive treatment costs and access to medical facilities, a stigma associated with BU exists in many regions due to a belief that the infection is a result of witchcraft. A case controlled study in Ghana determined that 59% of study respondents felt that witchcraft was involved in disease development (Stienstra *et al.*, 2002). Persons without BU reported avoiding patients suffering from the disease, and patients reported hiding symptoms from community members. Many respondents attributed the disease to a lack of hygiene by patients, and patients reported a fear of the "evil eye" and did want community members staring at wounds or watching dressing changes for fear that these activities would influence healing negatively. Importantly, many respondents did not believe that BU was a "hospital disease" because the infection was the result of a curse, and therefore, traditional healing methods would be the best treatment option.

### 1.4 Mycobacterium ulcerans

MU is a slow-growing, mycolactone-producing environmental mycobacterium (Merritt *et al.*, 2005). During the pre-ulcerative stage, acid-fast bacilli localize to fatty tissues under the skin where microcolony formation takes place (Dobos *et al.*, 1999). MU is unusual because of its extracellular activity and mycolactone secretion, a lipid toxin responsible for fat and subcutaneous tissue necrosis (George *et al.*, 1999) The mycolactone secretes an immunosuppressive property, indicated by the lack of a granulomatous inflammatory response in early lesion stages, allowing the disease to progress with little or no pain in the patient (Johnson *et al.*, 1999). Lack of a host immune response leaves the infection undetected by burulin skin tests that become positive only after the bacterium ceases to reproduce and healing begins (WHO, 2007).

Additional attributes set MU apart from related mycobacteria. Most notably, MU prefers lower temperatures and has a narrower temperature range than its counterparts, preferring temperatures between 28-34°C with an optimal growth range between 30-33°C in a laboratory setting (Merritt *et al.*, 2010). Although isolates from various regions show differences in temperature tolerance, for example, isolates from Africa are more thermo-tolerant than those from more temperate regions, survival at higher temperatures takes place without reproduction (Edyanni and Portaels, 2007). Further, MU is intolerant to ultra-violet (UV) light because it lacks pigments found in related mycobacterium, indicating that MU may be protected from sunlight in its natural environment (Stinear *et al.*, 2007).

Recent technological advances enabled researchers to detect MU DNA in a variety of environmental samples ranging from soils to invertebrates (for a complete review see Merritt *et al.*, 2010) using PCR probes based on detection of IS2404 (Ross *et al.*, 1997). Although IS2404

was believed to be specific to *M. ulcerans*, it was later determined that other mycobacteria also tested IS2404 positive; specifically, *M. marinum*, *M. liflandji*, and *M. pseudoshottsii* (Stragier *et al.*, 2007), but the advent of real-time PCR provided the tools necessary to differentiate MU from other mycobacteria testing IS2404 positive (Fyfe *et al.*, 2007).

A significant contribution involving a pure MU culture from an environmental sample took place recently in Benin (Portaels et al, 2008). The culture was obtained from a water strider, an aquatic insect (Hemiptera: Gerridae, *Gerris* sp.). This discovery made a substantial contribution to BU research because it was the first of its kind and confirmed MU existence in aquatic habitats (Merritt *et al.*, 2010).

#### 1.5 Hypothesized Modes of Transmission

The mode or modes of BU transmission are currently unknown. The occurrence of ulcer presentation at the site of previous skin trauma in some patients suggests a direct mode of transmission from the environment (Meyers *et al.*, 1974). Ulcer presentation in a patient in Togo, Africa was reported at the site of a wound from a large splinter of wood (Meyers *et al.*, 1996), and cleaning and covering cuts and abrasions is recommended in Victoria, Australia to help prevent inoculation with the disease (Johnson *et al.*, 2007).

Aerosol transmission is another mechanism proposed for MU inoculation based on the ability of *Mycobacteria intracellulare* to concentrate in air bubbles, suggesting that mycobacteria may be propelled into the air and dispersed by wind or waves upon gas bubble bursts occurring in water bodies in the natural environment (Hayman, 1991). Further speculation ensued when a study in Australia revealed that BU patients did not report having contact with environmental water other than the ocean before presenting with the disease, but a need exists for additional research to determine the plausibility of this hypothesis (Johnson *et al.*, 2005).

Researchers found MU DNA in biofilm of aquatic vegetation in Ghana, and subsequent testing determined that MU growth rates increased substantially after two green algae types were entered into the medium in a laboratory setting (Marsollier *et al.*, 2004b). Persons may come into direct contact with contaminated water and plants while bathing, farming or conducting domestic duties, or contaminated insects may act as mechanical vectors of the disease.

Past studies focused on the possibility of aquatic insects as primary BU vectors. In 1999, researchers investigated five aquatic invertebrate species found on the roots of various plants in Benin and Ghana and found they were MU positive, but no evidence surfaced of these insects passing the pathogen to humans, even though they were known to sometimes bite villagers (Portaels *et al.*, 1999). Further research determined that MU could survive and reproduce within the salivary glands of biting aquatic bugs (Marsollier *et al.*, 2003), and scientists observed ulcer presentation in mice bitten by infected aquatic bugs in the laboratory, although insect species native to West Africa were not used in these studies (Marsollier, 2002). Additional research demonstrated that aquatic snails may act as passive hosts, harboring MU within their bodies after eating contaminated aquatic vegetation, and that MU may be transferred to the salivary glands of biting insects after feeding on infected snails (Marsollier *et al.* 2004a).

Contrasting results from a field study involving 27 water body sites near BU positive and BU negative villages in Ghana determined that biting Hermiptera were not likely BU vectors after finding no positive correlation between Hemiptera abundance and endemic sties; MU positivity rates and endemic sites; MU positivity rates among Hemiptera versus other aquatic insects within endemic sites; or overall MU positivity and vector abundance (Benbow *et al.*, 2008). However, a recent field study conducted in Cameroon (Marion *et al.*, 2010) supported previous laboratory results, finding MU within biting hemiptera salivary glands, and contrary to

field results from Ghana, found insect density counts ten times higher in BU endemic study sites than in BU non-endemic sites.

Mosi *et al.* (2008) investigated MU colonization within the salivary glands of African giant water bugs (Belostomatidae) through MU-infected mosquito larvae ingestion in the laboratory. Results determined that MU preferred to accumulate on the exoskeleton as opposed to the guts or salivary glands, but persistent colonization without replication could occur, and therefore, these insects were capable of supporting the trophic transfer of MU within the environment.

Researchers in Australia investigated the role of mosquitoes in potential BU transmission after discovering that areas with BU outbreaks also had a large mosquito population (Johnson *et al.*, 2007). Although mosquitoes tested MU positive, it was inconclusive whether they were harboring MU within their bodies or whether they had acquired the pathogen externally from the environment. A recent study conducted in the laboratory determined that mosquito larvae fed MU-contaminated materials accumulated the bacterium in their mouths and midgets over four instars, although when fed closely-related *M. marinum*, bacterium was not detected (Tobias *et al.*, 2009). Additional research identified a correlation over a seven year time period between BU case notifications and Ross River virus case notifications, a mosquito-transmitted disease in Australia, although the authors conceded that suitable environmental conditions promoting both diseases may be driving the correlation (Johnson and Lavender, 2009).

Several investigations into potential MU reservoirs exist. Mammals and marsupials in Australia, including koalas, alpaca, a domestic cat, potaroos, two horses, black rats, and brushtail and ringtail possums tested MU positive, but these infections were limited within the geographic region of Australia (Mitchell *et al.*, 1984; Elsner *et al.*, 2008; van Zyl *et al.*, 2009). A recent

study in Australia found that 38% of captured ringtail possums and 24% of captured brushtail possums had lesions testing MU positive or feces testing MU positive in a BU endemic region, suggesting that these possums contribute to maintenance of the bacterium in the environment (Fyfe *et al.*, 2010). An additional study in Benin collected 326 rodents and 222 shrews around water bodies and in houses during the dry season and during the wet season in high BU endemic and low BU endemic areas, but MU was not identified in any of the collection samples (Durnez *et al.*, 2010). Finally, some researchers believe that migratory birds aid in disseminating MU between wetlands, but further research is needed to determine the potential of this hypothesis (Eddyani *et al.*, 2004).

#### 1.6 Risk Factors

The greatest risk factor for contracting BU is contact with an endemic area (Johnson *et al.*, 2007), although certain behavioral patterns may increase risk. A matched case-control study in three endemic districts of Ghana confirmed researchers' beliefs that BU is an environmentally-acquired infection associated with rivers and streams (Raghunathan *et al.*, 2005). The results also indicated that wading in a river or stream was a risk factor, that using certain soap products and wearing long trousers was protective against BU, and that wearing clothing that covered the upper body while farming was also protective against the disease. In a separate study conducted in Benin, wearing clothing during farming activities was not identified as a protective factor against BU infection, contact with stagnant water increased BU risk, while contact with flowing water and using soap decreased BU risk (Nackers *et al.*, 2007). Aiga *et al.* (2004) found that swimming in rivers and water use from rivers was a BU risk factor, but water use from piped sources was not a protective factor in Ghana, while Marston *et al.* (1995) found that swimming in rivers was not a BU risk factor Côte d'Ivoire.

In Cameroon, the use of bed nets was a strongly-associated protective factor against BU, but bed nets were not found to be protective in Ghana (Pouillot *et al.*, 2007). Applying insect repellant during outdoor activities reduced BU risk in Australia (Quek *et al.*, 2007), although mosquito coil use was a behavioral risk factor in Cameroon (Pouillot *et al.*, 2007). An association between BU-infected patients and mosquito bites on the arms and legs exists in Australia, but a direct link between insect bites and inoculation was not established (Quek *et al.*, 2007).

BU cases are known to occur surrounding slow-moving or stagnant water bodies or wetlands, and flooding is cited as a risk factor for the disease (CDC, 2005). The first recorded BU cases in Bairnsdale, Australia occurred two to three years after a major flooding event during Christmas of 1935 (Hayman, 1991). In 1978, Bairnsdale had its wettest year in recorded history, and in 1980 BU cases emerged. In 1962 and 1964 severe flooding took place in Uganda, and approximately two to three years later, BU cases surfaced (Dobos *et al.*, 1999). The first reported BU cases in Togo occurred in two children living near two separate rivers that experienced seasonal flooding (Meyers *et al.*, 1996), and in Papua New Guinea, cases occur near the Sepik and Kumusi Rivers where a spike in cases emerged following the flooding and widespread destruction from the Mount Lamington volcanic eruption in 1951 (WHO, 2000).

Empirical and anecdotal links exist between landscape alterations, including deforestation, agriculture irrigation, mining activities, and artificial dam creation and increased BU risk (Hayman 1991; Brou *et al.*, 2009; Duker *et al.*, 2004; Wagner *et al.*, 2008a; Wagner *et al.*, 2008b; WHO, 2000; Merritt *et al.*, 2005). Hayman (1991) postulated that closed rainforests contain MU, and disruption of the rainforest results in MU-contaminated runoff water, creating more concentrated MU quantities in water bodies, resulting in a bacteria bloom under favorable

environmental conditions. Deforestation contributes to increased flooding and erosion, creating ideal conditions for nutrient introduction into water bodies that contribute to higher water temperatures, decreased oxygen levels, and an increase in turbidity, all of which create a habitat that may be suitable to MU (Merritt *et al.*, 2005). Duker *et al.* (2004) found a relationship between the spatial distribution of BU cases and distance to gold mining sites and exposure to arsenic-contaminated soils in Ghana, and Wagner *et al.* (2008b) found that villages experiencing high BU rates were situated within low-lying areas at risk for flooding and surrounded by an agriculture matrix, suggesting that deforestation likely took place.

Several associations exist between artificial water body creation and river damming and increased BU risk. Students on the campus of the University of Ibadan in Nigeria began contracting BU after the creation of a dam on a small river running through campus in order to create an artificial lake (Oluwasanmi, 1975). BU cases also occurred following the building of large dams for agriculture irrigation north of Brisbane, Australia between 1957 and 1958 and in 1962 (Abrahams, 1964), and a recent study in Côte d'Ivoire found a relationship between disease rates and patients' proximities to dams and irrigated agricultures (Brou *et al.*, 2009). In Liberia, cases emerged after the installation of a swamp rice field that replaced an upland rice field and also in areas where the creation of dams expanded wetland areas (WHO, 2000).

Although little is known regarding MU growth and subsequent transmission, linkages between human activities and BU emergence suggest that identification of landscapes disturbed by anthropogenic activities may provide information needed to characterize risk while contributing to a better understanding of potential ecological drivers behind disease emergence.

### 1.7 Landscape Epidemiology/Ecology, GIS, and Remote Sensing

Landscape epidemiology is a multidisciplinary field focused on abiotic and biotic environmental conditions and their relationships to pathogen and vector ecology with an emphasis on mapping and predicting potential disease distributions based on ecological conditions (Pavlovsky, 1966; Ostfeld, 2005). Landscape epidemiology is nested partially within the field of landscape ecology, or the study of spatial and temporal landscape patterns and their interactions with ecological processes at multiple scales (Turner *et al.*, 2001). Observing landscape heterogeneity and its influences on ecological systems provides a substantial advantage when working with environmental data, leading to a better understanding of underlying mechanisms contributing ecosystem functions (Pickett and Cadenasso, 1995).

Emphases on spatial and temporal patterns are unique to landscape ecology in the broader ecology discipline because spatial homogeneity across ecological systems was the standard assumption until recently (Turner and Gardner, 1991; Wagner and Fortin, 2005). In general, landscape ecological studies observe larger spatial extents than those used in more traditional ecological studies with an understanding based on scale theory that finer-scale processes can act as mechanisms driving landscape dynamics within broader-scale patterns and that these broader-scale patterns can act as constraints limiting finer-scale processes (Turner *et al.*, 2001). Emphasis on neighborhood context is important under this framework and acknowledgement that environmental heterogeneity may occur at any spatial scale differentiates landscape ecology approaches further from traditional ecology methods (Wagner and Fortin, 2005).

Landscape epidemiology studies incorporate landscape ecology approaches regularly (Kitron, 1998), from identifying vector habitat distributions based on landscape composition to determining where anthrax risk from *Bacillus anthracis* exists in the United States using climate and soil variables (Beck *et al.*, 2000; Malone, 2005; Coetzee *et al.*, 2000; Blackburn *et al.*, 2007).

Several of these studies utilize geographic information systems (GIS), remote sensing technologies, and spatial analyses to identify where disease emergence is likely to take place.

GIS and remote sensing technologies provide the foundation from which to collect and process data to use in landscape ecological studies. GIS are unique in their ability to combine information from multiple sources with a shared location across a large geographic region. GIS are techniques to input, store, retrieve, manipulate, analyze, and output data that have spatial attributes associated with them (Otsfeld *et al.*, 2005). Common outputs include maps displaying features of interest, but the real power of GIS is that it provides a platform from which to organize a multitude of data for statistical and pattern analyses, for example natural environmental data, such as climate, LULC, and elevation data, along with anthropogenic attributes, such as demographic, road network, and socio-economic data.

GIS facilitates vector and raster data formats (Clarke 2003). A vector data format consists of points, lines and polygons to which information about specific attributes are stored, for example address locations, road networks, or administrative boundaries, while a raster format consists of a grid of equally-sized cells. Cell sizes are referred to as the spatial resolution of the grid; for example, a 30m resolution grid consists of cells measuring 30m on each side, representing an area equal to 900 square meters total. Each cell contains information such as elevation, temperature, or land cover classification values, and the possibility exists for calculations between grids when cells correspond to the same geographic locations.

Satellite sensors that monitor the Earth from space generate remotely-sensed satellite imagery (Jensen and Hodgson, 2004). The majority of remotely-sensed satellite products are available in raster format. A variety of products exist, each measuring reflectance from the Earth's surface across the electromagnetic spectrum (EMS) (Turner *et al.*, 2003). These images

are useful particularly when observing land cover patterns, water turbidity, or when measuring elevation.

Quantitative approaches characterizing landscape patterns often utilize landscape metric calculations derived from raster images that are classified into different land cover categories (McGarigal and Marks, 1995). Landscape metrics quantify landscape patterns based on composition, or the presence of specific landscape components in a geographic area, and landscape configuration, or the spatial arrangement of landscape components in an area (Turner, 2005; McGarigal and Marks, 1995). Outputs from these metrics are then interpreted and analyzed statistically to gain a better understanding of patterns that may be influencing ecological processes in a geographic area.

Of particular interest are landscape metrics that identify landscape disturbances linked to anthropogenic activities. A disturbance is defined as "any relatively discrete event in time that disrupts ecosystem, community, or population structure and changes resources, substrate availability, or the physical environment" (Pickett and White, 1985). These disturbances include habitat fragmentation, or a disruption in landscape connectivity (With *et al.*, 1997) resulting from large land cover expanses transforming into small patch sizes that become isolated by land cover types alternative to the natural vegetation (Wilcove *et al.*, 1986), and agriculture intensification, which takes place when cultivated land is altered to produce high-yield crops through the use of fertilizers and pesticides, increased irrigation methods, or mechanization (Matson *et al.*, 1997).

Observing land cover patch sizes and shape patterns using landscape metrics, along with landscape composition, can provide insight into human activities in a region; for example, Krummel *et al.* (1987) found that deciduous forest patches with more uniform shapes, such as

squares or rectangles, indicated managed forest cover and forest cover adjacent to agricultural land using a fractal dimension index.

A study conducted by Iverson (1988) assessing land cover changes over a160 year period in Illinois used several landscape metrics, including number of patches, mean patch area, perimeter-to-area ratio, and fractal dimension indices by land cover type, to characterize anthropogenic influence on the landscape. Results determined that a relationship existed between high perimeter-to-area ratios and the presence of road networks; natural wetlands had highly-complex shapes because they were not confined to regularly-shaped boundaries imposed by human activities; surface mines, quarries, and gravel pits had highly-regular shapes because of human management; and forest cover patches often had regular shapes because of adjacency to agriculture land cover.

A landscape index quantifying the number of landscape patches was used to characterize habitat fragmentation in a study area in Iowa (Narumalani *et al.*, 2004), and a study observing forest clearing patterns in Oregon used a landscape metric that employed a weighted patch edge calculation to compare forest patches in privately-owned land versus in publically-owned land between 1972 and 1988 (Spies *et al.*, 1994). Results determined that privately-owned land had a smaller percentage of interior forest patch habitat compared to publically-owned land, suggesting a more fragmented forest landscape.

Landscape epidemiology studies use landscape metrics frequently to relate landscape patterns to disease incidence. Graham *et al.* (2004) determined that mean shape index values at the landscape-level within concentric polygons surrounding disease incidence locations were important when investigating human alveolar echinococossis in China. Brownstein *et al.* (2005) quantified a link between forest fragmentation and tick densities and numbers of infected ticks

responsible for Lyme disease transmission to humans in Connecticut using observations of patch size and patch isolation. Results identified a positive relationship between fragmentation and entomologic risk, but a negative relationship between fragmentation and human disease incidence.

A study investigating and predicting schistosomiasis-harboring mollusk densities in two mountainous regions in China used an integrated approach, quantifying landscape patterns and then employing Bayesian spatial modeling methods (Yang et al., 2008). Researchers analyzed mean shape index values and Shannon's evenness index values along with a variety of environmental variables. Generation of non-spatial and spatial model results emphasized the importance of using spatial statistical approaches when investigating natural phenomena. Final results determined a positive relationship existed between mean shape index values and mollusk densities, indicating that mollusks clustered in irregularly-shaped land cover patches such as irrigation ditches. Using spatial statistical methods to predict mollusk densities took advantage of information provided by landscape metric calculations while accounting for spatial autocorrelation in the data, an important factor that can introduce bias and that many researchers ignore when working with environmental data.

### 1.8 Spatial Autocorrelation

Tobler's first law of geography states that everything is related to everything else, but near things are more related than distant things (Tobler, 1970), or are spatially autocorrelated. Ignoring positive spatial autocorrelation, a common phenomenon when working with ecological data, can produce falsely-precise model estimates, the most common of which is to overestimate regression coefficient significance leading to Type I errors by rejecting null hypotheses when they are true (Legendre and Fortin, 1989; Wagner and Fortin, 2005; Lennon, 2000). These errors

lead not only to inaccurate parameter estimates contributing to erroneous model prediction, but promote a misunderstanding of processes driving ecological patterns (Lennon, 2000).

Spatial autocorrelation in environmental data can occur for a variety of reasons, including processes inherent to the organism under investigation or because of spatial dependency of the organism to spatially-structured environmental drivers (de Knegt *et al.*, 2010) Further, the processes driving spatial dependence may occur at different scales than which derivation of data observations and variables took place (Keitt, 2002). Omission of important covariates will bias  $\beta$  estimations, and if these covariates have a spatial structure, spatial autocorrelation in model residuals will likely result (Waller and Gotway, 2004). Failure to account for spatially autocorrelated model residuals violates the assumption of independently and identically distributed errors, leading to inflated degrees of freedom, resulting in the overestimation of coefficient significance mentioned above (de Knegt *et al.*, 2010; Legendre and Fortin, 1989; Wagner and Fortin, 2005; Lennon, 2000; Keitt, 2002; Waller and Gotway, 2004).

Spatial modeling approaches, for example the one employed by Yang *et al.* (2008), mitigate spatial dependency problems by accounting for spatial autocorrelation in the modeling process. Several spatial modeling approaches exist, each of which was designed to incorporate different data formats and to achieve different goals. For a review of spatial statistical models and methods see Schabenberger and Gotway (2005).

## 1.9 Past BU Landscape Studies

GIS, remote sensing technologies, and statistical analyses were used in several BU studies investigating environmental features related to disease incidence, but to our knowledge studies quantifying landscape patterns using landscape metrics do not exist, and, with the

exception of Duker *et al.* (2006) and Wagner *et al.* (2008a, 2008b), these studies failed to account for spatial autocorrelation among observations, variables, and model residuals.

A study investigating the relationship between arsenic-rich floodplains and BU incidence in the Amasie West District of Ghana analyzed several human and environmental variables using GIS and satellite imagery (Duker *et al.*, 2004). BU incidence per settlement and settlement population were mapped along with stream sediment sample locations and corresponding arsenic concentration values. Farmlands lying below a specified elevation threshold were identified, along with proximities to arsenic-enriched streams. A land use and land cover map generated from Advanced Spaceborne Thermal Emission and Reflection Radiometer (ASTER) imagery determined that 21% of total farmlands in the study area lie within arsenic-enriched areas. Although the results revealed a correlation existed between BU cases and arsenic-enriched, lowlying farmlands, researchers did not determine whether the flooded lowlands or arsenic levels contributed more to BU risk.

Duker et al. (2006) conducted another analysis in the Amansie West district of Ghana targeting spatial patterns of BU incidence in the district. Stream sediment samples from 1992 and 37 ground water samples from 2003 were related to single year BU incidence reports obtained from a 1999 national case search, along with BU average incidence from 2000-2003 for each settlement within the district using a conditional autoregressive (CAR) statistical model. This approach assumed that covariates from neighboring districts influenced BU prevalence in the target district, and districts were defined as regions bordering each other or those that were within a fixed 15km distance from one another. Results suggested that a relationship existed between mean arsenic levels in soil and BU spatial distributions and distances to gold mining sites and BU spatial distributions.

The RESPOND Health Mapping Activity Ivory Coast study investigated BU occurrence in the Ivory Coast (Côte d'Ivoire) using remote sensing and GIS to identify areas with a high BU risk (RESPOND 2006). Landsat satellite imagery along with Moderate Resolution Imaging Spectroradiometer (MODIS) data were used to classify vegetation and wetland conditions. A digital elevation model using Shuttle Radar Topography Mission (SRTM) data was used to search for low-lying areas prone to water accumulation. The results of the study indicated definite vegetation trends in the area of interest, but researchers were unable to obtain the necessary epidemiological data to complete their analysis.

A more recent country-wide study by Brou et al. (2008) investigated landscape variables related to BU incidence in Côte d'Ivoire. Forest surface area in hectares, irrigated rice production, banana production, and dam surface areas were mapped and quantified using GIS in preparation for a multivariate statistical analysis. Logistic regression results suggested that closer proximities to irrigated rice fields and to dams increased BU risk, but spatial autocorrelation in the observed data, the environmental covariates, or the model residuals were not considered.

A study investigating the role of landscape features related to BU rates at a country-wide scale in Benin used satellite imagery and GIS to prepare data for statistical analyses (Wagner *et al.*, 2008a). BU case data from 2004 and 2005 were mapped to corresponding village locations. Concentric buffers with radii ranging from 100m to 50 km from village centers were generated to analyze land cover composition, elevation, and potential wetness patterns, and distances from village centers to the nearest river were quantified. A negative binomial statistical analysis including random district effects determined that villages lying at low elevations within drainage basins with variable wetness patterns that are surrounded by forest cover have a high BU risk. A spatial scan statistic identified spatial disease clusters with higher than expected BU rates near

the Zou and Ouémé Rivers located toward the eastern side of the country and along the Couffo River located toward the western side of the country. Lower than expected BU rates occurred near the coastline and toward the northern region of Benin.

A second study by Wagner *et al.* (2008b) used LULC variables to construct a probability model related to BU infection. Latitude, longitude, distance to nearest river, elevation, total population and seven LULC class percentages were analyzed statistically using a multilevel Bayesian logistic regression model with district-level random effects. This modeling approach used data derived at different scales and the district-level random effects mitigated correlation in residuals due to unknown covariates at the district-level. Model residual plots revealed that spatial autocorrelation was no longer present in the data set. The results indicated that the probability of BU incidence increased with percentage surrounding agricultural land cover, and the probability of BU incidence decreased as the percentage of surrounding urban land use increased at large scales. A set of "best" models predicted BU rates from the mean posterior distribution of each model at validation sites in Benin and also in Ghana. The models predicted BU positive sites more accurately than BU negative sites.

A study investigating BU incidence in Victoria, Australia from 1980 to 2009 performed a network analysis to determine whether BU cases occurred randomly before the analysis of climate, landscape, and socioeconomic data (van Ravensway *et al.*, IN PREP). Network analysis results determined that BU cases did not occur randomly; therefore, administrative data equivalent to U.S. census tract-level data demarcated town boundaries from which derivation of several environmental and sociological data variables took place. Statistical analyses used multilevel Poisson regression models with random effects for endemic locations. Two model sets were produced, one investigating an approximate lag time between human infection and

symptom presentation, with the assumption that mosquitoes play a direct role in transmission and that infection occurred during high mosquito abundance periods, and referred to as the mosquito abundance prediction (MAP) model. The second model set investigated landscape, occupational, and climate (LOC) variables related to BU incidence in the study region.

The MAP models used climate variables as a proxy for high mosquito abundance periods, wetland land cover and low elevations represented mosquito habitats, and outdoor occupation variables represented proportion of humans at risk within each town. MAP model results suggested that towns with high percentages of water and low elevations with increased precipitation and minimum temperatures nine months prior to BU symptom presentation with large proportions of the population working in agriculture, mining, or parks and gardens professions were at a higher BU risk, but direct links to mosquitoes as vectors are still under investigation. The LOC model results indicated that towns at lower elevations with high percentages of forest and agriculture land cover, along with decreased maximum temperatures 14 months prior to symptom presentation, followed by increased precipitation 11 months prior to symptom presentation are at a higher BU risk. This study was the first of its kind to incorporate climate, social, and landscape variables into its analyses and the first to investigate a specific vector habitat in relation to BU incidence.

While these studies investigated important environmental features related to BU risk, landscape components focused on compositional features, rather than exploring landscape configurations. Further, many of these studies investigated relationships between specific anthropogenic activities, for example proximity to dams or percentage of surrounding agriculture, while insight into overall landscape disturbance was not gained.

Additionally, although these studies observed variables spatial in nature, with the exception of Duker *et al.* (2006) and Wagner *et al.* (2008a, 2008b), quantified relationships failed to account for potential spatial autocorrelation in model residuals, and while several studies included random effects to help account for unobserved variables contributing to BU prevalence, no studies incorporated spatial random effects that identify whether a spatial structure exists for these unobserved covariates. Incorporating spatial random effects into the modeling process while accounting for spatial autocorrelation among model residuals provides a powerful tool from which to predict BU risk at new locations and to identify potential covariates through observations of spatial characteristics related to unknown covariates.

#### 1.10 Objectives

This study builds upon knowledge gain from previous studies in Benin by relating BU occurrence to landscape patterns (Wagner *et al.*, 2008a; Wagner *et al.*, 2008b). Previous research in this region related specific land cover composition to BU risk across large spatial extents. The primary objective of this research is to observe landscape configurations in addition to landscape composition related to BU rates at a medium spatial extent, ranging from 400m to 2k from village centers. Observing closer proximities allowed quantification of habitats traversed regularly by village residents, while maintaining study areas large enough to quantify landscape patterns.

The specific objectives of this thesis were to

1) determine whether landscape patch configurations, quantified using landscape metrics and used as indicators of potential anthropogenic-related landscape disturbances, are related to BU rates in Benin, West Africa,

- 2) whether specific land cover configurations specific to individual land cover composition types are related to BU rates,
- 3) whether compound topographic index values using 30m resolution data were consistent with previous research outcomes implicating a relationship between stagnant water and BU rates.
- 4) identify whether a spatial structure exists for underlying processes contributing to BU rates and finally
- 5) create a BU risk surface based on identified contributing landscape characteristics and underlying spatial processes in the study area.

Further, the goal of this study is not to identify specific ecological processes contributing to MU growth and BU transmission in Benin, but to determine whether human disturbance indicators as characterized by landscape patterns are linked to and can be used to identify high BU risk landscapes.

### 1.11 Hypotheses

Previous research suggesting that a relationship exists between anthropogenic landscape disturbances and BU risk (Merritt *et al.*, 2005; Hayman 1991; Brou *et al.* 2009; Wagner *et al.*, 2008; Duker *et al.*, 2004; WHO, 2000) provided the basis for the first set of hypotheses. The first hypothesis is that disturbed landscapes characterized by uniformly-shaped land cover patches and low aggregation levels, representative of potential anthropogenic landscape disturbances, surround villages with higher BU rates. The second hypothesis is that a positive relationship exists between BU rates and land cover patch configurations representative of potential anthropogenic landscape disturbances corresponding to specific land cover composition types; for example, uniformly-shaped agriculture or forest patches. Previous research findings

demonstrating that BU cases occur near slow-moving or stagnant bodies of water or in low-lying areas within drainage basins (CDC, 2005; WHO, 2007; Wagner *et al.*, 2008) provided the basis for the final hypothesis that landscapes with higher average compound topographic, or wetness index, values surround villages with higher BU rates.

A strong inference approach, involving the exploration of multiple, biologically plausible hypotheses followed by identification of the model that provides the best approximation of the data, will provide the basis from which inference may be drawn to predict disease risk across the study domain (Plowright *et al.*, 2008).

# **Chapter 2 MATERIALS AND METHODS**

#### 2.1 Study Area

The southern regions of Benin and Togo, West Africa comprise the study area for this investigation. The study area falls within a 185 x 185 km area that is equal to one Landsat satellite image extent located in WRS path 192 row 55, with latitudes ranging from approximately 8.167 N to 6.300 N and longitudes ranging from approximately 0.842 E to 2.482 E. The study area encompasses all or parts of several administrative districts, including Atlantique, Mono, Plateau, Couffo, Zou, and Collines located in Benin and Centre, Plateaux, and Maritime in Togo. Four major rivers flow through the study area, including the Couffu, Oueme and Zou Rivers in Benin, and the Mono River which delineates the border between Togo and Benin in the southern regions of the countries (Figure 2-1).

Buruli ulcer is endemic in Benin and Togo, but limitations exist regarding data corresponding to disease incidence in Togo. Therefore, this study used BU case data and corresponding environmental data from Benin to predict BU risk across the landscape, into regions within the boundary of Togo.

The Republic of Benin is a coastal country located in West Africa along the Gulf of Guinea, bounded by the countries of Togo, Burkina Faso, Niger, and Nigeria. Benin is a former French colony that gained independence on August 1, 1960. The country encompasses a total surface area of 112,622 sq km, with 110,622 sq km of land and 2,000 sq km of water (CIA). The 2010 estimated population is 9,056,010 people, and the average life expectancy at birth is 62.3 years for women and 60.1 years for men (United Nations Statistical Division). French is the official language in Benin, but several groups speak local, indigenous languages, including the Fon, Yorouba, Boun, Bariba, Somba, Aizo, Mina, and Dendi (United Nations Benin, 2010).

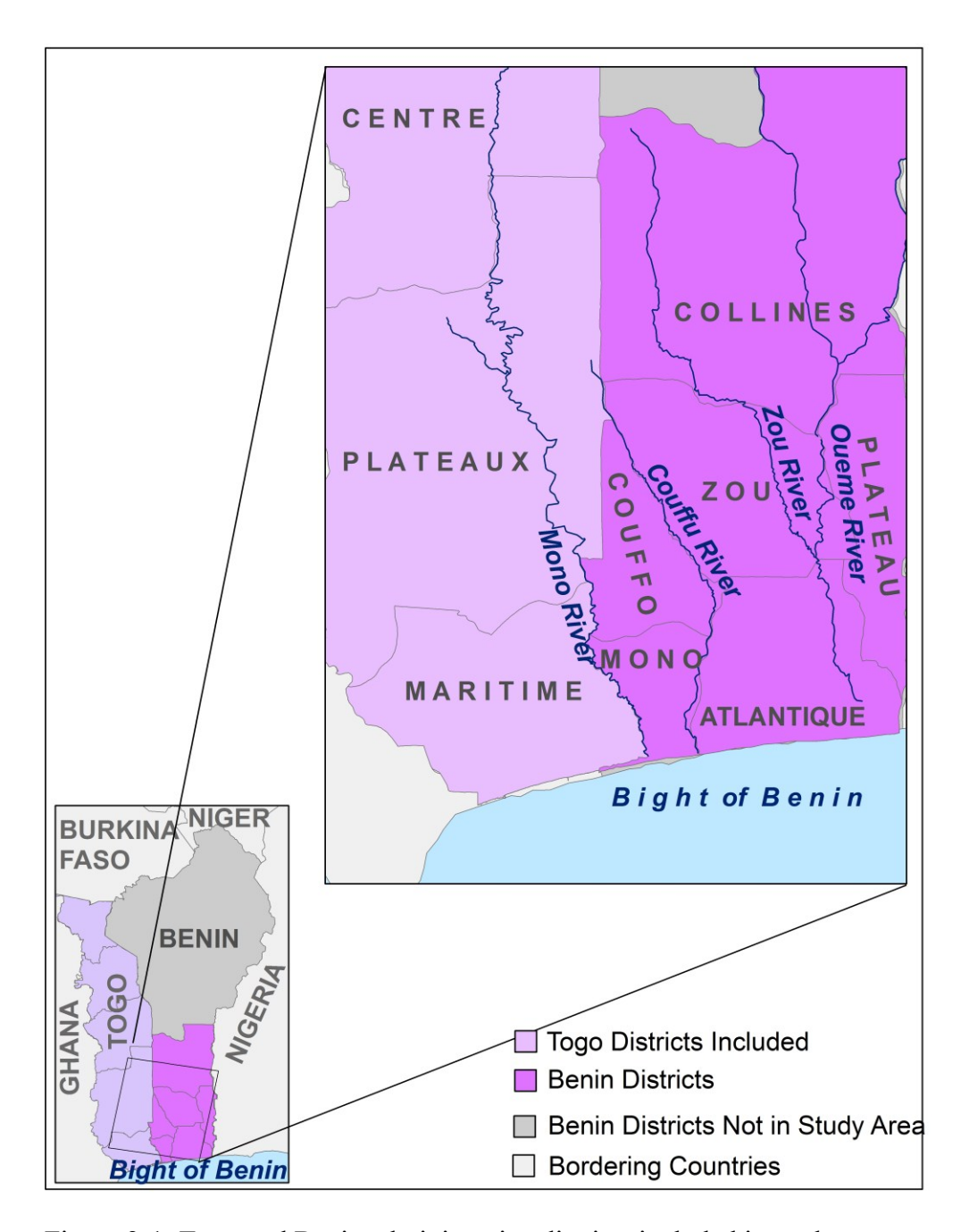


Figure 2-1. Togo and Benin administrative districts included in study area

Subsistence farming is the main form of agriculture production, but for-profit agriculture products include cotton, corn, cassava, yams, beans, palm oil, peanuts, cashews and livestock (CIA). Benin's landscape consists primarily of woodland and savannas, followed by cultivated woodland and shrub savanna, then fallow fields mixed with cultivated fields; semi-deciduous

forests are present in the southern region of the country and occupied an estimated 1-2% of the land surface in 2007 (USAID, 2007). Deforestation and environmental degradation is an ongoing problem in Benin, and the landscape continues to change rapidly. Food-crop and cotton cultivation expanded by 265% and 79% between 1986 and 1997, while firewood extraction and charcoal production contributed to a 30,000 ha per year deforestation rate, along with additional deforestation taking place to construct fish corrals (USAID, 2007).

Southern Benin falls within an a sub-equatorial climate zone, often referred to as the Dahomey Gap, with bimodal seasonal distributions; two rainy seasons extend from April to July and from September to November, while two dry seasons extend from December to March and in the month of August each year (Dossou and Gléhouenou-Dossou, 2007).

#### 2.2 BU Case Data

The Programme National de Lutte contre la Lèpre et l'ulcère de Buruli (PNLLUB) provided a subset of Benin 2004 and 2005 BU positive and BU negative villages to use in this analysis. Processing of these data included three levels. Initially, volunteers and trained personnel reported cases at the village level under the supervision of health care workers from nearby facilities, and then a trained nurse reported cases at the regional level using BU02 standardized forms, which were then summed quarterly at the national level (Sopah *et al.* 2007).

A total of 292 villages, 183 positive and 109 negative, from the data subset were located within the study area (Figure 2-2); 558 cases occurred total, ranging between 1 case per village to 29 cases per village. A village was identified as positive if at least one case occurred in 2004 or 2005. The data set consisted of BU case counts, population counts, and latitude and longitude coordinates of villages. No correlation between population and BU incidence existed.

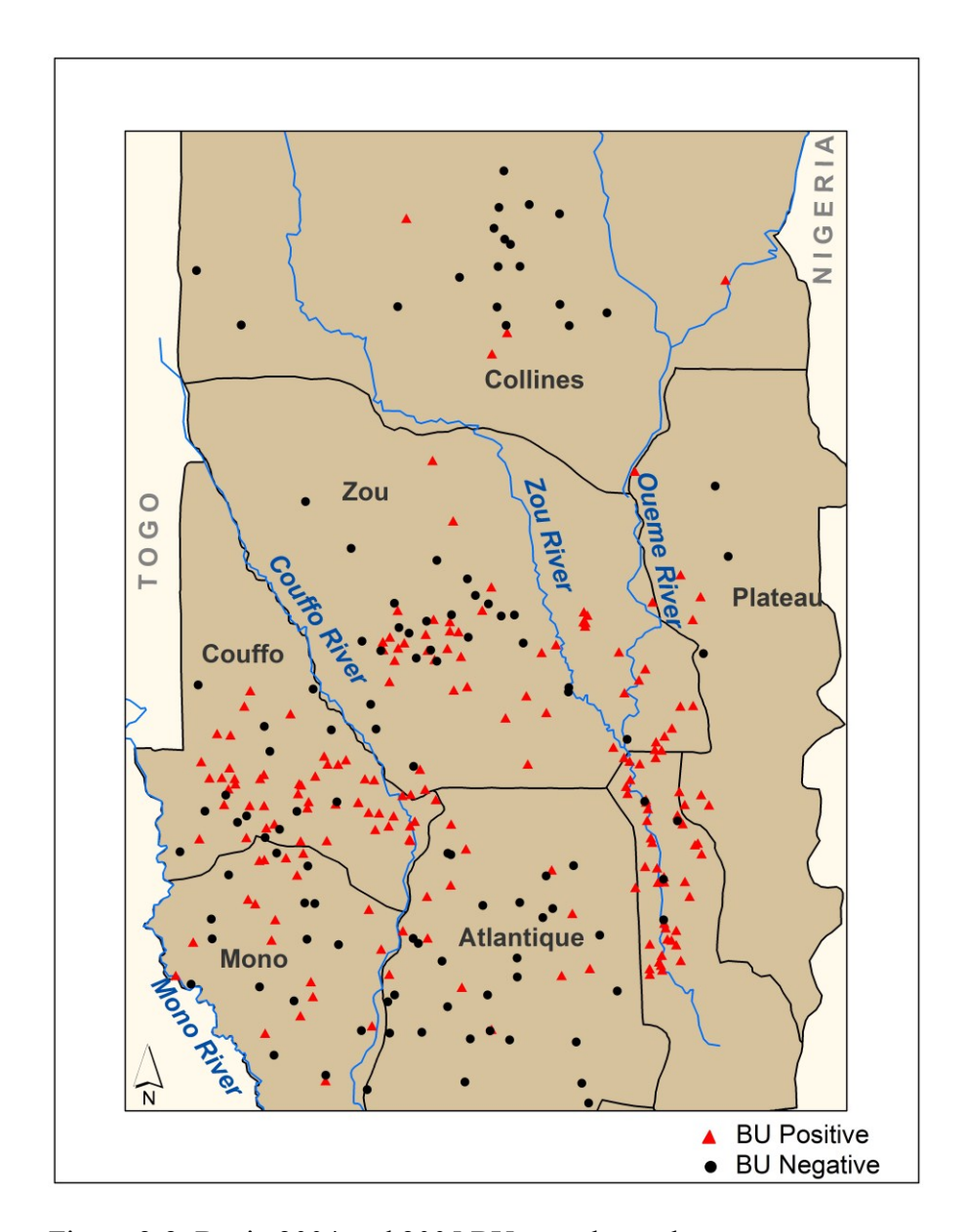


Figure 2-2. Benin 2004 and 2005 BU case data subset

Wagner *et al.* (2008a) identified disease clusters with higher than expected and lower than expected BU rates located across southern Benin using the same data set. A primary cluster comprised of higher than expected BU rates was located across the Atlantic, Zou, and Couffo districts and falls within the study area for this analysis.

# 2.3 Satellite imagery and derivatives

Land use and land cover data was derived from December 13, 2000 Landsat ETM+ imagery obtained from the University of Maryland Global Land Cover Facility (http://glcf.umiacs.umd.edu/index.shtml). The imagery was geometrically rectified and projected (UTM Zone 31N) before performing an unsupervised classification (Lillesand and Kiefer, 2000) using an ISODATA algorithm with100 initial classes on the principal axis, set to approximate true color for 10 iterations or 0.95 convergence in Erdas Imagine software program. The initial 100 classes were then reduced to 22 classes, which were then reduced further to 10 classes, following Anderson's Level I classification scheme, with the exception of a mixed class and the agriculture class (Table 2-1; Figure 2-3; Anderson, 1976). The final classification consisted of three mixed agriculture classes because a dominant agriculture class did not emerge from the classification algorithm and a mixed class that included pixels classified with greater than two categories. Execution of a 5x5 statistical majority filter helped to eliminate classification noise (Mather, 2004).

Lack of ground truth data points from this region and during this time period limited the ability to assign spectral signatures to specific land cover categories; therefore, visual interpretation methods were used to delineate land cover classes and aggregated land cover classes were intended to help mitigate classification error.

Table 2-1. Land use and cover classification categories

Land Use and Land Cover Classes							
Class Number	Class Name	Class Description					
1	Urban	Mixed Urban or Built-up Land, Other Urban or Built-up Land, Transportation					
2	Not Present	Agriculture: see classes 9, 10, and 11					
3	Rangeland	Shrub and Brush Rangeland: Shrub and Shrubland					
4	Forest	Riparian Forest, Evergreen Forest, Forest					
5	Water	Streams and Canals, Lakes, Reservoirs, Bays and Estuaries					
6	Wetland	Wetland and Forested and Non-forested Wetland: Water/Wetland, Wetland/Shrub, Wetland/Riparian Vegetation					
7	Barren	Sand/Salt					
8	Mixed	Evergreen/Ag/Shrub, Shrub/Ag/Wetland, Wetland/Shrub/Urban, Shrub/Ag/Urban					
9	Agriculture 1	Shrub/Agriculture					
10	Agriculture 2	Agriculture/Forest					
11	Agriculture 3	Agriculture/Urban					
Class categories correspond to Level I classification scheme except for class 8 (Mixed) and classes 9-11 (Mixed Agriculture) (Anderson <i>et al.</i> , 1976)							

Quantifying landscape patterns within concentric polygons is a common approach in landscape analyses (see Condeso and Meentemeyer, 2007; Graham *et al.*, 2004; Danson *et al.*, 2004; Brownstein *et al.*, 2005; Wagner *et al.*, 2008a, Wagner *et al.*, 2008b). Concentric polygons with radii set at 100m intervals, from 400m to 2k, from village centroids acted as buffers from which LULC classification data was obtained for pattern analysis (Figure 2-4).

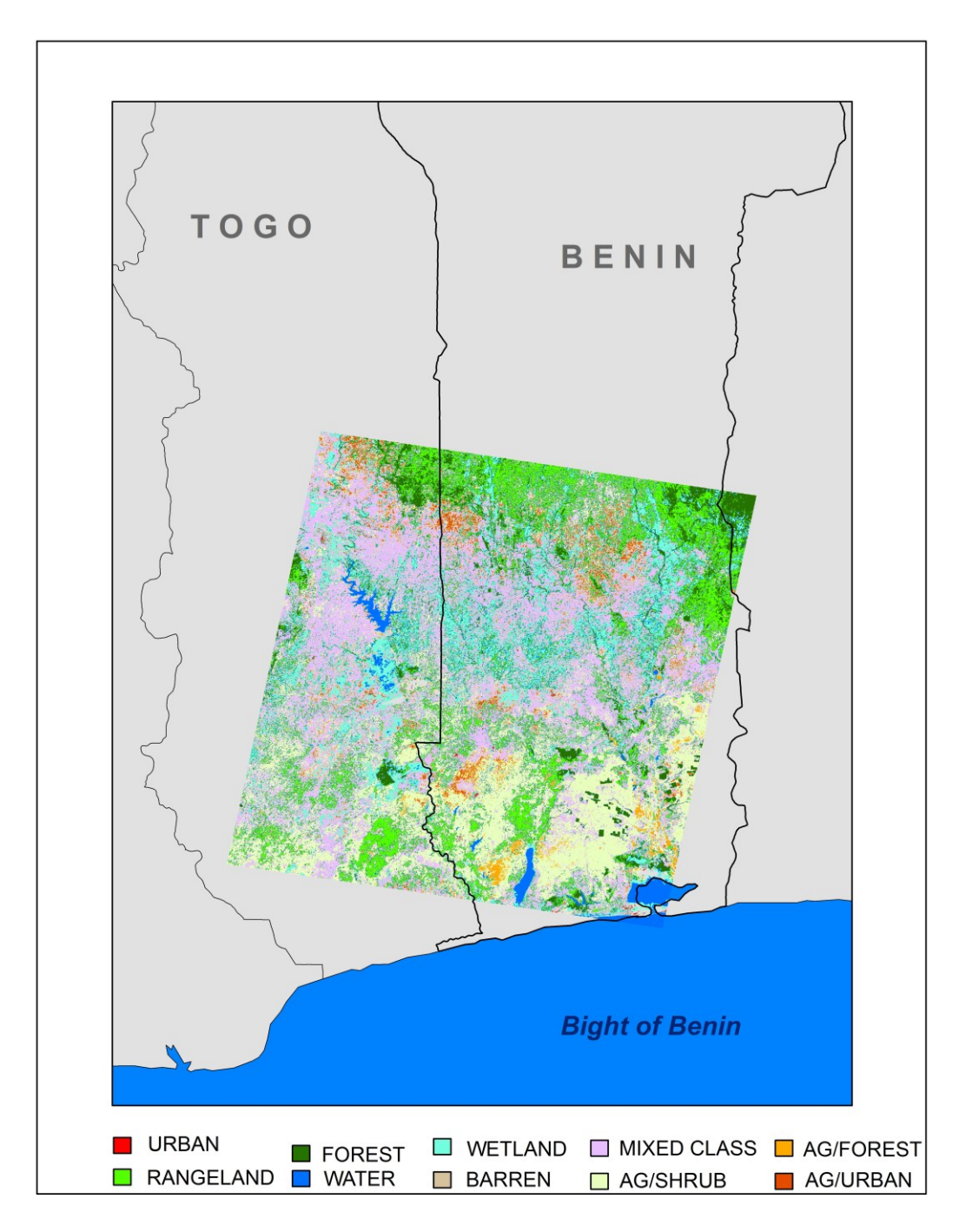


Figure 2-3. Land use and land cover classification.

The LULC within each buffer was clipped and reformatted for compatibility within FRAGSTATS software package. A total of 292 individual buffers representing each village location were created at each distance interval, with 16 distance intervals total.

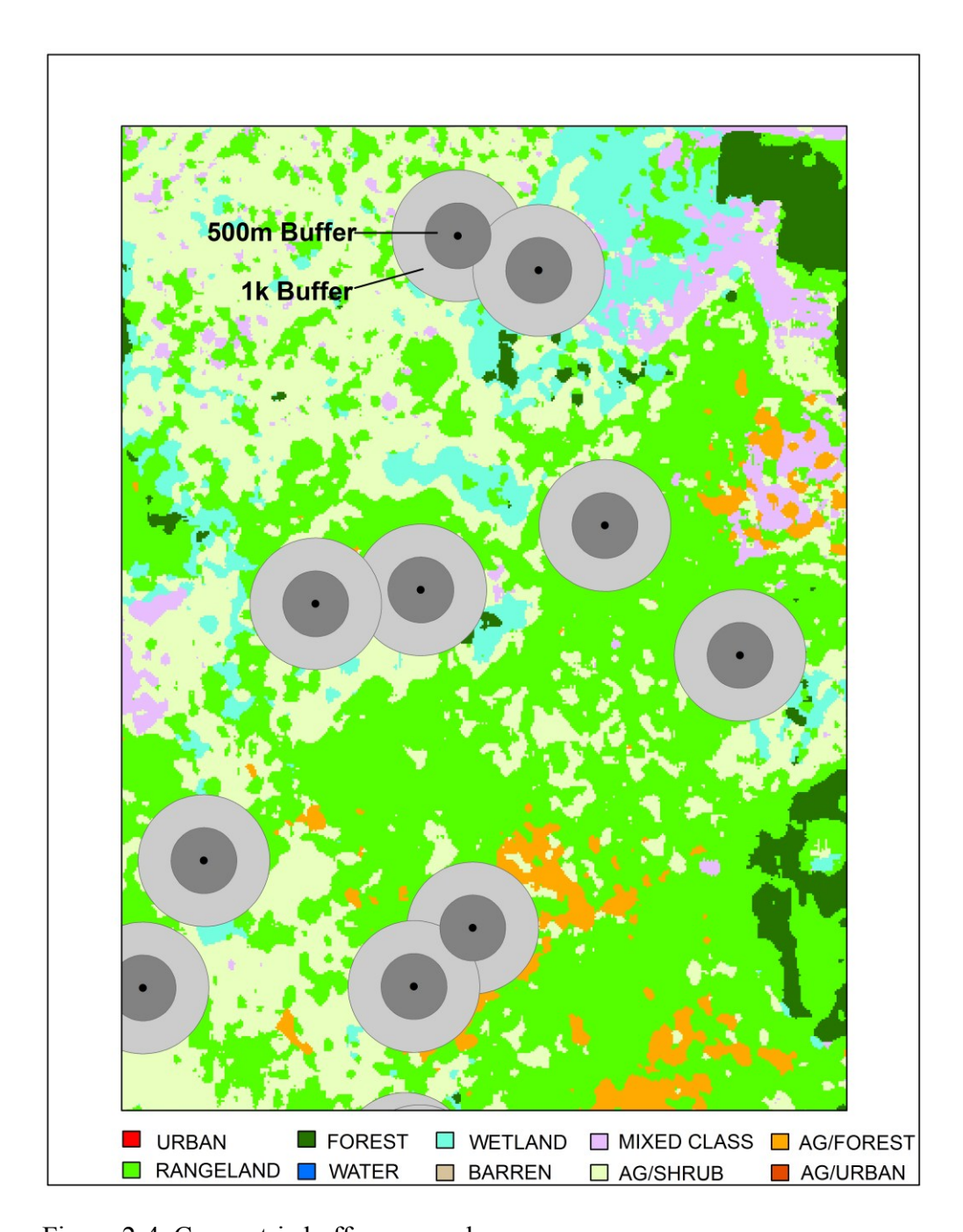


Figure 2-4. Concentric buffers example

Compound topographic index, or wetness index, derivation was completed using 30m resolution ASTER Global Digital Elevation Model data (https://wist.echo.nasa.gov/wist-bin/api/ims.cgi?mode=MAINSRCH&JS=1). DEM sinks were filled, and elevation slope was calculated in degrees using ArcGIS software program. Flow direction was modeled using a D-8

algorthim (O'Callaghan and Mark, 1984) from which flow accumulation and the wetness index were calculated using the following equation (Equation 2-1; Beven and Kirby, 1979):

Equation 2-1

$$wi = \ln(A_S / \tan \beta)$$

where  $A_S$  is the catchment area at a point, or flow accumulation, and  $\tan \beta$  is the local slope gradient (Figure 2-5; Schmidt and Persson, 2003). Wetness index averages within each buffer were calculated using the Zonal Statistics function within Hawth's Tools in ArcGIS.

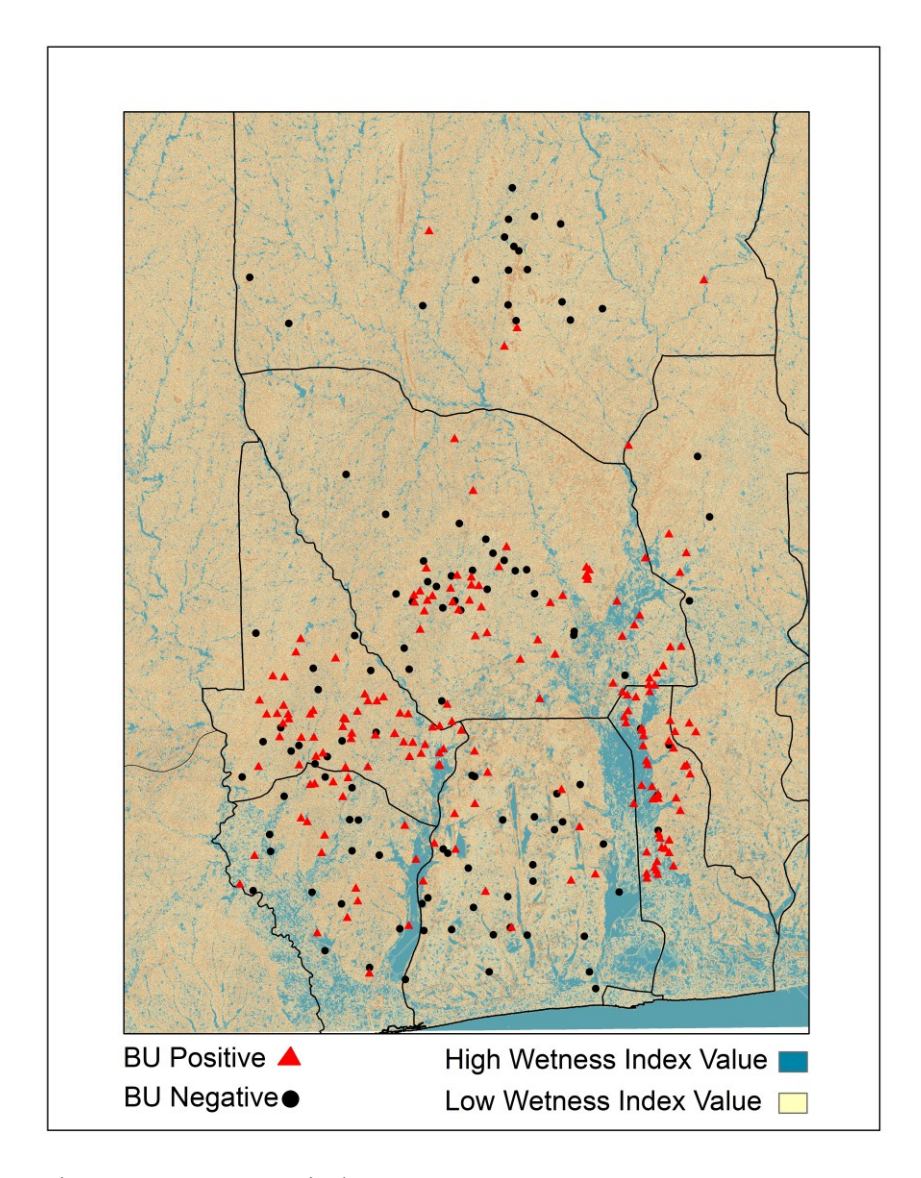


Figure 2-5. Wetness index map.

### 2.4 Statistical Modeling

Model sets were created at the landscape level, characterizing landscape configuration for all classes across the study area, and at the class level, characterizing landscape configuration for specific classes across the study area.

Following the integrated approach of Yang *et al.* (2008), a landscape analysis approach and a hierarchical Bayesian spatial modeling approach employing Markov Chain Monte Carlo (MCMC) simulation were used to identify important covariates and to predict the spatial distribution of BU risk across the study domain. Figure 2-6 outlines the methods and approaches used to generate the final predictive surface.

### 2.5 Landscape-level Configuration Analysis

A variety of landscape-level metrics were calculated within FRAGSTATS software package using the clipped LULC data. These calculations employed an 8-neighbor rule that included neighboring cells with flat adjacencies and those with diagonal adjacencies to the focal cell (Gergel and Turner, 2002). The ability to characterize potential human disturbances to the landscape expressed through relatively high fragmentation values, potential for ecological edge effects, and potential biodiversity loss provided the basis for landscape metric selection (Table 2-2).

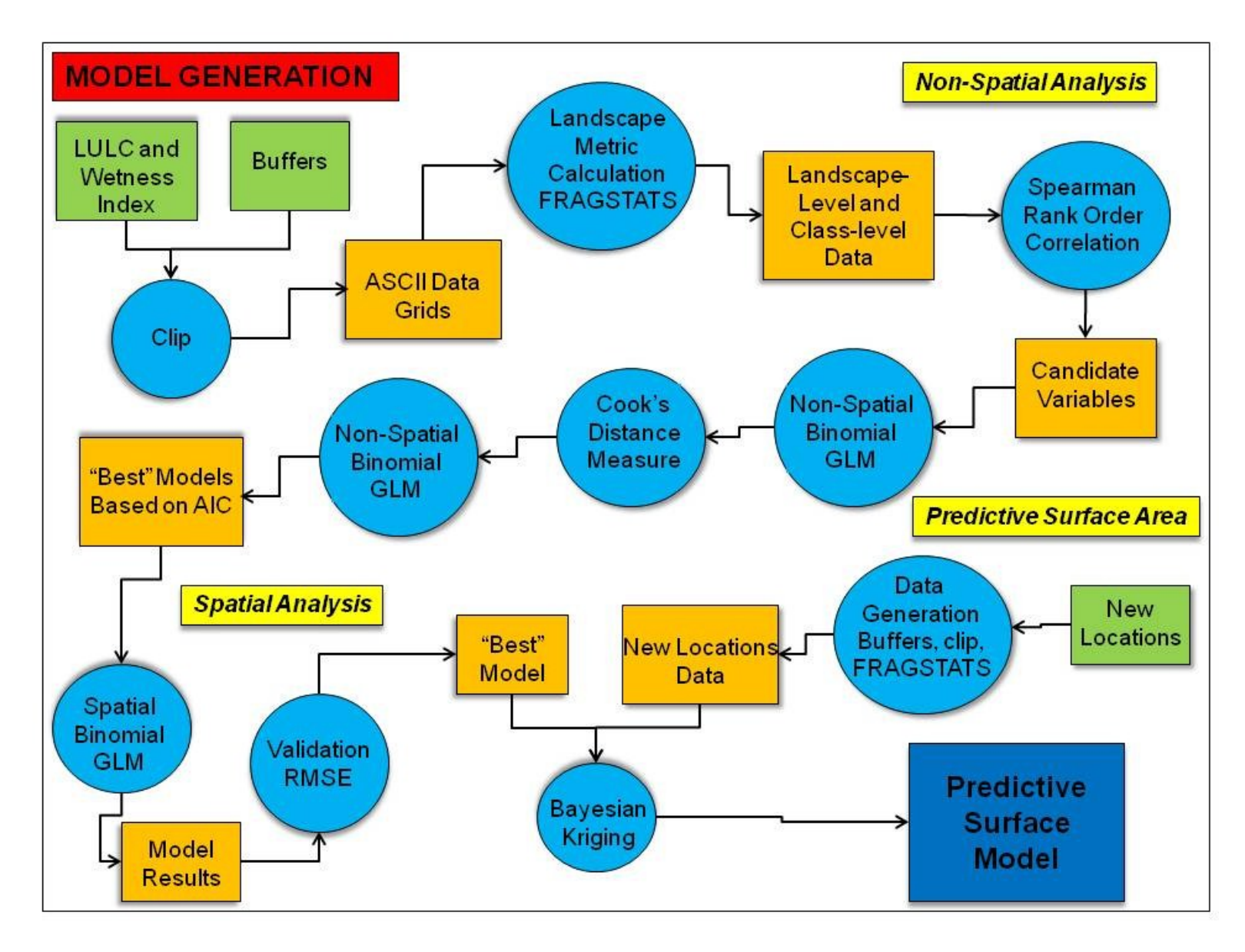


Figure 2-6. Methods and approaches used for final model generation

Table 2-2. Initial landscape metrics calculations.

Landscape-level Initial Landscape Metrics								
Metric	Abreviation	Description	Interest					
Landscape Shape Index	LSI	Standardized aggregation index based on total edge	Fragmentation					
Shape Index Mean	SHAPE_MN	Standardized land cover patch edge complexity measurement	Altered land cover shapes					
Fractal Dimension Index Mean	FRAC_MN	Land cover patch edge complexity measurement	Altered land cover shapes					
Perimeter-to-area Ratio Mean	PARA_MN	Land cover shape complexity measurement	Altered land cover shapes					
Percent Land Cover Adjacency	PLANDJ	Land cover type aggregation measurement	Fragmentation					
Patch Richness Density	PRD	Standardized landcover diversity measurement	Heterogeneity					
Shannon's Diversity Index	SHDI	Land cover diversity measurement	Heterogeneity					
Number of Patches	NP	Measures number of individual patches present in area	Fragmentation					

Redundancy among landscape metrics is a common problem (Riitters  $\it et al., 1995$ ); therefore, a Spearman's rank order correlation matrix identified mulitcolinearity between metrics, and only those metrics that exhibited an r < 0.60 with one another across all distance intervals were selected for candidate regression models. Correlation matrices generated for this study are available in Appendix A.

Metrics were divided into groups representing shape complexity, potential fragmentation, and land cover diversity. Candidate model generation used non-spatial binomial generalized linear regression models (GLMs) with BU rates as the response variable and landscape metric values and average wetness index values as independent variables. BU rates were derived by dividing BU counts by the total population at each location. The binomial GLM model

distribution is  $y_i \mid p_i \sim binomial(n_i, p_i)$  where  $p_i$  is the success probability and links to the regression covariate  $x_i$  through a logit transformation (Equation 2-2; SAS/STAT(R)):

Equation 2-2

$$\log it(p_i) = \log(\frac{p_i}{1 - p_i}) = \alpha + \beta x_i$$

Nested models were generated at 100m distance intervals from 400m to 2k; data was not combined across distances. High leverage points were identified using Cook's distance measure, and data locations with a value > 1.0 that impacted sign direction and model results substantially were removed from the data set (Cook, 1977). Fourteen high leverage points were removed from the landscape-level analysis, and removal of high leverage points at the class-level occurred on an individual model basis (Appendix B). Final candidate models consisted of data points that were never high leverage points at any distance interval between 400m and 2k. Observations of Akaike Information Criterion (AIC) values (Akaike, 1974) determined the "best model" to use in the final analysis. Two "best" model sets were created at the landscape-level because metrics representing diversity and fragmentation were correlated with one another, but both model sets demonstrated explanatory potential. Complete non-spatial candidate model results are available in Appendix C.

# 2.6 Landscape-level Configuration Analysis Predictor Variables

Characterization of land cover shape complexity used the shape index mean. Selection of the shape index mean over the fractal dimension index mean occurred because the fractal dimension index mean has the potential to introduce bias when working with small areas, as was the case when working with buffers with shorter radii from village centers (Turner, 2005). Shape index mean values characterize land cover patch shape complexity using an equation that adjusts for a square standard, thereby eliminating problems introduced from changing perimeter-to-area ratios (McGarigal and Marks, 1995). The shape index mean is calculated in FRAGSTATS software package as follows (Equation 2-3):

Equation 2-3

$$SHAPE = \frac{p_{ij}}{\min p_{ij}}$$

where  $p_{ij}$  = perimeter of patch ij in terms of number of cell surfaces and  $p_{ij}$  = minimum perimeter of patch ij in terms of number of cell surfaces. Values closer to 1.0 indicate more uniformly-shaped land cover patches with complexity increasing as values increase. A plot of the shape index mean surface at the landscape level plotted areas with more uniform patch shapes in blue and more complex shapes in red (Figure 2-7).

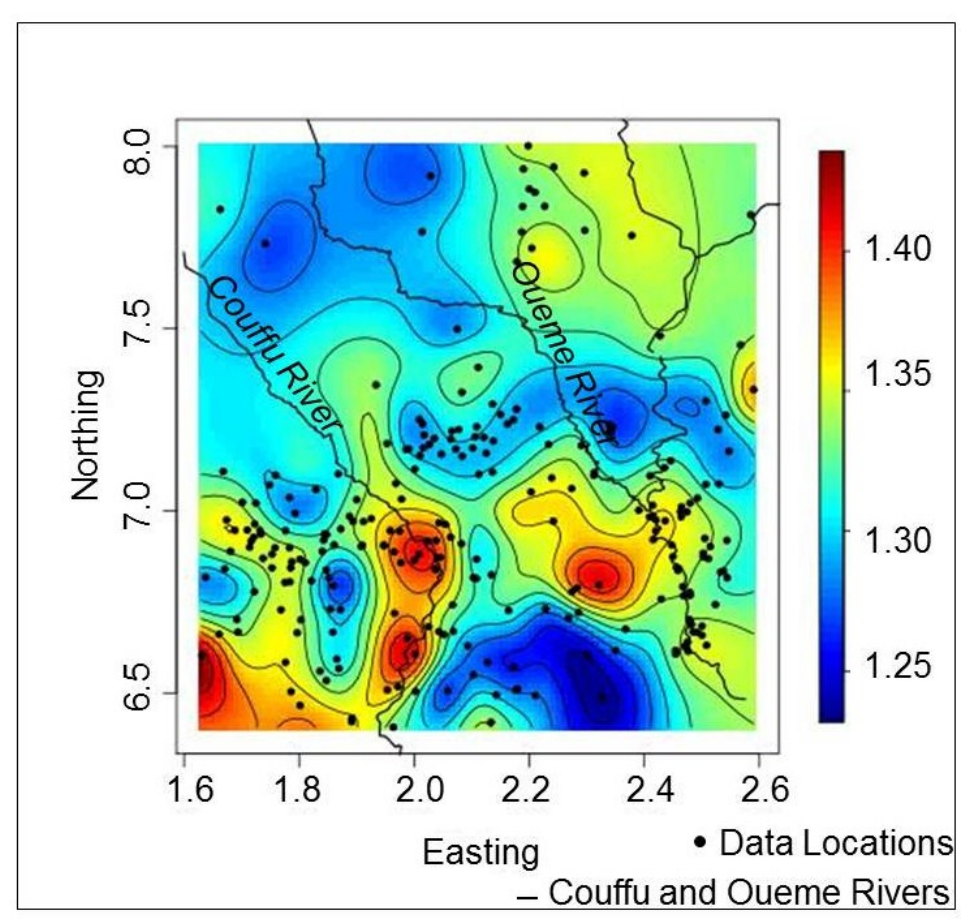


Figure 2-7. Shape index mean surface

Number of patches is a measurement of potential habitat fragmentation. Number of patches is calculated within FRAGSTATS as follows (Equation 2-4):

Equation 2-4

$$NP = N$$

where NP is equal to the number of patches in a landscape and N is equal to the number of patches in the landscape (McGarigal and Marks, 1995). High numbers of patches correspond to greater fragmentation potential, while lower numbers of patches indicate a more aggregated landscape. No background or border cells were included in the calculation, and patch attributes, for example total area or land cover type, were not described in this metric (Figure 2-8).

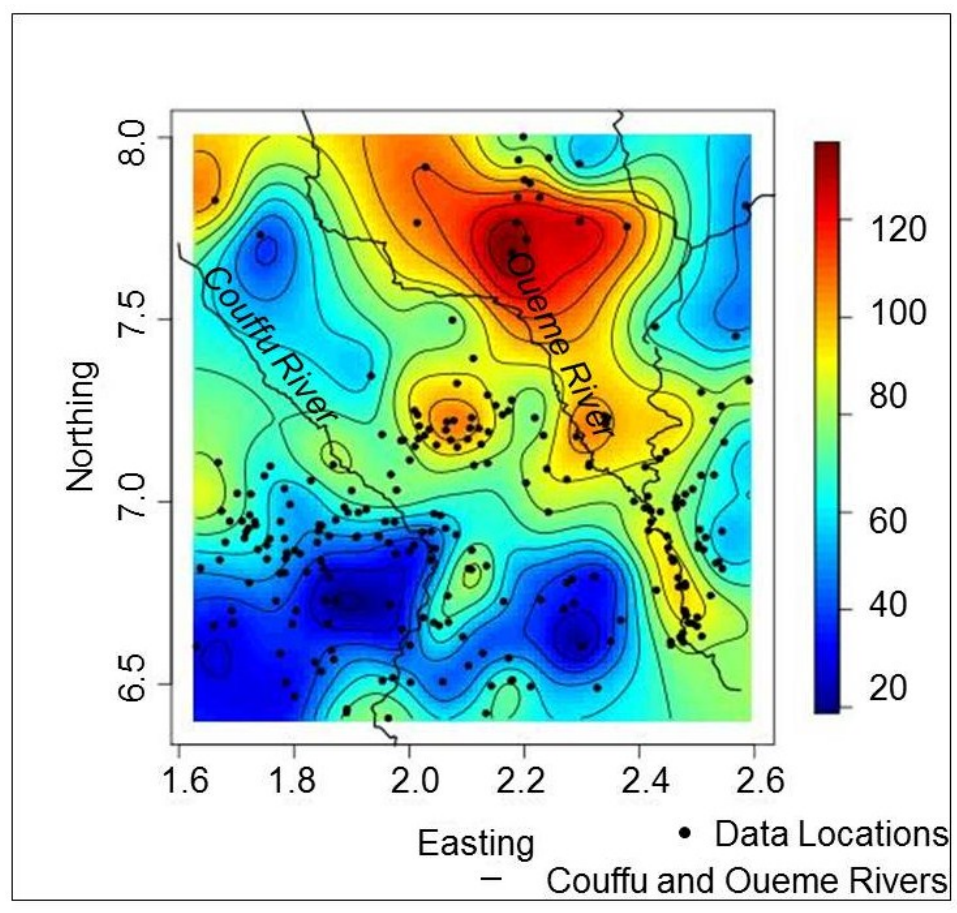


Figure 2-8. Number of patches surface

Average wetness index value was the third landscape-level predictor variable. As outlined above, a wetness index identifies areas in a landscape where water is likely to accumulate during a precipitation event (See Equation 1; Bevin and Kirby, 1979). High wetness index values indicate greater accumulation potential, while low wetness index values indicate a lower accumulation potential. A plot of wetness index values across the study region highlights areas of high accumulation potential in blue and areas with low accumulation potential in red (Figure 2-9).

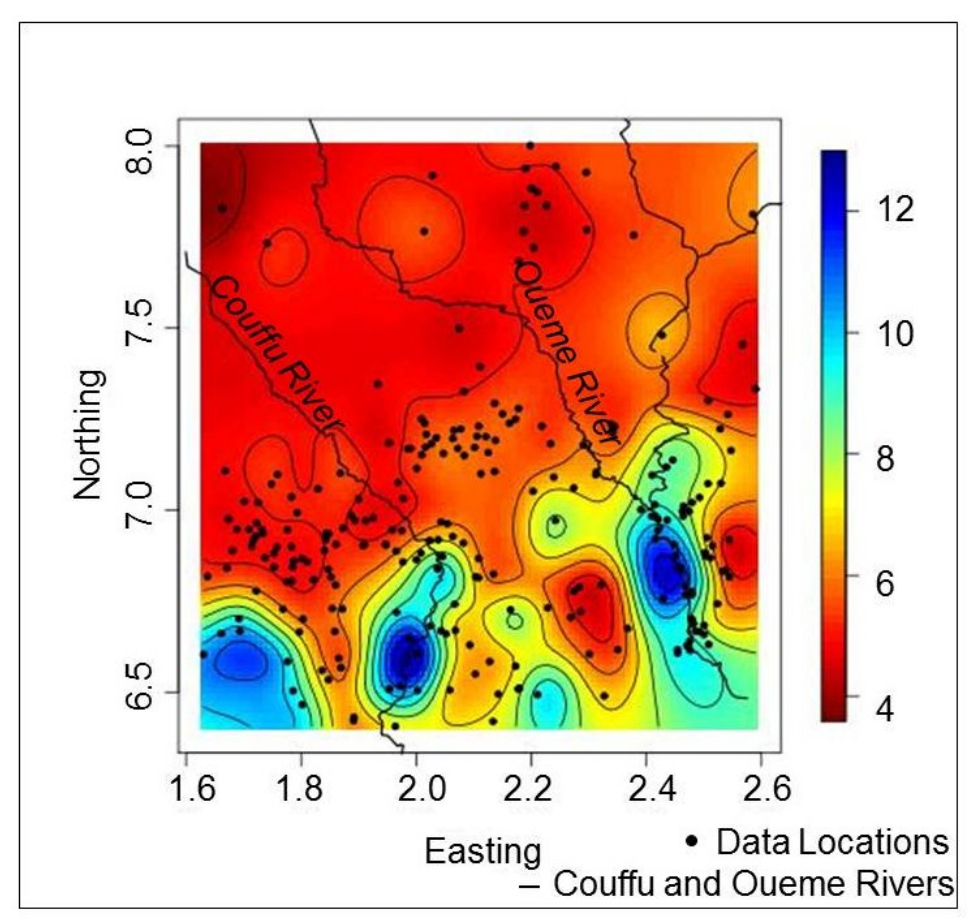


Figure 2-9. Wetness index average surface

Limitations of mean approaches include the possibility of unusually high or low values within a buffer distance affecting the mean value disproportionately, although using a large number of data locations and the elimination of high leverage points was intended to help mitigate this problem.

The patch richness density metric quantifies the number of different land cover types in a landscape and then standardizes this measurement in order to facilitate comparison across landscapes (McGarigal and Marks, 1995). Patch richness density was calculated in FRAGSTATS as follows (Equation 2-5):

### Equation 2-5

$$PRD = \frac{m}{A}(10,000)(100)$$

where m = number of patch types present in the landscape, excluding the landscape border if present and A = total landscape area  $m^2$  (McGarigal and Marks, 1995). Higher values represent more diverse landscapes, while lower values represent more homogeneous landscapes. Regions with higher numbers of land cover types were plotted in red and those with lower numbers of land cover types were plotted in blue in Figure 2-10.

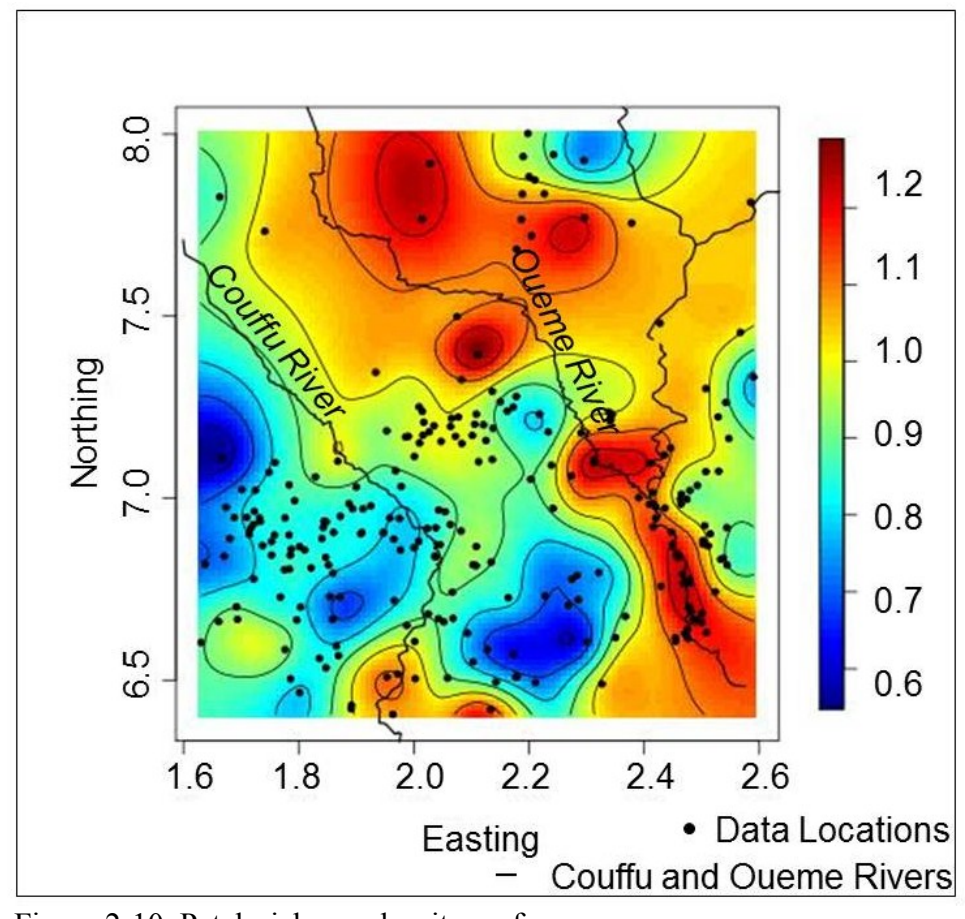


Figure 2-10. Patch richness density surface

### 2.7 Class-level Configuration Analysis

Additional model generation at the class-level included predictor variables characterizing land cover patch configurations corresponding to specific land cover types. Shape index mean values and an additional variable group characterizing class-level fragmentation were calculated in FRAGSTATS (Table 2-3).

Table 2-3. Class-level initial landscape metric candidates

Class-level Initial Landscape Metrics								
Metric	Abbreviation	Description	Interest					
Shape Index Mean	SHAPE_MN	Standardized land cover patch edge complexity measurement	Altered land cover shapes					
Landscape Shape Index	LSI	Standardized aggregation index based on total edge	Fragmentation					
Percent Land Cover Adjacency	PLANDJ	Land cover type aggregation measurement	Fragmentation					
Number of Patches	NP	Measures number of individual patches present in area	Fragmentation					
Clumpiness Index	CLUMPY	Land cover type aggregation measurement	Fragmentation					
Aggregation Index	AI	Land cover type aggregation measurement	Fragmentation					

As outlined in the landscape-level analysis, a Spearman's rank order correlation matrix identified potential multicolinearity between variables (Appendix A), and non-spatial binomial GLMs were generated for land cover types using BU rates as the response variable and landscape metric values corresponding to specific land cover classes as independent variables. Three land cover classes were explored: agriculture/forest, forest, and wetland because these land cover classes represented land cover types or uses noted in the literature as having anecdotal or empirical links to BU incidence in past studies.

Data sets changed as distance increased from village centers because a buffer at a 400m distance did not necessarily contain forest patches, while a buffer at 2k might contain several forest patches. Therefore, models were produced individually for each land cover type within buffers at 800m, 1\_2k, 1\_6k, and 2k distances. Identification of high leverage points occurred on an individual model basis using Cook's distance measure (Appendix B); therefore, a "best" model for each distance interval was not identified using lowest AIC values, but was determined by variable significance values.

#### 2.8 Class-level Configuration Analysis Predictor Variables

Shape index mean acted as a predictor variable to quantify relationships between land cover patch shape complexity and BU rates. Calculation of this metric was identical to the landscape-level shape index mean (Equation 3) with the exception of quantifying individual classes rather than all classes encompassing the landscape across the study region.

Percent land cover adjacency measured land cover class aggregation (Equation 2-6)

Equation 2-6

$$PLADJ = \begin{pmatrix} g_{ij} \\ \hline m \\ \sum_{k=1}^{m} g_{ik} \end{pmatrix}$$

where  $\mathcal{E}_{ij}$  = the number of like adjacencies (joins) between pixels of patch type (class) i based on a double-count method, and  $\mathcal{E}_{ik}$  = the number of adjacencies (joins) between pixels of patch types (classes) i and k are based on a double-count method (McGarigal and Marks, 1995).

High PLADJ values represent a more aggregated land cover class, while low PLADJ values represent a more fragmented land cover class. An example of PLADJ for the 2k wetland class demonstrates high aggregation values in the northern study area plotted in red, and low aggregation in the southeastern corner of the study area plotted in blue (Figure 2-11).

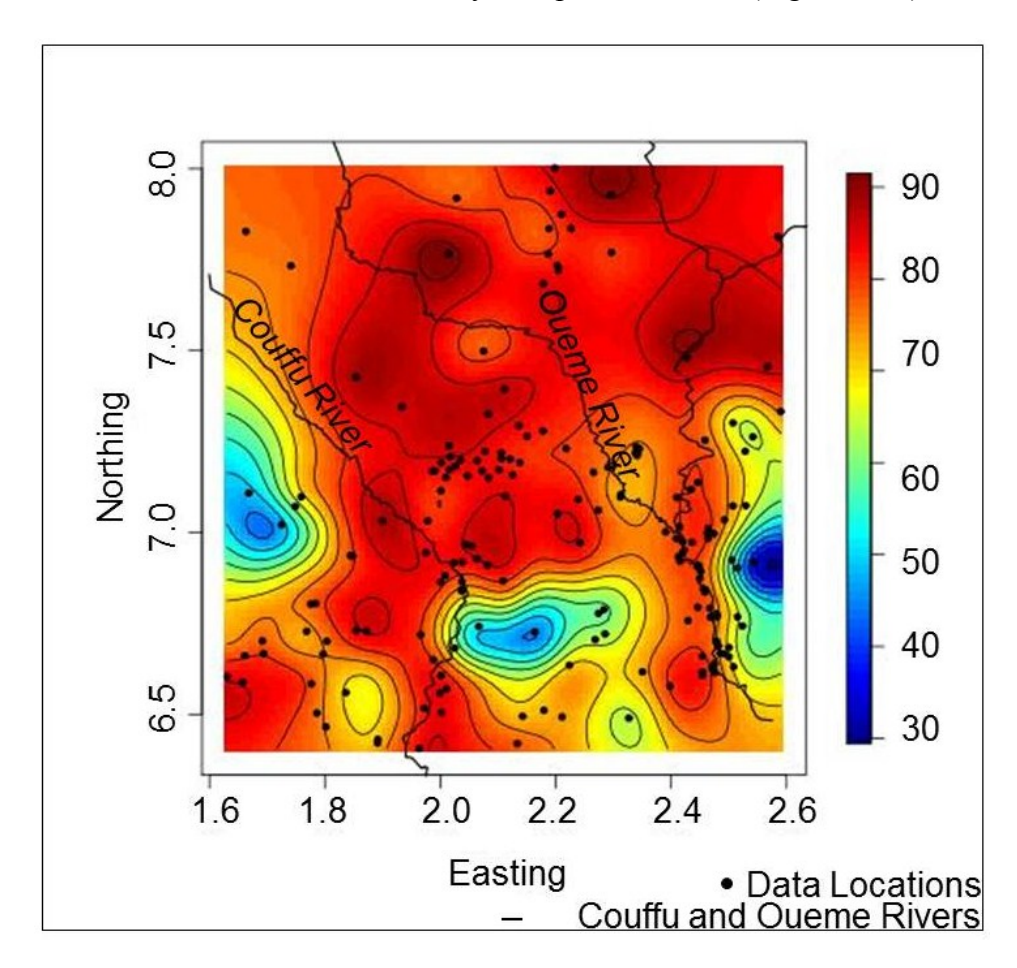


Figure 2-11. Percent land cover adjacency surface 2k wetland class

The landscape shape index (LSI) is another land cover patch aggregation measurement.

LSI was calculated within FRAGSTATS using the following equation (Equation 2-7):

### Equation 2-7

$$LSI = \frac{e_i}{\min e_i}$$

where  $e_i^{\phantom{i}}$  = total length of edge (or perimeter) of class i in terms of number of cell surfaces, includes all landscape boundary and background edge segments involving class i, and  $\min e_i^{\phantom{i}}$  = minimum total length of edge (or perimeter) of class i in terms of number of cell surfaces (Figure 2-12; McGarigal and Marks, 1995).

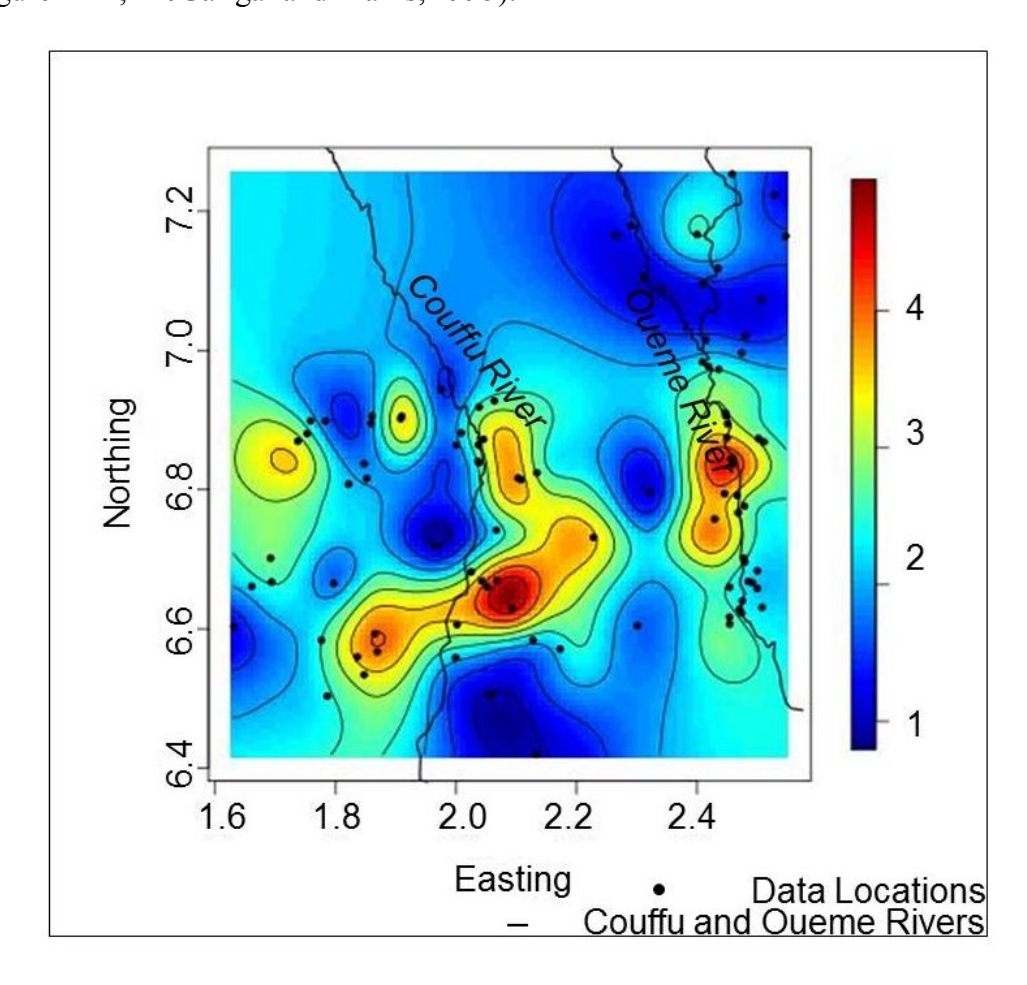


Figure 2-12. 1\_2k agriculture/forest class landscape shape index surface

### 2.9 Spatial GLM

The binomial GLMs used to identify significant BU rate predictor variables assumed model residuals were independent and identically distributed across the study domain (Keitt *et al.*, 2002). While this approach is adequate in the absence of spatial autocorrelation in model residuals, this assumption was unrealistic given the spatial structure of the observations and the heterogeneity of the environmental covariates (Boyd *et al.*, 2005).

In order to mitigate this problem, a hierarchical modeling approach was used to adapt the non-spatial GLM with a correlation matrix based on the spatial structure of the model residuals, adding a spatial random effects component that accounted for missing, spatially-structured covariates (Waller and Gotway, 2004).

Our interest was in modeling the number of cases Y(s) at n observed locations. Here, s denotes the geographic location, assuming  $s \in D \subseteq \Re^2$ . A set of p spatially referenced predictors x(s) were calculated at each location. Given the population at each location, N(s), we assumed Y(s) followed a binomial distribution. For the i-th location  $(Y(s_i)|\eta(s_i) \sim Binomial(N(s_i),p(\eta(s_i))) \text{ where } p(\eta(s_i)) \text{ is the success probability at } s_i$  and  $\eta(s_i) = x(s_i)'\beta + w(s_i)$ . A logit link function

$$p(\eta(s_i)) = \exp(\eta(s_i)) / (1 + \exp(\eta(s_i)))$$
 was assumed for this model.

The process specification for w(s) is a mean 0 Gaussian Process with covariance function,  $C(s_1, s_2)$ , denoted  $GP(0, C(s_1, s_2))$ . In application, we specify

$$C(s_1, s_2) = \sigma^2 p(s_1, s_2; \phi)$$
 where  $p(\cdot; \phi)$  is a correlation function and  $\phi$  is the spatial decay

parameter. The exponential spatial correlation was assumed for  $p(\cdot)$ . Prior distributions on the remaining parameters complete the hierarchical model. Customarily, the regression effect  $\beta$  is assigned a multivariate Gaussian prior, (i.e.  $\beta \sim N(\mu_{\beta}, \Sigma \beta)$ , while the latent variance component  $\sigma^2$  is assigned  $IG(\cdot, \cdot)$  priors. The process correlation parameter,  $\phi$ , was assigned an informative prior (e.g., uniform over a finite range) based upon the underlying spatial domain.

Model parameter distributions were estimated using Markov Chain Monte Carlo (MCMC) methods employing an adaptive Metropolis (AM) algorithm with a 43% acceptance rate. MCMC employs an iterative sampling process, the goal of which is to converge to a stationary state representing the target distribution, or in the Bayesian approach, the true distribution of the model parameters, from which inference may be drawn (Brooks and Gelman, 1998).

The AM algorithm differs from a traditional Metropolis algorithm because accumulated information from all previous chains are incorporated into each sampling iteration as opposed to only the prior chain's information contributing to the calculation (Brooks and Gelman, 1998). This sampling method speeds convergence, or the point at which equilibrium between parameter mean and variance commences.

Starting values were obtained from non-spatial models and posterior inference was based on 3 chains at 500,000 post burn-in iterations measured at 1\_2k, 1\_6k, and 2k for landscape-level models, and 3 chains at 50,000 to 100,000 iterations measured at 800m, 1\_2k, 1\_6k, and 2k for the class-level models, depending on the individual model. Burn-in occurred at 10,000 iterations and thinning took place at every 100 samples. All model generation was completed using the

spGLM function in spBayes R package, and summaries are available in Appendix D of this document.

The Gelman-Rubin diagnostic measure assessed model convergence within 5,000 MCMC sample iterations. This diagnostic observed within chain and between chain variance with values closer to 1.0 indicating that convergence likely took place (Brooks and Gelman, 1998).

Comparison of deviance information criterion (DIC) values from non-spatial models and from spatial models determined whether the spatial models achieved a better fit. A similarity exists between DIC values and AIC values; a lower DIC value indicates a better model fit, but DIC value are used with Bayesian hierarchical models because they can be calculated from MCMC samples directly (Spiegelhalter *et al.*, 2002).

#### 2.10 Model Verification

A random sample consisting of 10% of village locations was withheld from each model data set for verification purposes. Spatial GLMs were calculated at the landscape-level at 1\_2k, 1\_6k, and 2k distance intervals using 90% of the data set as training locations, and at the class-level at 800m, 1\_2k, 1\_6k, and 2k distance intervals using 90% of the data set as training locations. Training model results predicted BU rates at the remaining 10% verification data set locations using the spPredict function in spBayes R. Predicted values were compared to actual values at these locations, and a root mean squared error (RMSE) determined the model that achieved the best fit (Figure 2-8).

$$RMSE = \sum_{i=1}^{m} \sqrt{(\hat{y}_{i}(s_{O}) - y_{i}(s_{O}))^{2} / m}$$

where  $\hat{y}(s_o)$  are the estimated rates,  $y(s_o)$  are the actual rates, and m is equal to the number of data points (Bolstad, 2005). The model exhibiting the lowest RMSE value was chosen as the "best" model from which to predict to new, unsampled data locations.

## 2.11 Risk Surface

A BU risk surface was created employing Bayesian, or model-based, kriging methods using samples drawn from the mean posterior distribution of the predictor variables from the best spatial binomial GLM to predict BU rates at new, unsampled locations. Incorporation of the random spatial effects component accounted for unknown predictor variables and spatial autocorrelation, improving prediction accuracy.

Kriging is a geostatistical interpolation method that uses data from observed locations to predict to new, unsampled locations (Schabenberger and Gotway, 2005). Kriging is a probabilistic approach; therefore, it has standard errors associated with model predictions, enabling quantification of uncertainty related to model outputs (Waller and Gotway, 2004). Several kriging approaches exist. A Bayesian kriging approach differs from traditional kriging approaches because model parameters are treated as random variables rather than estimated (Helbert *et al.*, 2009), and while traditional kriging methods ignore uncertainty introduced when estimating the covariance structure, Bayesian kriging incorporates parameter uncertainty into model predictions (Moyeed and Papritz, 2002).

A total of 1030 new locations generated at 5km intervals within the boundary of the study area represent locations to which BU rates were predicted (Figure 2-13). Gaps in new location points represent areas where derivation of predictor variables could not occur because a lack of data existed corresponding to the "best" model covariates and distance interval.

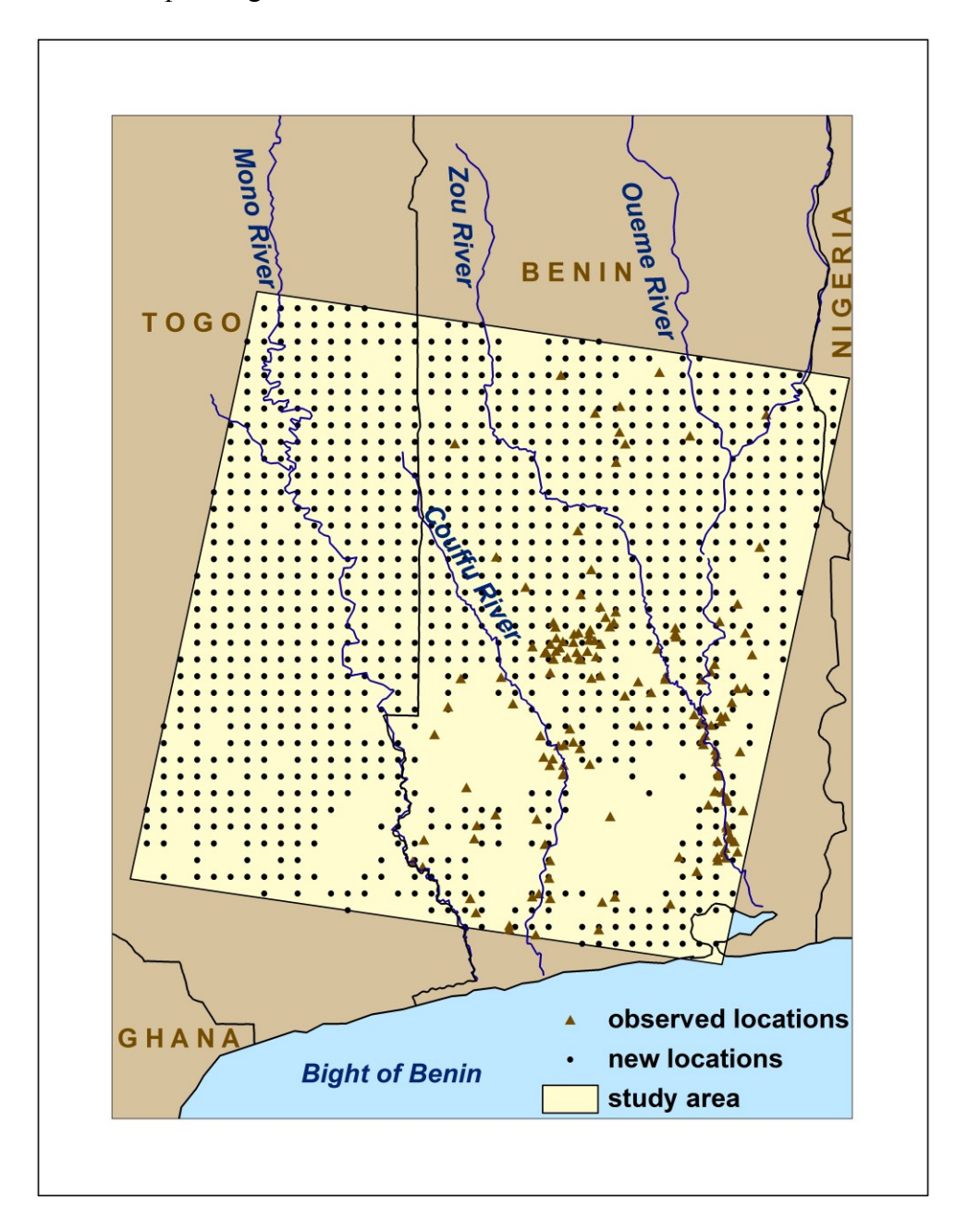


Figure 2-13. New locations and observed locations used to create risk surface

Circular buffers with radii equal to the best-fitting spatial model were created surrounding each new location, and a polygon created at approximately 5k inside the study area boundary prevented the introduction of uncertainty due to potential edge effects (Haase, 1995). Derivation of predictor variables followed methods outlined in section 2.4, and a surface based on the mean posterior predictive distribution and associated uncertainty was created across the entire study area using the spPredict function in spBayes R.

A population of 100,000 persons was assumed at each location to calculate meaningful rates, although these locations were not necessarily occupied by villages or residents. These location points were generated to characterize risk associated with landscape variables across the study region, but do not suggest that BU transmission is taking place. Unreliable and incomplete population data and villages with questionable coordinate information prompted pseudo-location generation.

# **Chapter 3 RESULTS**

# 3.1 Non-Spatial vs. Spatial Model Results

Spatial model results determined that several non-spatial models overestimated the significance of one or more predictor variables, indicating that spatial autocorrelation was present in model residuals. Lower DIC values corresponding to the spatial GLMs compared to the non-spatial GLMs demonstrated that the spatial models achieved a better fit in every circumstance (Table 3-1).

Table 3-1. Non-spatial and spatial GLM DIC values.

			-	DIC	DIC Value	
			Post	Non-		
Scale	Model	Variables	Burn-in	Spatial	Spatial	
		WIAVG + SHAPE_MN +				
	1_2k	PRD	500,000	7542.948	6774.835	
		WIAVG + SHAPE_MN +				
	1_2k	NP	500,000	7558.832	6775.580	
		WIAVG + SHAPE_MN +				
Landscape-	1_6k	PRD	500,000	7526.302	6775.539	
level		WIAVG + SHAPE_MN +				
	1_6k	NP	500,000	7558.955	6777.154	
		WIAVG + SHAPE_MN +				
	2k	PRD	500,000	7533.240	6776.804	
		WIAVG + SHAPE_MN +				
	2k	NP	500,000	7539.006	6777.211	
	800 Forest	SHAPE_MN + PLADJ	100,000	1927.261	1780.473	
	800 Wetland	SHAPE_MN + PLADJ	50,000	3918.085	3483.809	
	800 Ag/Forest	SHAPE_MN + LSI	50,000	2000.561	1859.042	
	1_2k Forest	SHAPE_MN + LSI	100,000	3661.611	3289.170	
	1_2k Wetland	SHAPE_MN + LSI	100,000	5335.240	4781.834	
Class Issal	1 2k Ag/Forest	SHAPE MN + LSI	100,000	3901.120	3644.391	
Class-level	1 6k Forest	SHAPE MN	50,000	3668.271	3257.107	
	1 6k Wetland	SHAPE MN + LSI	100,000	5937.132	5218.884	
	1 6k Ag/Forest	SHAPE MN + LSI	50,000	4344.966	4071.081	
	2k Forest	PLADJ	50,000	4394.660	3883.277	
	2k Wetland	PLADJ	50,000	6558.870	5780.372	
	2k Ag/Forest	SHAPE MN + LSI	50,000	4712.282	4316.881	

Table 3-2 provides a comparison of non-spatial and spatial model variable significance results, with full model results available in Appendices C and D.

Table 3-2. Non-spatial vs. spatial binomial GLM variable significance.

	•		Significa	ınce
			Non-Spatial	Spatial
	Model	Variable	Model	Model
		Wetness index average	Y	N
	1_2k LS	Shape Index Mean	Y	N
		Number of Patches	Y	N
		Wetness index average	Y	N
	1_2k LS	Shape Index Mean	Y	N
		Patch Richness Density	Y	Y
			Y	N
	1_6k LS	_	Y	N
Landscape-		Number of Patches	Y	Y
level		Wetness index average	Y	N
	1 6k LS	Shape Index Mean	Y	N
	_	1	Y	N
		Patch Richness Density Wetness index average Shape Index Mean Number of Patches Wetness index average Shape Index Mean	Y	Y
2	2k LS	•	Y	Y
		Shape Index Mean Number of Patches Wetness index average	Y	N
			Y	Y
	2k LS	_	Y	N
		Wetness index average Shape Index Mean Number of Patches Wetness index average Shape Index Mean Patch Richness Density Wetness index average Shape Index Mean Number of Patches Wetness index average Shape Index Mean Patch Richness Density Wetness index average Shape Index Mean Number of Patches Wetness index average Shape Index Mean Number of Patches Wetness index average Shape Index Mean Patch Richness Density Shape Index Mean Patch Richness Density Shape Index Mean Percent Land Cover Adjacency Shape Index Mean Landscape Shape Index Shape Index Mean	Y	N
		•	Y	N
	800m Forest	1		
			Y	N
	800m Wetland	2 2	Y	Y
	800	1	Y	Y
	Agriculture/Forest	*	Y	Y
		<del></del>	Y	Y
	1_2k Forest	<u> </u>	Y	N
Class-Level —			Y	N
	1_2k Wetland	-	Y	N
	1 2k	1 1	Y	Y
	Agriculture/Forest	1	Y	Y
	1 6k Forest		Y	N
	_		Y	N
	1_6k Wetland		Y	N
	1 6k		Y	Y
	Agriculture/Forest	*	Y	Y
	2k Forest		-	

			Significance	
Class-Level			Non-Spatial	Spatial
	Model	Variable	Model	Model
	2k Wetland	Percent Land Cover		
	2k Wetland	Adjacency	Y	N
	2k	Shape Index Mean	Y	Y
	Agriculture/Forest	Landscape Shape Index	Y	Y

### 3.2 Model Output Interpretation

Model results contain two components. The first component consists of a table reporting variable significance for each model under the Bayesian credible interval approach. Similarities exist between credible interval interpretations used in Bayesian statistical analyses and confidence interval interpretations used in frequentist statistical approaches, although exact meanings vary between the two approaches (Bland and Altman, 1998). The Bayesian approach determines that a 95% probability exists that a value lies within a distribution, while the frequentist approach assumes that a population value is fixed and then constructs a 95% confidence interval around the fixed value.

Under a Bayesian approach, when parameter value directions do not change between the lower 2.5% and the upper 97.5% credible tails, the variable may be interpreted as significant at a 95% confidence level; for example, in this study, patch richness density maintained a positive direction in both tails at a 1\_2k distance (Table 3-3), indicating that BU rates increased as patch richness density increased. The output tables also include the effect range which is the distance at which the spatial correlation drops to 0.05 (i.e., -log(0.05)/phi).

The second model output component consists of a Gelman-Rubin diagnostic table that outlines the likelihood that convergence took place within 5,000 MCMC sample iterations. Values close to 1.0 indicate that convergence likely took place.

### 3.3 Landscape-level Configuration Analysis Results

The following tables and figures outline spatial GLM landscape-level results. No models maintained significance in all variables under the spatial modeling framework, but four out of six models maintained significance in at least one variable. The first model to maintain a significant variable was the 1\_2k patch richness density model mentioned above. Results indicated that as patch richness density increased, BU rates increased, although wetness index average and shape index mean values were no longer significant under the spatial modeling framework (Table 3-3).

Table 3-3. 1\_2k number of patches spatial binomial GLM model summary

Summary 1_2k Landscape-level 3 Chains at 500,000			
Parameters	50.0%	2.5%	97.5%
Intercept	-12.94	-14.991	-7.244
Wetness Index Average	0.151	-0.035	0.223
Shape Index Mean	0.913	-2.765	2.487
<b>Patch Richness Density</b>	2.397	1.458	2.89
sigma.sq	3.285	3.097	3.922
Phi	24.388	13.647	29.623
effective range 3/phi	0.123	0.101	0.224
max intersite distance	1.254		

The Gelman-Rubin diagnostic measure determined that convergence likely took place with values presenting close to 1.0 in all parameters (Table 3-4).

Table 3-4. Gelman diagnostic 1\_2k patch richness density model

Gelman-Rubin Diagnostic 1_2k Landscape-level			
	Point	97.5	
	est.	quantile	
Intercept	1.13		1.39
Wetness Index Average	1.00		1.01
Shape Index Mean	1.12		1.34
Patch Richness Density	1.01		1.03
sigma.sq	1.00		1.00
phi	1.03		1.03
Multivariate $psrf = 1.08$			

The second model that maintained significance in one variable was at a 1\_6k distance (Table 3-5). Results indicated that a relationship exists between high BU rates and a higher number of patches surrounding villages within a 1\_6k distance. Wetness index average and shape index mean values were no longer significant.

Table 3-5. 1 6k number of patches spatial binomial GLM model summary

Summary 1_6k Landscape-level 3 Chains at 500,000			
Parameters	50.0%	2.5%	97.5%
Intercept	-11.107	-12.728	-9.653
Wetness Index Average	0.077	-0.004	0.241
Shape Index Mean	1.586	-0.645	2.052
<b>Number of Patches</b>	0.007	0.004	0.009
sigma.sq	3.41	2.698	4.21
Phi	21.639	21.517	46.297
effective range 3/phi	0.139	0.067	0.139
max intersite distance	1.254		

The Gelman-Rubin diagnostic calculation determined that convergence likely took place in all model parameters (Table 3-6).

Table 3-6. Gelman diagnostic 1\_6k numbers of patches model

Gelman-Rubin Diagnostic 1_6k Landscape-level			
	Point	97.5	
	est.	quantile	
Intercept	1.05	1.15	
Wetness Index Average	1.01	1.03	
Shape Index Mean	1.06	1.16	
Number of Patches	1.01	1.02	
sigma.sq	1.00	1.01	
Phi	1.02	1.02	
Multivariate $psrf = 1.03$	•		

Results from the spatial model including wetness index average, shape index means, and numbers of patches at a 2k distance maintained significance in two variables (Table 3-7). Results

suggested that higher wetness index averages and more uniformly-shaped land cover patches surrounded villages with higher BU rates within a 2k distance of village centers.

Table 3-7. 2k numbers of patches spatial binomial GLM model summary

Summary 2k Landscape-level 3 Chains at 500,000			
Parameters	50.0%	2.5%	97.5%
Intercept	-9.084	-10.252	-7.187
Wetness Index Average	0.254	0.213	0.268
<b>Shape Index Mean</b>	-1.021	-1.996	-0.095
Number of Patches	0.000	-0.001	0.006
sigma.sq	3.411	3.109	3.430
Phi	24.873	17.339	29.020
effective range 3/phi	0.121	0.104	0.174
max intersite distance	1.254		

A Gelman-Rubin diagnostic calculation determined that convergence likely took place in all model parameters (Table 3-8).

Table 3-8. Gelman diagnostic 2k number of patches model

Gelman-Rubin Diagnostic 2k Landscape-level			
	Point	97.5	
	est.	quantile	
Intercept	1.09	1.27	
Wetness Index Average	1.00	1.01	
Shape Index Mean	1.10	1.30	
Number of Patches	1.01	1.04	
sigma.sq	1.00	1.01	
phi	1.03	1.03	
Multivariate $psrf = 1.07$	-		

The final model to maintain significance in at least one variable also occurred at a 2k distance (Table 3-9). This model included wetness index averages, shape index means, and patch richness density values. Results suggested that a positive relationship exists between higher BU rates and higher wetness index values within a 2km distance of village centers, but shape index mean values were not significant.

Table 3-9. 2k patch richness density spatial binomial GLM summary

Summary 2k Landscape-level 3 Chains at 500,000			
Parameters	50.0%	2.5%	97.5%
Intercept	-8.986	-9.983	-7.754
Wetness Index Average	0.126	0.111	0.283
Shape Index Mean	-0.942	-1.411	0.711
Patch Richness Density	-0.273	-1.831	2.954
sigma.sq	3.251	3.010	3.886
Phi	22.260	21.599	26.227
effective range 3/phi	0.135	0.115	0.139
max intersite distance	1.254		

The Gelman-Rubin diagnostic measure determined that convergence likely took place in all parameters with the exception of the shape index mean, which had a value of 2.10 (Table 3-10).

Table 3-10. Gelman diagnostic 2k patch richness density model

Gelman-Rubin Diagnostic 2k Landscape-level			
	Point	97.5	
	est.	quantile	
Intercept	1.38	2.10	
Wetness Index Average	1.00	1.00	
Shape Index Mean	1.38	2.10	
Patch Richness Density	1.00	1.01	
sigma.sq	1.02	1.06	
phi	1.05	1.08	
Multivariate $psrf = 1.26$			

## 3.4 Class-level Composition and Configuration Analysis

Seven out of twelve class-level candidate models maintained significance in all model variables under the spatial modeling framework, the results of which are outlined in following tables.

Results from the 800m wetland class model (Table 3-11) indicated that a relationship exists between high BU rates and wetland patches with high patch shape complexity.

Table 3-11. 800m wetland class spatial model results

Summary 800m Wetland 3 Chains at 50,000			
Parameters	50.0%	2.5%	97.5%
Intercept	-10.022	-10.095	-8.918
Shape Index Mean	0.986	0.722	1.096
sigma.sq	3.503	3.158	3.869
Phi	15.224	12.006	21.354
effective range 3/phi	0.197	0.141	0.251
max intersite distance $= 1.260$			

The Gelman-Rubin diagnostic (Table 3-12) indicated that convergence likely took place in all model parameters with values presenting close to 1.0.

Table 3-12. 800m wetland class convergence diagnostic

Gelman-Rubin Diagnostic 800m Wetland			
	Point		
	est.	97.5 quantile	
Intercept	1.02	1.07	
Shape Index Mean	1.01	1.02	
sigma.sq	1.00	1.01	
Phi	1.02	1.02	
Multivariate $psrf = 1.03$			

Results summarizing the 800m agriculture/forest class model (Table 3-13) suggested that a relationship exists between mixed agriculture/forest land cover patches with more complex shapes that are highly aggregated with one another and higher BU rates.

Table 3-13. 800m agriculture/forest class spatial model results

Summary 800m Agriculture/Forest 3 Chains at 50,000			
Parameters	50.0%	2.5%	97.5%
Intercept	-8.868	-9.844	-8.245
Shape Index Mean	2.319	1.774	2.500
Landscape Shape Index	-0.549	-0.776	-0.192
sigma.sq	1.345	1.142	2.309
Phi	283.921	234.639	551.114
effective range 3/phi	0.011	0.006	0.013

The Gelman-Rubin diagnostic (Table 3-14) indicated that convergence likely took place with all values presenting close to 1.0.

Table 3-14. 800m agriculture/forest class convergence diagnostic

Gelman-Rubin Diagnostic 800m Agriculture/Forest			
	Point		
	est.	97.5 quantile	
Intercept	1.01	1.01	
Shape Index Mean	1.01	1.02	
Landscape Shape Index	1.00	1.00	
sigma.sq	1.00	1.00	
phi	1.00	1.00	
Multivariate $psrf = 1.00$	·		

The 1\_2k forest model (Table 3-15) indicated that more complex forest shapes and more aggregated forest patches surround villages with higher BU rates within a 1\_2k distance from village centers.

Table 3-15. 1 2k forest spatial model results

Summary 1_2k Forest 3 Chains at 100,000			
Parameters	50.0%	2.5%	97.5%
Intercept	11.411	15.723	-8.792
Shape Index Mean	3.439	1.076	6.52
Landscape Shape Index	-0.31	-0.45	-0.07
sigma.sq	4.392	4.304	4.449
Phi	75.14	18.076	189.105
effective range 3/phi	0.04	0.017	0.191
Max intersite distance = 1.260			

Gelman-Rubin diagnostic results indicated that convergence likely took place in all parameters with the exception of the shape index mean, which had a value of 2.15 (Table 3-16).

Table 3-16. 1 2k forest class convergence diagnostic

Gelman-Rubin Diagnostic 1_2k Forest			
	Point		
	est.	97.5 quantile	
Intercept	1.46	2.34	
Shape Index Mean	1.41	2.15	
Percent Land Cover Adjacency	1.03	1.11	
sigma.sq	1.00	1.01	
Phi	1.02	1.08	
Multivariate psrf = 1.28			

The 1\_2k mixed class agriculture/forest model indicated that a relationship exists between villages with high BU rates and agriculture/forest land cover patches with complex shapes that are highly aggregated within a 1\_2k distance from village centers (Table 3-17).

Table 3-17. 1\_2k agriculture/forest spatial model results

Summary 1_2k Agriculture/Forest 3 Chains at 100,000			
Parameters	50.0%	2.5%	97.5%
Intercept	-9.096	-10.403	-6.957
Shape Index Mean	2.240	0.555	3.582
Landscape Shape Index	-0.255	-0.424	-0.242
sigma.sq	1.547	1.112	1.733
Phi	449.736	319.780	592.320
effective range 3/phi	0.007	0.005	0.009
max intersite distance $= 1.230$	•		

The Gelman-Rubin diagnostic measure (Table 3-18) indicated that convergence likely took place with all values presenting close to 1.0.

Table 3-18. 1\_2k agriculture/forest class convergence diagnostic

Gelman-Rubin Diagnostic 1_2k Agriculture/Forest		
	Point	
	est.	97.5 quantile
Intercept	1.04	1.14
Shape Index Mean	1.05	1.15
Landscape Shape Index	1.00	1.01
sigma.sq	1.00	1.00
Phi	1.00	1.00
Multivariate $psrf = 1.04$		

Results corresponding to the 1\_6k agriculture/forest model (Table 3-19) suggested that a relationship exists between higher BU rates and more complexly-shaped agriculture/forest land cover patches that are aggregated with one another within a 1\_6k distance from village centers.

Table 3-19.1 6k agriculture/forest spatial model results

Summary 1_6k Agriculture/Forest 3 Chains at 50,000			
Parameters	50.0%	2.5%	97.5%
Intercept	10.739	11.111	10.168
Shape Index Mean	3.635	3.004	3.741
Landscape Shape Index	-0.248	-0.319	-0.208
sigma.sq	1.921	1.334	2.199
Phi	16.864	10.402	33.195
effective range 3/phi	0.178	0.093	0.292
max intersite distance = 1.224			

The Gelman-Rubin diagnostic model indicated that convergence likely took place with all parameter values presenting close to 1.0 (Table 3-20).

Table 3-20. 1\_6k agriculture/forest class convergence diagnostic

Gelman-Rubin Diagnostic 1_6k Agriculture/Forest		
	Point	
	est.	97.5 quantile
Intercept	1.10	1.31
Shape Index Mean	1.09	1.27
Landscape Shape Index	1.01	1.02
sigma.sq	1.01	1.02
Phi	1.01	1.02
Multivariate $psrf = 1.08$	·	

The 2k forest model indicated that a relationship exists between higher BU rates and higher percentages of adjacent forest land cover patches within a 2k distance of village centers (Table 3-21).

Table 3-21. 2k forest class spatial model results

Summary 2k Forest 3 Chains at 50,000			
Parameters	50.0%	2.5%	97.5%
Intercept	-10.811	-11.266	-9.358
Percent Land Cover Adjacency	0.024	0.014	0.029
sigma.sq	5.164	4.708	5.165
Phi	18.343	15.803	23.018
effective range 3/phi	0.164	0.131	0.190
max intersite distance = 1.174	•		

The Gelman-Rubin diagnostic model suggested that convergence likely took place in all model parameters (Table 3-22).

Table 3-22. 2k forest class model convergence diagnostic

Gelman-Rubin Diagnostic 2k Forest			
Point			
	est.	97.5 quantile	
Intercept	1.04	1.06	
Percent Land Cover Adjacency	1.04	1.08	
sigma.sq	1.00	1.00	
Phi	1.04	1.04	
Multivariate $psrf = 1.01$			

Results corresponding to the 2k agriculture/forest model indicated that a relationship exists between high BU rates and more complexly-shaped agriculture/forest land cover patches that are aggregated with one another within 2k distances of village centers (Table 3-23).

Table 3-23. 2k agriculture/forest class spatial model results

Summary 2k Agriculture/Forest 3 Chains at 50,000			
Parameters	50.0%	2.5%	97.5%
Intercept	-9.434	-11.430	-8.954
Shape Index Mean	2.448	1.700	4.771
Landscape Shape Index	-0.253	-0.492	-0.120
sigma.sq	2.232	1.873	2.707
Phi	366.493	334.177	489.995
effective range 3/phi	0.008	0.006	0.009
max intersite distance = $1.256$	•		

The Gelman-Rubin diagnostic indicated that convergence likely took place, although the shape index mean value exhibited a higher value at 1.67 (Table 3-24).

Table 3-24. 2k agriculture/forest model convergence diagnostic

Gelman-Rubin Diagnostic 2k Agriculture/Forest		
	Point	
	est.	97.5 quantile
Intercept	1.19	1.61
Shape Index Mean	1.21	1.67
Landscape Shape Index	1.06	1.21
sigma.sq	1.01	1.03
Phi	1.00	1.00
Multivariate $psrf = 1.08$	1.15	

## 3.5 Model Verification

Withheld data equal to 10% of each significant model's data set acted as locations for model verification. Predicted values were compared to observed values and calculation of the RMSE for each model determined the "best" model to use to predict to new locations.

Table 3-25 outlines the RMSE results for the landscape-level and class-level models with models with the lowest RMSE values from each model set highlighted in bold text.

Table 3-25. Root mean square error results

Root Mean Square Error (RMSE)								
				Post-Burn- In				
Scale	Model	Variables	RMSE	Iterations				
	1_2k	WI+SHAPE_MN+NP	333.780	500,000				
	1_2k	WI+SHAPE_MN+PRD	347.565	500,000				
Landscape-	1_6k	WI+SHAPE_MN+NP	311.843	500,000				
level	1_6k	WI+SHAPE_MN+PRD	294.507	500,000				
	$2\overline{\mathbf{k}}$	WI+SHAPE MN+NP	274.337	500,000				
	2k	WI+SHAPE_MN+PRD	291.361	500,000				
	800m forest	SHAPE_MN+PLADJ	559.395	100,000				
	800m wetland	SHAPE_MN	396.001	50,000				
	800m							
	agriculture/forest	SHAPE_MN+LSI	552.751	50,000				
	1_2k forest	SHAPE_MN+LSI	332.261	100,000				
	<b>1_2k wetland</b> 1 2k	SHAPE_MN+LSI	160.557	100,000				
Class-level	agriculture/forest	SHAPE_MN+LSI	311.324	100,000				
	1_6k forest	SHAPE_MN	485.752	50,000				
	1_6k wetland	SHAPE_MN+LSI	251.310	100,000				
	1_6k							
	agriculture/forest	SHAPE_MN+LSI	361.176	50,000				
	2k forest	PLADJ	213.547	50,000				
	2k wetland	PLADJ	420.077	50,000				
	2k agriculture/forest	SHAPE_MN+LSI	231.294	50,000				

RMSE values determined that the landscape-level 2k model including BU rates as the response variable and wetness index averages, shape index means, and number of patches as independent variables was the best-fitting landscape-level model with an RMSE of 274.337. The best-fitting class-level model, also the overall best-fitting model, was the 1\_2k wetland model that included BU rates as the response variable and shape index means and landscape shape index values as independent variables with an RMSE of 160.557. Fitted rates are similar to observed rates across Benin (Figure 3-1, Figure 3-2).

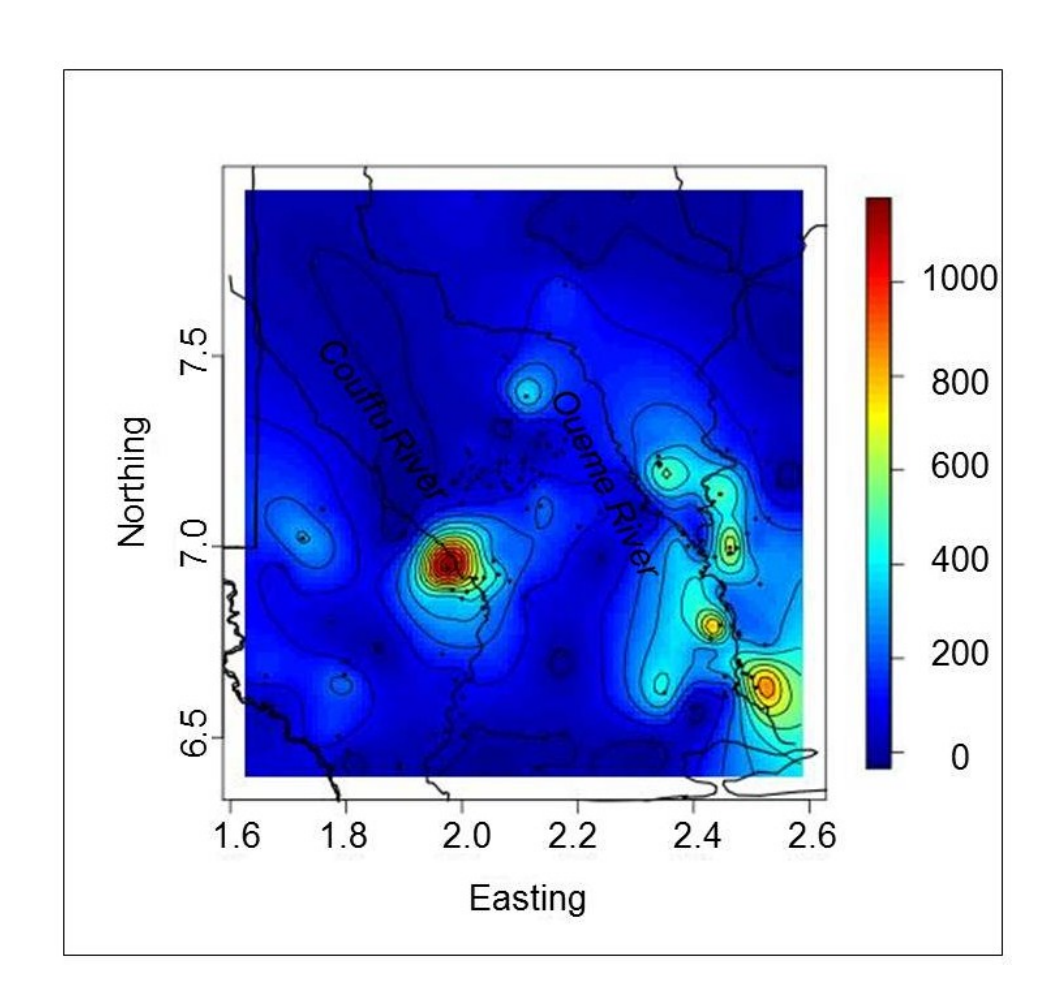


Figure 3-1. 1\_2k wetland class observed rates, 90% data

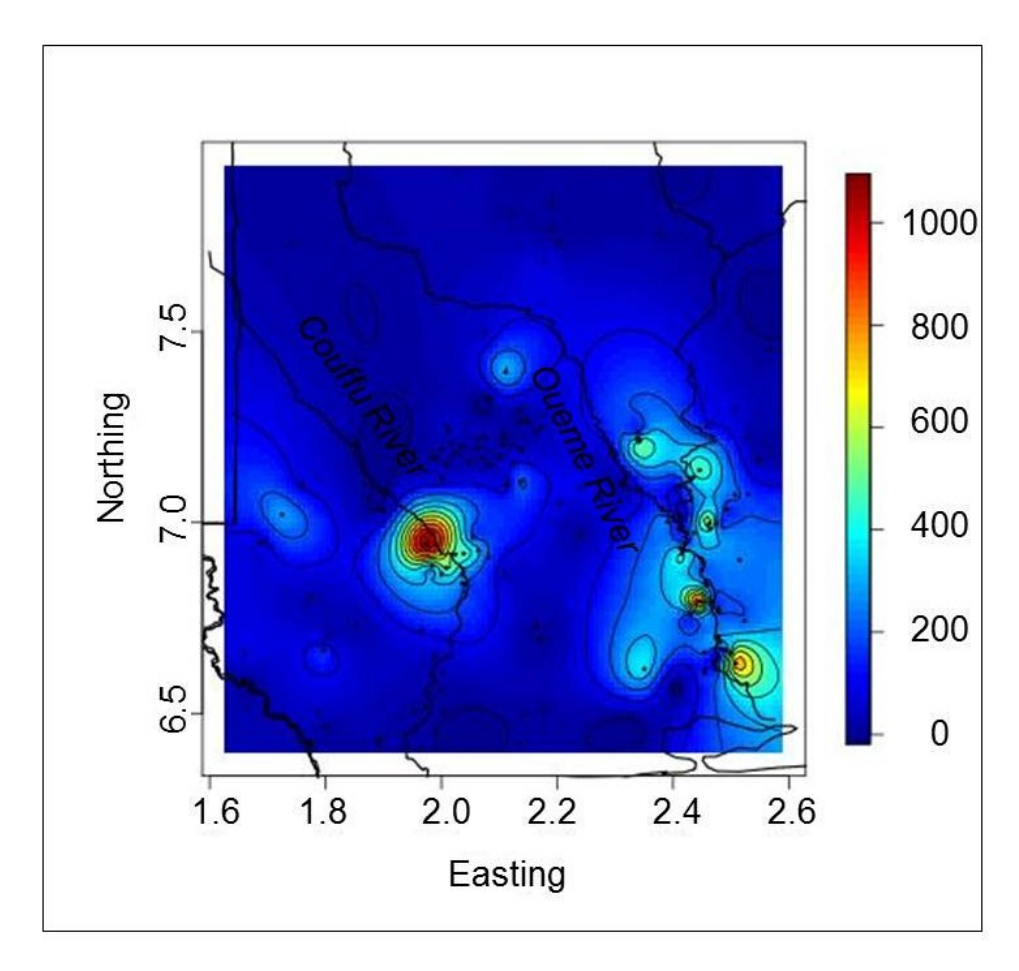


Figure 3-2. 1 2k wetland class fitted model, 90% data

The random spatial effects component contributed a large amount to the overall model fit; areas plotted in red represent higher spatial random effects, while areas plotted in blue represent lower spatial random effects (Figure 3-3). Areas exhibiting high spatial random effects correspond to areas with higher predicted rates, demonstrating their presence in the overall model fit.

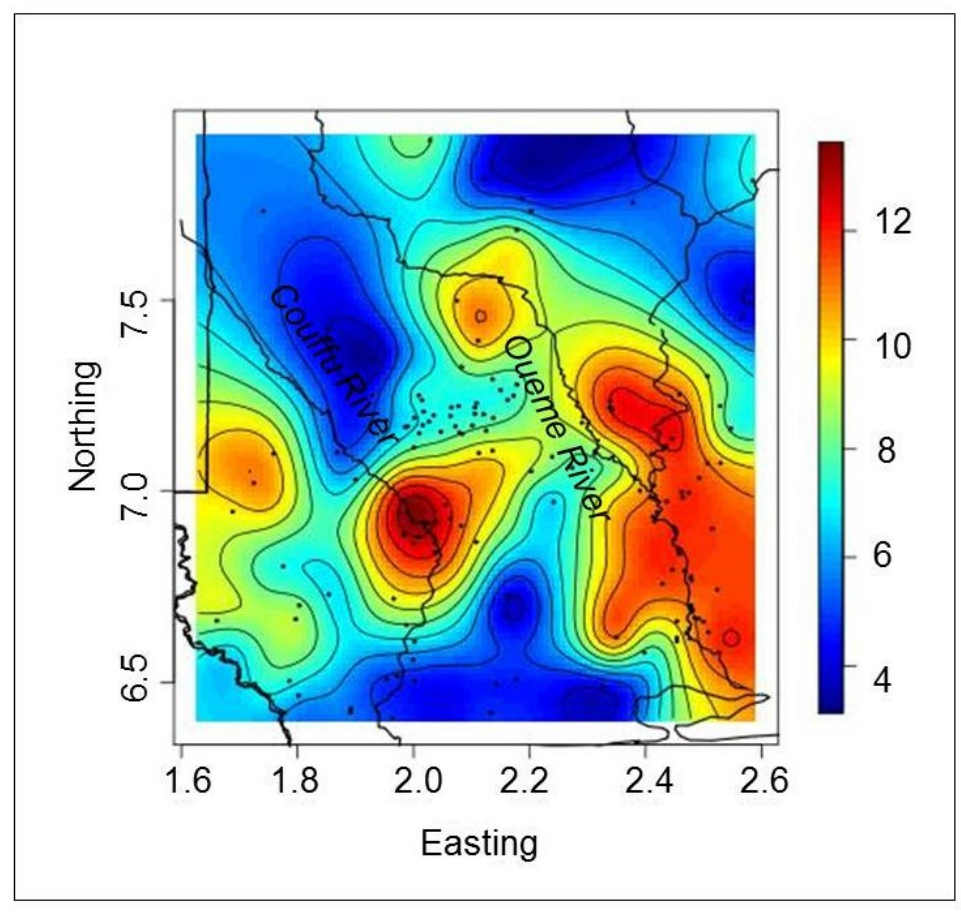


Figure 3-3. 1\_2k wetland class spatial random effects

## 3.6 Predictive Surface Model

Predicted BU rates at new locations across the study region identified areas at risk for BU cases based on landscape configuration metrics and unknown, spatially-structured covariates characterized by random spatial effects generated from the 1\_2k wetland spatial binomial GLM (Figure 3-4). Although this surface represents predictive BU rates, this model does not account for population absences in a region or for any socio-behavioral activities leading to transmission; therefore, although areas might be identified as high-risk areas, it does not necessarily mean that transmission will take place.

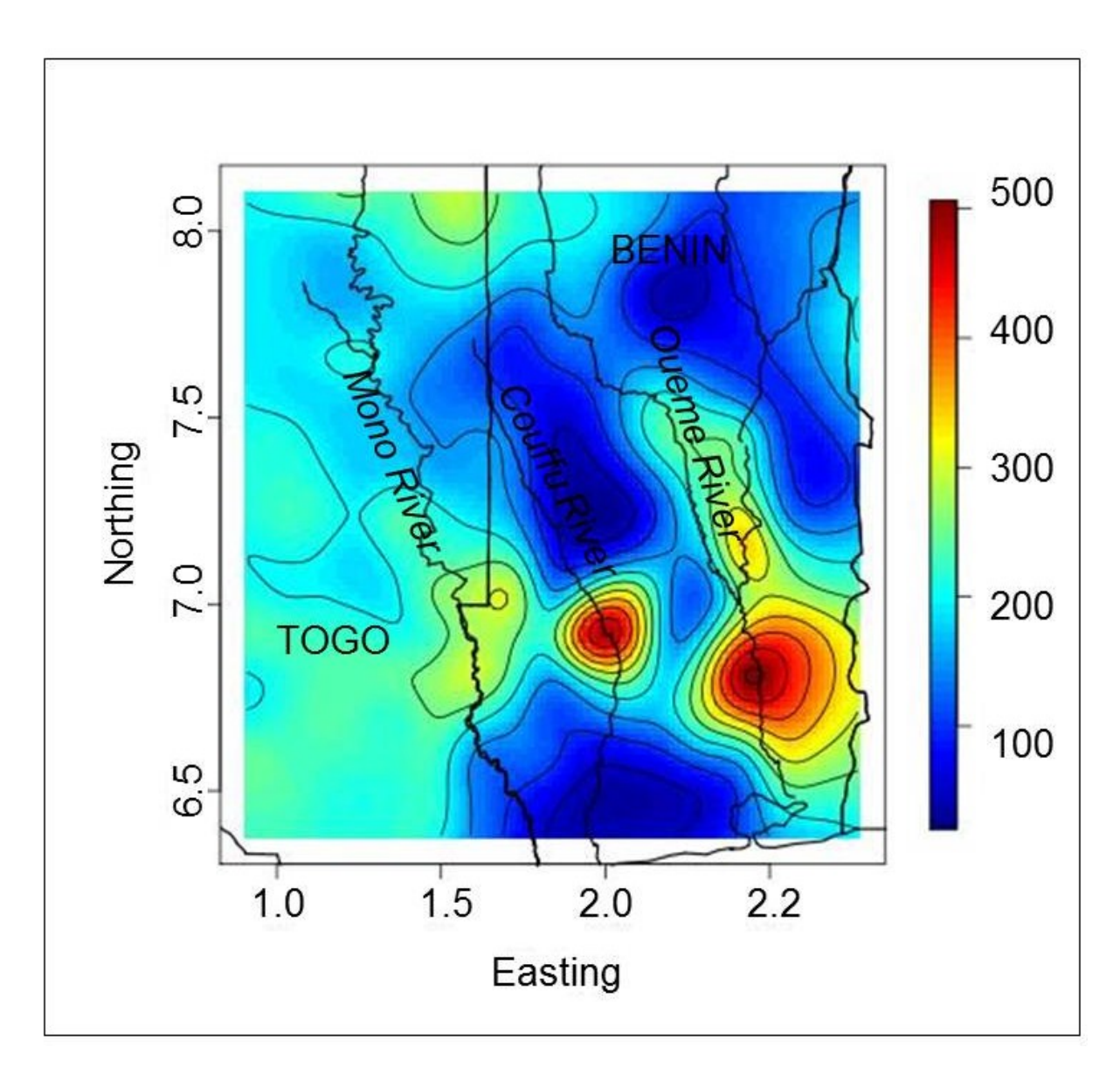


Figure 3-4. Predictive BU rates surface across the study domain

The highest predicted rates occurred within the boundary of Benin along the southern portions of the Oueme and Couffu Rivers. These predictions were consistent with observed rates in these areas. Low risk areas consisted of the northern region and areas along the southern coast in Benin. Moderate risk was identified across large portions of the study area located within the boundary of Togo and along the Oueme River, north of high risk areas.

## **Chapter 4 DISCUSSION AND LIMITATIONS**

#### 4.1 Discussion

This study was a first attempt to quantify relationships between land cover patch patterns indicative of anthropogenic disturbances and BU incidence in Benin. The methods used and the approach taken to quantify these attributes were novel to BU research and highlighted the importance of using spatial statistical methods when investigating environmental phenomena.

The first set of results demonstrated that using non-spatial statistical methods when investigating positively, spatially-autocorrelated ecological variables can lead to overestimations in variable significance. Non-spatial binomial GLMs inflated the influence of predictor variables for all landscape-level models and for several class-level models. Although non-spatial models exhibited significance in all covariates, these methods failed to account for spatial autocorrelation among model residuals, leading to false assumptions regarding their contributions to BU rates. Spatial binomial GLMs mitigated these effects, while identifying important variables related to BU rates at observed locations. The addition of a random spatial effects component partitioned unobserved covariates contributing to BU rates while identifying a spatial structure associated with these covariates, promoting more accurate predictions at new, unsampled locations.

Model sets constructed at a landscape-level and at a class-level enabled an in depth analysis of land cover patch configuration relationships to BU rates within the study region. Several model results determined that land cover patch configurations related to high BU rates at the landscape-level supported study hypotheses that more fragmented landscapes with more uniformly-shaped land cover patches, lying within areas more likely to accumulate water during precipitation events surround villages with higher BU rates, although no models supported all

three scenarios simultaneously, and no variables emerged as dominant indicators of BU risk across all distance intervals. These results were not surprising considering the complexity of factors involved in determining variable selection and when deciding the scale at which to measure natural environmental variables.

Although consistency in variable significance lacked across distances at the landscape level, significance direction in individual variables did not change between models. Further, the best-fitting model in the landscape-level set supported two components of the study hypotheses, and although not the primary focus of this study, additional model results provided several opportunities for a glimpse into potential ecological connections between land cover patch configurations and BU rates.

Notable results included a positive relationship between patch richness density surrounding villages with high BU rates at a 1\_2k distance. Variable significance occurred at a 1\_2k distance only, but the outcome suggested that a relationship exists between more diverse landscapes closer to village centers and higher BU rates. A positive relationship between numbers of patches at a 1\_6k distance and BU rates supported the hypothesis that more fragmented landscapes, potentially disturbed by anthropogenic activities, surround villages with higher disease rates. Although variable significance took place at a 1\_6k distance only, these results warrant further investigation at larger distance intervals to determine whether this phenomenon is indicative of BU risk across broader geographic regions.

Models generated at a 2k distance produced differing results, but both models indicated that a relationship exists between higher average wetness index values and higher BU rates, supporting the hypothesis that areas more likely to accumulate water during a precipitation event surround villages with higher BU rates. Interestingly, average wetness index value variable

significance did not occur at distances closer to village centers, suggesting that a sufficient distance may be needed to encounter rivers and tributaries of a magnitude large enough to create local flooding events on a seasonal basis or during extreme weather events.

Two models created at 2k distances from village centers exhibited different results related to shape index mean values. Low shape index mean values were significant at a 2km distance when paired with numbers of patches and wetness index averages as model covariates, although shape index mean values were not significant at a 2km distance when paired with patch richness density and wetness index averages. One contributing factor to this difference was that shape index mean convergence likely did not take place in the model including patch richness density values; therefore, this model was not representative of the shape index mean distribution at a 2k distance from village centers.

Results from the 2k model including wetness index averages, shape index means, and numbers of patches had the lowest RMSE value of all models produced at the landscape-level and supported the hypothesis that more uniformly-shaped land cover patches, a characteristic of anthropogenically-disturbed landscapes, located in areas more likely to accumulate water during a precipitation event surround villages with higher BU rates. Further investigation into these factors at greater distances from village centers could reveal important trends in larger-scale processes constraining finer-scale phenomena related to BU ecology in the study region.

Class-level models exhibited several consistent results at various distances and across individual class types, fulfilling the second objective of this study to determine whether a relationship exists between land cover patch configurations indicative of potential anthropogenic disturbances corresponding to specific land cover types and high BU rates. While several significant model outcomes occurred, these results did not support the study hypotheses.

Significant forest, wetland, and mixed agriculture/forest patch shape index mean values suggested that more natural or undisturbed patch shapes corresponding to these classes surround villages with higher BU rates, and consistent model outcomes occurred across all distance intervals.

While results corresponding to patch shape complexity did not support the study hypothesis, these results were particularly interesting when observing the mixed agriculture/forest class because the composition of this class included some level of anthropogenic disturbance inherently; therefore, model outcomes provided insight into potential disturbance patterns. Natural patch shape complexities corresponding to this land cover class suggested characteristics representative of natural forest cover because vegetation planted by humans could not likely produce this pattern, indicating that agriculture plots likely intrude into forest patches undisturbed previously. The agriculture/forest class models maintained significance at all distance intervals, signifying that a need exists for further investigation into agriculture planting practices within forested areas and relationships to BU emergence.

Additionally, individual forest, wetland or mixed agriculture/forest class aggregation values related to higher BU rates did not support the study hypothesis that more fragmented land cover corresponding to these classes surrounds villages with higher BU rates. Significant model outcomes reported lower landscape shape index values and higher percent land cover adjacency values consistently, suggesting that more aggregated land cover patches corresponding to these classes surround villages with higher BU rates across all distance intervals.

Several potential reasons may explain class-level model outcomes. One possibility is that anthropogenic disturbance patterns related to the individual classes investigated in this study may not follow patterns recognized previously. Studies demonstrating uniformly-shaped land cover

patches as those created by anthropogenic activities took place largely in European countries and within the United States where access to heavy farming machinery was readily available and long-standing property boundaries may demarcate land cover patches more abruptly.

While disturbance patterns may not follow those quantified in western studies, a more likely explanation has to do with the scale at which the quantification of the study area took place. Ikonos 4m resolution satellite imagery from January 2009 revealed several anthropogenic landscape disturbances demarcated by uniform shapes across a 10k x 10k BU endemic area in the mid-western portion of the study region. Of particular interest were partitioned rice paddy plots within natural wetland boundaries (Figure 4-1). These areas appeared undisturbed until observed at a finer resolution, suggesting that 30m resolution Landsat imagery could not identify within patch anthropogenic disturbance revealed at a finer resolution, and this factor may have influenced class-level results.



Figure 4-1. Anthropogenic disturbance within wetland land cover patch

A third possible explanation may have to do with MU pathogen abundance in the environment. To date, unknown ecological factors drive MU abundance, but landscapes experiencing early disturbance stages may experience elevated pathogen levels. As residents begin to intrude into habitats undisturbed previously to plant agriculture or to collect fuel wood, their activities likely follow natural land cover boundaries before significant landscape alterations take place. Future quantitative PCR applications have the potential to provide knowledge related to pathogen abundance in the environment, the results of which could provide critical information linking MU presence and abundance to specific land cover types and uses during multiple succession stages (Merritt *et al.*, 2005).

Finally, landscape-level model results differed from class-level model results and supported the study hypotheses, suggesting that important land cover categories may not have been included at the class-level in this study. Alternatively, while uniformly-shaped patches corresponding to specific classes did not exhibit significance, when measurement of these patch shapes took place in conjunction with measurements from the entire landscape, uniformly-shaped patches emerged as an important predictor variable; therefore, the importance of this phenomenon may be unrelated to specific class types.

The "best" model with the lowest RMSE value from both model sets corresponded to the 1\_2k wetland class model with BU rates as the response variable and shape index mean values and landscape shape index values as the independent variables. Interestingly, the independent variables did not maintain significance in the spatial GLM; therefore, the spatial random effects component contributed to the majority of the model fit. These results confirmed that a spatial structure exists for processes driving BU rates in Benin, although at the end of this study, these covariates remain unknown.

Although measuring the contribution of land cover composition alone was not the primary objective behind class-level model construction, the fact that the "best" model corresponded to the wetland class while land cover configuration variables corresponding to this class and at this distance were not significant is an important development. These results suggest that wetland land cover composition within relatively close distances from village centers may play an important role in the distribution of BU rates in Benin because additional models at 1\_2k distances, even those maintaining significant variables, exhibited higher RMSE values. These results supported previous studies implicating close proximities to slow-moving or stagnant water bodies as a BU risk factor; consequently, a need exists for further investigation into wetland characteristics at multiple scales near villages experiencing high BU rates.

The creation of a continuous risk surface map across the study region fulfilled the final study objective. Although "best" model predictor variables alone could not predict BU rates effectively, the incorporation of the random spatial effects component enabled accurate predictions at new, unsampled locations while accounting for uncertainty across the study domain. To our knowledge, this study was the first to produce a continuous risk surface based on environmental covariates and the only study to account for and to utilize unknown, spatial covariates driving disease incidence in model predictions.

Predicted rates derived from the mean posterior predictive distribution of the "best" model produced a BU risk surface map from which to identify high risk regions across the study domain (Figure 3-4). Predicted rates in Benin followed a similar pattern to the observed case data with higher rates along the Oueme River in the east and along the Couffu River in the western section of the country. A large floodplain exists in the eastern portion of the country where the Oueme and Zou Rivers join before draining into the Gulf of Guinea. Land cover consists of

mixed agriculture, forest, and shrubland with wetlands situated in the south where the river flows into Lake Nokoué before emptying into the Bight of Benin. Several wetlands extend from the Couffu River with one group situated near the town of Tandji, located within a high predicted rate area, around which BU cases occur regularly. Land cover within this region consists primarily of mixed agriculture/shrub, forest, mixed agriculture/forest, and wetlands.

Low prediction rates along the southern coast coincided with few observed cases in the region, where brackish waters may impact environmental conditions suitable to the MU pathogen, and toward the northern portion of the study region where higher elevations separate the two endemic regions and farther north where climate conditions begin to change to a dryer, less humid environment.

Predicted rates in the study area within the boundary of Togo exhibited moderate values with less variability than rates predicted within the boundary of Benin. This may be due to increased distance from observed locations. As distance from known values exceeds the effective range determined by the spatial structure of the observed data set, predicted rates have a tendency to move toward a mean predictive value, and although this phenomenon may have impacted predicted rates within Togo, the results were still interesting and relevant.

Southern Togo shares a similar climate to southern Benin, falling within the Dahomey Gap. Swampy floodplains reside along the southern portion of the Mono River beginning at an approximate latitude of 6.9333 N, stretching to the southern coast, while an additional wetland consisting of herb swamp, swampy forest, and grassy floodplain lies across the border with Benin (Hughes and Hughes, 1992). The lagoon system in Togo does not experience tidal flow except during periods of high rainfall, and therefore, is considered a freshwater system.

Most notable were moderate-to-high rates predicted along the Mono River west of the Tandji foci in Benin at the border between the two countries. Although located within a wetland system, few reported BU cases exist in this region following construction of the Nangbeto dam in 1987 (R. Christian Johnson, personal communication, March 24, 2009). One hypothesis is that a reduction in cases occurred because of controlled fluctuations in water levels, reducing seasonal flooding impacts in the region. While the environmental conditions may be comparable to those identified as high risk environments in Benin, the model could not account for anthropogenic interference with river flow and identified this area as having a moderate-to-high BU risk.

The region south of the Nangbeto dam may prove to be an important surveillance area. Although the dam construction reduced seasonal flooding risk in the Mono River region, unusually high rainfall contributed to tragedy when the opening of a sluice gate relieved water pressure in the reservoir behind the dam, causing the river to burst its banks, wiping away houses and farms on November 2, 2010 (Ghana News Link, 2010). While troubling, these flooding events may provide a unique control from which to observe whether BU cases emerge, providing an opportunity to gain a better understanding of the role in which flooding contributes to BU incidence.

While multiple, unknown, environmental variables must interact for the bacterium to flourish and transmission to humans likely requires specific socio-behavioral factors unaccounted for in this model, a risk surface incorporating the spatial structure of these unknown variables provided an ideal tool from which to identify high BU risk regions despite little knowledge regarding environmental factors contributing to the disease. Further, BU disease does not observe administrative boundaries; therefore, the creation of a continuous surface

transcending artificial borders eliminated areal data set constraints, the benefits of which were demonstrated in predicted rates across Togo where little case data exists.

Although a temptation exists to observe this risk surface as absolute, the natural environment is not a static phenomenon, nor is BU incidence. This risk surface represents one snapshot in time, based on land cover configurations derived from one satellite image during one season and from the spatial structure of factors contributing to BU incidence in 2004 and 2005. However, observing where BU transmission could likely take place if persons encountered similar environments provides a first step toward surveillance and prevention, while creating a framework from which to target future environmental sampling and research efforts.

#### 4.2 Limitations

Several limitations existed in this study, some of which related directly to data used in the analysis. LULC data derived from 2000 satellite imagery was used to analyze 2004 and 2005 BU case data. Challenges existed in acquiring suitable satellite imagery from the study region because of the presence of cloud cover in a large proportion of the imagery; therefore, this study assumed that the LULC within the study region did not change substantially within a 3-4 year time period. Suitable ground truth data were not available to validate the LULC classification. A 10 year gap between image acquisition and limited ground truth data existed; therefore, this study relied on visual interpretation methods along with aggregated land cover classes to create the land cover classification.

Characterization of land cover configurations took place at one scale using 30m resolution data. Important organism responses may be linked to these variables, but could occur at scales differing from those at which variable measurement took place. A 30m resolution may not be the appropriate resolution to characterize processes driving MU growth and BU

emergence; therefore, a need exists for additional investigation into land cover configuration patterns related to BU rates at different spatial resolutions.

Although active surveillance by government health officials identified BU cases within the study region, underreporting may have impacted study results. Further, identification of BU negative villages corresponded to a 2004 and 2005 time period; these villages may have had positive cases in previous or subsequent years. Additionally, this study assumed that BU transmission occurred near the village of residence. Travel between regions and migration was not known and therefore, was not incorporated into this study.

Environmental variables with a seasonal or a highly temporal nature were not included in this study; for example, precipitation, temperature, or relative humidity factors. Six weather stations with incomplete inventories exist within the study region, making data interpolation across the study domain questionable. Beyond data quality issues, unknown lag times between suitable environmental conditions and pathogen proliferation, inoculation and ulcer presentation, and ulcer presentation and hospital treatment make linking BU cases to specific environmental events challenging. Coarser resolution climate data were considered and an exploratory analysis of several BioClim 30 year average variables did not reveal significant relationships between these variables and BU rates. Likely, the data was too coarse both spatially and temporally to identify important relationships. A need exists for further investigation into the relationship between climate variables and BU cases in West Africa.

Finally, scaling of model coordinates to correspond to a one-to-one surface area may have introduced uncertainty, although the location of the study area close to the equator reduced the impact of this phenomenon.

#### 4.3 Conclusions and Future Directions

The role of anthropogenic ecosystem disturbances in the emergence of environmental bacterial infections is poorly understood. This study was a first attempt to link land cover configurations representative of anthropogenic disturbances to the environmental bacterial infection Buruli ulcer disease. Although mixed results did not suggest a definite trend toward positive linkages between land cover patch configurations representative of anthropogenic disturbances and BU rates, study results identified several significant variables, warranting future investigations into these factors at different scales.

Beyond the novel exploratory analysis outlined above, a major contribution of this study included the incorporation of a modeling component that partitioned the spatial structure of missing variables, providing a structure from which to predict BU rates to new locations without strong knowledge of environmental factors contributing to disease distribution. The resulting continuous BU risk surface is the first of its kind and marks the potential to develop and to target surveillance efforts. The ability to predict potential risk adequately to locations where little data availability exists provided a first step toward prevention, while creating a tool from which a more systematic and controlled site selection process may be used to target future environmental sampling research.

Future directions include model refinement and comparisons of model outcomes generated from this study with additional modeling approaches, for example those using an extreme value link function that accounts for data sets where the number of zeros is vastly greater than the number of ones. Acquisition of climate variables corresponding to endemic regions may reveal valuable linkages between weather events and landscape attributes related to disease incidence, and future studies into wetland land cover using higher resolution satellite

imagery in conjunction with environmental samples could identify relevant links between anthropogenic wetland disturbances and BU disease emergence.

Finally and most importantly, continued acquisition of accurate, and georeferenced case data along with georeferenced pathogen data will provide the best opportunity for robust empirical studies of linkages between ecological factors, anthropogenic activities, and BU transmission. Combining these data with the continued efforts of multidisciplinary research teams, international governments, and aid agencies will provide the tools necessary to one day understand the mystery behind Buruli ulcer disease.

# **APPENDICES**

# Appendix A

Correlation Matrices

Table A-1. Landscape-level 400m correlation matrix

400m Spearman Rank Order Correlation Matrix										
	BU RATE	NP	LSI	SHAPE MN	FRAC MN	PARA MN	PLADJ	PRD	SHDI	WIAVGG
BU RATE	1.000	0.048	0.056	0.138	0.137	0.028	-0.050	0.008	0.033	0.042
NP	0.048	1.000	0.906	-0.073	0.000	0.514	-0.910	0.642	0.814	0.072
LSI	0.056	0.906	1.000	0.263	0.272	0.302	-0.992	0.554	0.870	0.048
SHAPE MN	0.138	0.073	0.263	1.000	0.899	-0.278	-0.255	0.105	0.181	-0.071
FRAC MN	0.137	0.000	0.272	0.899	1.000	-0.318	-0.263	0.022	0.205	-0.034
PARA MN	0.028	0.514	0.302	-0.278	-0.318	1.000	-0.317	0.345	0.169	-0.007
PLADJ	-0.050	0.910	0.992	-0.255	-0.263	-0.317	1.000	0.548	0.868	-0.047
PRD	0.008	0.642	0.554	-0.105	-0.022	0.345	-0.548	1.000	0.660	0.096
SHDI	0.033	0.814	0.870	0.181	0.205	0.169	-0.868	0.660	1.000	0.131
WIAVGG	0.042	0.072	0.048	-0.071	-0.034	-0.007	-0.047	0.096	0.131	1.000

Table A-2. Landscape-level 500m correlation matrix

500m Spearman Rank Order Correlation Matrix										
	BU RATE	NP	LSI	SHAPE MN	FRAC MN	PARA MN	PLADJ	PRD	SHDI	WIAVGG
BU RATE	1.000	0.005	0.035	0.123	0.142	-0.099	-0.028	0.001	0.043	0.068
NP	0.005	1.000	0.900	-0.036	0.015	0.463	-0.902	0.669	0.791	0.100
LSI	0.035	0.900	1.000	0.321	0.306	0.229	-0.991	0.573	0.853	0.068
SHAPE MN	0.123	0.036	0.321	1.000	0.913	-0.395	-0.322	-0.045	0.277	-0.054
FRAC MN	0.142	0.015	0.306	0.913	1.000	-0.448	-0.309	0.007	0.289	0.024
PARA MN	0.099	0.463	0.229	-0.395	-0.448	1.000	-0.229	0.287	0.067	-0.022
PLADJ	0.028	0.902	0.991	-0.322	-0.309	-0.229	1.000	-0.571	-0.853	-0.071
PRD	0.001	0.669	0.573	-0.045	0.007	0.287	-0.571	1.000	0.688	0.152
SHDI	0.043	0.791	0.853	0.277	0.289	0.067	-0.853	0.688	1.000	0.139
WIAVGG	0.068	0.100	0.068	-0.054	0.024	-0.022	-0.071	0.152	0.139	1.000

Table A-3. Landscape-level 600m correlation matrix

600m Spearman Rank Order Correlation Matrix										
	BU RATE	NP	LSI	SHAPE MN	FRAC MN	PARA MN	PLADJ	PRD	SHDI	WIAVGG
<b>BU RATE</b>	1.000	0.014	0.029	0.057	0.032	-0.087	-0.022	0.014	0.057	0.089
NP	0.014	1.000	0.908	-0.081	-0.010	0.393	-0.910	0.613	0.773	0.078
LSI	0.029	0.908	1.000	0.255	0.258	0.168	-0.991	0.512	0.831	0.069
SHAPE MN	0.057	0.081	0.255	1.000	0.903	-0.452	-0.255	0.085	0.229	-0.011
FRAC MN	0.032	0.010	0.258	0.903	1.000	-0.479	-0.257	0.027	0.245	0.006
PARA MN	0.087	0.393	0.168	-0.452	-0.479	1.000	-0.180	0.195	0.015	-0.021
PLADJ	0.022	0.910	0.991	-0.255	-0.257	-0.180	1.000	0.518	0.837	-0.072
PRD	0.014	0.613	0.512	-0.085	0.027	0.195	-0.518	1.000	0.629	0.131
SHDI	0.057	0.773	0.831	0.229	0.245	0.015	-0.837	0.629	1.000	0.143
WIAVGG	0.089	0.078	0.069	-0.011	0.006	-0.021	-0.072	0.131	0.143	1.000

Table A-4. Landscape-level 700m correlation matrix

		7	'00m Spe	earman Rai	nk Order	Correlatio	n Matrix			
	BU RATE	NP	LSI	SHAPE MN	FRAC MN	PARA MN	PLADJ	PRD	SHDI	WIAVGG
BU RATE	1.000	0.016	0.022	0.088	0.044	0.057	-0.013	0.060	0.065	0.111
NP	0.016	1.000	0.897	-0.049	0.021	0.440	-0.902	0.572	0.745	0.073
LSI	0.022	0.897	1.000	0.316	0.268	0.201	-0.991	0.469	0.806	0.044
SHAPE MN	0.088	0.049	0.316	1.000	0.896	0.466	-0.307	0.096	0.270	-0.042
FRAC MN	0.044	0.021	0.268	0.896	1.000	0.507	-0.261	0.034	0.257	0.004
PARA MN	-0.057	0.440	0.201	-0.466	0.507	1.000	-0.209	0.209	0.039	-0.047
PLADJ	-0.013	0.902	0.991	-0.307	0.261	0.209	1.000	0.478	0.814	-0.045
PRD	0.060	0.572	0.469	-0.096	0.034	0.209	-0.478	1.000	0.621	0.185
SHDI	0.065	0.745	0.806	0.270	0.257	0.039	-0.814	0.621	1.000	0.137
WIAVGG	0.111	0.073	0.044	-0.042	0.004	0.047	-0.045	0.185	0.137	1.000

Table A-5. Landscape-level 800m correlation matrix

			800m S	Spearman R	ank Orde	r Correlati	ion Matrix			
	BU RATE	NP	LSI	SHAPE MN	FRAC MN	PARA MN	PLADJ	PRD	SHDI	WIAVGG
BU RATE	1.000	0.009	0.024	0.118	0.073	0.142	-0.013	0.052	0.074	0.131
NP	0.009	1.000	0.910	-0.110	0.073	0.472	-0.914	0.556	0.741	0.091
LSI	0.024	0.910	1.000	0.232	0.202	0.270	-0.989	0.447	0.782	0.045
SHAPE MN	0.118	0.110	0.232	1.000	0.909	0.511	-0.225	0.126	0.236	-0.024
FRAC MN	0.073	0.073	0.202	0.909	1.000	0.598	-0.196	0.054	0.234	0.019
PARA MN	0.142	0.472	0.270	-0.511	-0.598	1.000	-0.280	0.231	0.094	-0.012
PLADJ	0.013	0.914	0.989	-0.225	-0.196	-0.280	1.000	0.459	0.794	-0.051
PRD	0.052	0.556	0.447	-0.126	-0.054	0.231	-0.459	1.000	0.621	0.206
SHDI	0.074	0.741	0.782	0.236	0.234	0.094	-0.794	0.621	1.000	0.161
WIAVGG	0.131	0.091	0.045	-0.024	0.019	-0.012	-0.051	0.206	0.161	1.000

Table A-6. Landscape-level 900m correlation matrix

			900m Sp	earman Raı	nk Order (	Correlation	n Matrix			
	BU RATE	NP	LSI	SHAPE MN	FRAC MN	PARA MN	PLADJ	PRD	SHDI	WIAVGG
BU RATE	1.000	0.013	0.025	0.122	0.071	-0.137	-0.013	0.070	0.076	0.135
NP	-0.013	1.000	0.901	-0.108	0.037	0.421	-0.907	0.545	0.732	0.076
LSI	0.025	0.901	1.000	0.249	0.239	0.200	-0.987	0.438	0.767	0.050
SHAPE MN	0.122	0.108	0.249	1.000	0.889	-0.484	-0.238	0.130	0.221	-0.002
FRAC MN	0.071	0.037	0.239	0.889	1.000	-0.558	-0.231	0.057	0.262	0.009
PARA MN	-0.137	0.421	0.200	-0.484	0.558	1.000	-0.217	0.200	0.011	-0.034
PLADJ	-0.013	0.907	0.987	-0.238	0.231	-0.217	1.000	0.450	-0.783	-0.057
PRD	0.070	0.545	0.438	-0.130	0.057	0.200	-0.450	1.000	0.611	0.199
SHDI	0.076	0.732	0.767	0.221	0.262	0.011	-0.783	0.611	1.000	0.169
WIAVGG	0.135	0.076	0.050	-0.002	0.009	-0.034	-0.057	0.199	0.169	1.000

Table A-7. Landscape-level 1k correlation matrix

			1k Sp	earman Ran	k Order Co	orrelation N	<b>Matrix</b>			
	BU RATE	NP	LSI	SHAPE MN	FRAC MN	PARA MN	PLADJ	PRD	SHDI	WIAVGG
BU RATE	1.000	0.005	0.030	0.112	0.080	-0.083	-0.016	0.083	0.084	0.133
NP	0.005	1.000	0.906	-0.084	0.004	0.431	-0.911	0.541	0.706	0.061
LSI	0.030	0.906	1.000	0.257	0.278	0.228	-0.986	0.445	0.751	0.048
SHAPE MN	0.112	0.084	0.257	1.000	0.910	-0.497	-0.249	0.087	0.266	0.036
FRAC MN	0.080	0.004	0.278	0.910	1.000	-0.565	-0.271	0.010	0.324	0.059
PARA MN	0.083	0.431	0.228	-0.497	-0.565	1.000	-0.244	0.201	0.000	-0.033
PLADJ	0.016	0.911	0.986	-0.249	-0.271	-0.244	1.000	0.461	0.767	-0.055
PRD	0.083	0.541	0.445	-0.087	0.010	0.201	-0.461	1.000	0.597	0.236
SHDI	0.084	0.706	0.751	0.266	0.324	0.000	-0.767	0.597	1.000	0.165
WIAVGG	0.133	0.061	0.048	0.036	0.059	-0.033	-0.055	0.236	0.165	1.000

Table A-8. Landscape-level 1\_1k correlation matrix

			1_1k Sp	earman Rai	nk Order (	Correlation	n Matrix			
	BU RATE	NP	LSI	SHAPE MN	FRAC MN	PARA MN	PLADJ	PRD	SHDI	WIAVGG
BU RATE	1.000	0.000	0.038	0.120	0.100	-0.143	-0.024	0.127	0.095	0.133
NP	0.000	1.000	0.906	-0.088	0.043	0.438	-0.913	0.543	0.698	0.051
LSI	0.038	0.906	1.000	0.254	0.313	0.234	-0.985	0.474	0.744	0.039
SHAPE MN	0.120	-0.088	0.254	1.000	0.907	-0.468	-0.244	-0.033	0.282	0.039
FRAC MN	0.100	0.043	0.313	0.907	1.000	-0.478	-0.303	0.083	0.382	0.052
PARA MN	0.143	0.438	0.234	-0.468	-0.478	1.000	-0.249	0.158	0.006	-0.058
PLADJ	0.024	-0.913	-0.985	-0.244	-0.303	-0.249	1.000	-0.491	-0.762	-0.049
PRD	0.127	0.543	0.474	-0.033	0.083	0.158	-0.491	1.000	0.616	0.282
SHDI	0.095	0.698	0.744	0.282	0.382	0.006	-0.762	0.616	1.000	0.174
WIAVGG	0.133	0.051	0.039	0.039	0.052	-0.058	-0.049	0.282	0.174	1.000

Table A-9. Landscape-level 1\_2k correlation matrix

			1_2k Sp	earman Rai	nk Order (	Correlation	n Matrix			
	BU RATE	NP	LSI	SHAPE MN	FRAC MN	PARA MN	PLADJ	PRD	SHDI	WIAVGG
BU RATE	1.000	0.006	0.044	0.094	0.029	-0.072	-0.029	0.137	0.093	0.141
NP	0.006	1.000	0.908	-0.090	0.007	0.453	-0.914	0.532	0.684	0.039
LSI	0.044	0.908	1.000	0.252	0.280	0.248	-0.985	0.473	0.734	0.036
SHAPE MN	0.094	-0.090	0.252	1.000	0.895	-0.502	-0.245	0.004	0.296	0.058
FRAC MN	0.029	0.007	0.280	0.895	1.000	-0.550	-0.278	0.073	0.344	0.066
PARA MN	0.072	0.453	0.248	-0.502	-0.550	1.000	-0.260	0.188	0.038	-0.077
PLADJ	0.029	-0.914	-0.985	-0.245	-0.278	-0.260	1.000	-0.490	-0.750	-0.047
PRD	0.137	0.532	0.473	0.004	0.073	0.188	-0.490	1.000	0.607	0.302
SHDI	0.093	0.684	0.734	0.296	0.344	0.038	-0.750	0.607	1.000	0.178
WIAVGG	0.141	0.039	0.036	0.058	0.066	-0.077	-0.047	0.302	0.178	1.000

Table A-10. Landscape-level 1\_3k correlation matrix

			1_3k Sp	earman Rai	nk Order (	Correlation	n Matrix			
	BU RATE	NP	LSI	SHAPE MN	FRAC MN	PARA MN	PLADJ	PRD	SHDI	WIAVGG
BU RATE	1.000	0.020	0.053	0.126	0.075	-0.062	-0.038	0.144	0.094	0.145
NP	0.020	1.000	0.913	-0.088	0.014	0.462	-0.923	0.509	0.686	0.020
LSI	0.053	0.913	1.000	0.237	0.277	0.268	-0.985	0.457	0.728	0.018
SHAPE MN	0.126	-0.088	0.237	1.000	0.907	-0.478	-0.227	0.022	0.287	0.038
FRAC MN	0.075	0.014	0.277	0.907	1.000	-0.520	-0.267	0.111	0.360	0.046
PARA MN	0.062	0.462	0.268	-0.478	-0.520	1.000	-0.288	0.143	0.049	-0.076
PLADJ	0.038	-0.923	-0.985	-0.227	-0.267	-0.288	1.000	-0.472	-0.744	-0.029
PRD	0.144	0.509	0.457	0.022	0.111	0.143	-0.472	1.000	0.603	0.338
SHDI	0.094	0.686	0.728	0.287	0.360	0.049	-0.744	0.603	1.000	0.172
WIAVGG	0.145	0.020	0.018	0.038	0.046	-0.076	-0.029	0.338	0.172	1.000

Table A-11. Landscape-level 1\_5k correlation matrix

			1_5k Sp	earman Rai	nk Order (	Correlation	n Matrix			
	BU RATE	NP	LSI	SHAPE MN	FRAC MN	PARA MN	PLADJ	PRD	SHDI	WIAVGG
RATE	1.000	0.029	0.055	0.110	0.057	-0.069	-0.040	0.142	0.093	0.146
NP	0.029	1.000	0.915	-0.107	0.013	0.526	-0.925	0.490	0.665	0.011
LSI	0.055	0.915	1.000	0.215	0.267	0.356	-0.985	0.431	0.710	0.010
SHAPE MN	0.110	-0.107	0.215	1.000	0.880	-0.442	-0.200	0.030	0.280	0.073
FRAC MN	0.057	0.013	0.267	0.880	1.000	-0.508	-0.252	0.122	0.345	0.086
PARA MN	0.069	0.526	0.356	-0.442	-0.508	1.000	-0.377	0.182	0.136	-0.065
PLADJ	0.040	-0.925	-0.985	-0.200	-0.252	-0.377	1.000	-0.446	-0.725	-0.022
PRD	0.142	0.490	0.431	0.030	0.122	0.182	-0.446	1.000	0.588	0.341
SHDI	0.093	0.665	0.710	0.280	0.345	0.136	-0.725	0.588	1.000	0.175
WIAVGG	0.146	0.011	0.010	0.073	0.086	-0.065	-0.022	0.341	0.175	1.000

Table A-12. Landscape-level 1\_6k correlation matrix

			1_6k Sp	earman Rar	nk Order C	Correlation	Matrix			
	BU RATE	NP	LSI	SHAPE MN	FRAC MN	PARA MN	PLADJ	PRD	SHDI	WIAVGG
BU RATE	1.000	0.028	0.055	0.079	0.030	0.030	-0.039	0.118	0.089	0.146
NP	0.028	1.000	0.915	-0.057	0.089	0.508	-0.925	0.476	0.671	0.011
LSI	0.055	0.915	1.000	0.257	0.323	0.343	-0.987	0.409	0.706	0.011
SHAPE MN	0.079	0.057	0.257	1.000	0.875	0.390	-0.245	0.040	0.303	0.067
FRAC MN	0.030	0.089	0.323	0.875	1.000	0.458	-0.313	0.139	0.386	0.068
PARA MN	0.030	0.508	0.343	-0.390	-0.458	1.000	-0.363	0.186	0.144	-0.082
PLADJ	0.039	0.925	0.987	-0.245	-0.313	0.363	1.000	0.426	0.718	-0.020
PRD	0.118	0.476	0.409	0.040	0.139	0.186	-0.426	1.000	0.595	0.317
SHDI	0.089	0.671	0.706	0.303	0.386	0.144	-0.718	0.595	1.000	0.182
WIAVGG	0.146	0.011	0.011	0.067	0.068	0.082	-0.020	0.317	0.182	1.000

Table A-13. Landscape-level 1\_7k correlation matrix

			1_7k Sp	pearman Ra	nk Order (	Correlation	n Matrix			
	RATE	NP	LSI	SHAPE MN	FRAC MN	PARA MN	PLADJ	PRD	SHDI	WIAVGG
RATE	1.000	0.028	0.054	0.097	0.081	-0.042	-0.039	0.112	0.090	0.146
NP	0.028	1.000	0.914	-0.086	0.042	0.497	-0.924	0.451	0.666	0.006
LSI	0.054	0.914	1.000	0.232	0.289	0.331	-0.988	0.399	0.702	0.009
SHAPE MN	0.097	-0.086	0.232	1.000	0.877	-0.413	-0.219	0.055	0.282	0.065
FRAC MN	0.081	0.042	0.289	0.877	1.000	-0.484	-0.275	0.138	0.360	0.066
PARA MN	0.042	0.497	0.331	-0.413	-0.484	1.000	-0.350	0.159	0.140	-0.086
PLADJ	0.039	-0.924	-0.988	-0.219	-0.275	-0.350	1.000	-0.416	-0.714	-0.018
PRD	0.112	0.451	0.399	0.055	0.138	0.159	-0.416	1.000	0.592	0.337
SHDI	0.090	0.666	0.702	0.282	0.360	0.140	-0.714	0.592	1.000	0.190
WIAVGG	0.146	0.006	0.009	0.065	0.066	-0.086	-0.018	0.337	0.190	1.000

Table A-14. Landscape-level 1\_8k correlation matrix

			1_8k S <sub>1</sub>	pearman Rai	nk Order (	Correlation	Matrix			
	RATE	NP	LSI	SHAPE MN	FRAC MN	PARA MN	PLADJ	PRD	SHDI	WIAVGG
RATE	1.000	0.035	0.058	0.089	0.054	-0.040	-0.045	0.118	0.093	0.148
NP	0.035	1.000	0.914	-0.102	0.023	0.520	-0.922	0.462	0.658	-0.004
LSI	0.058	0.914	1.000	0.218	0.271	0.357	-0.988	0.404	0.698	0.005
SHAPE MN	0.089	-0.102	0.218	1.000	0.889	-0.444	-0.208	0.050	0.289	0.058
FRAC MN	0.054	0.023	0.271	0.889	1.000	-0.512	-0.259	0.127	0.376	0.068
PARA MN	0.040	0.520	0.357	-0.444	-0.512	1.000	-0.373	0.168	0.125	-0.093
PLADJ	0.045	-0.922	-0.988	-0.208	-0.259	-0.373	1.000	-0.418	-0.710	-0.012
PRD	0.118	0.462	0.404	0.050	0.127	0.168	-0.418	1.000	0.586	0.340
SHDI	0.093	0.658	0.698	0.289	0.376	0.125	-0.710	0.586	1.000	0.193
WIAVGG	0.148	-0.004	0.005	0.058	0.068	-0.093	-0.012	0.340	0.193	1.000

Table A-15. Landscape-level 1\_9k correlation matrix

	1_9k Spearman Rank Order Correlation Matrix										
	RATE	NP	LSI	SHAPE MN	FRAC MN	PARA MN	PLADJ	PRD	SHDI	WIAVGG	
RATE	1.000	0.034	0.058	0.088	0.064	-0.028	-0.044	0.129	0.091	0.150	
NP	0.034	1.000	0.912	-0.083	0.068	0.526	-0.920	0.453	0.642	-0.021	
LSI	0.058	0.912	1.000	0.241	0.320	0.355	-0.989	0.403	0.689	-0.005	
SHAPE MN	0.088	-0.083	0.241	1.000	0.885	-0.423	-0.229	0.094	0.310	0.082	
FRAC MN	0.064	0.068	0.320	0.885	1.000	-0.467	-0.307	0.171	0.398	0.064	
PARA MN	0.028	0.526	0.355	-0.423	-0.467	1.000	-0.369	0.191	0.156	-0.106	
PLADJ	0.044	-0.920	-0.989	-0.229	-0.307	-0.369	1.000	-0.418	-0.703	-0.002	
PRD	0.129	0.453	0.403	0.094	0.171	0.191	-0.418	1.000	0.594	0.344	
SHDI	0.091	0.642	0.689	0.310	0.398	0.156	-0.703	0.594	1.000	0.197	
WIAVGG	0.150	-0.021	-0.005	0.082	0.064	-0.106	-0.002	0.344	0.197	1.000	

Table A-16. Landscape-level 2k correlation matrix

	2k Spearman Rank Order Correlation Matrix										
	BU RATE	NP	LSI	SHAPE MN	FRAC MN	PARA MN	PLADJ	PRD	SHDI	WIAVGG	
BU RATE	1.000	0.033	0.055	0.091	0.056	-0.042	-0.042	0.121	0.089	0.149	
NP	0.033	1.000	0.913	-0.092	0.088	0.555	-0.920	0.447	0.636	-0.029	
LSI	0.055	0.913	1.000	0.226	0.330	0.394	-0.990	0.388	0.681	-0.017	
SHAPE MN	0.091	-0.092	0.226	1.000	0.866	-0.390	-0.214	0.099	0.309	0.089	
FRAC MN	0.056	0.088	0.330	0.866	1.000	-0.422	-0.317	0.191	0.410	0.056	
PARA MN	0.042	0.555	0.394	-0.390	-0.422	1.000	-0.406	0.173	0.176	-0.087	
PLADJ	0.042	-0.920	-0.990	-0.214	-0.317	-0.406	1.000	-0.402	-0.694	0.009	
PRD	0.121	0.447	0.388	0.099	0.191	0.173	-0.402	1.000	0.580	0.344	
SHDI	0.089	0.636	0.681	0.309	0.410	0.176	-0.694	0.580	1.000	0.198	
WIAVGG	0.149	-0.029	-0.017	0.089	0.056	-0.087	0.009	0.344	0.198	1.000	

Table A-17. 800m forest class correlation matrix

800m Forest Class Spearman Rank Order Correlation Matrix									
	NP	LSI	SHAPE MN	CLUMPY	PLADJ	AI			
NP	1.000	0.853	-0.003	-0.463	0.019	-0.442			
LSI	0.853	1.000	0.444	-0.335	0.257	-0.305			
SHAPE MN	-0.003	0.444	1.000	0.247	0.606	0.271			
CLUMPY	-0.463	-0.335	0.247	1.000	0.709	0.998			
PLADJ	0.019	0.257	0.606	0.709	1.000	0.727			
AI	-0.442	-0.305	0.271	0.998	0.727	1.000			

Table A-18. 800m wetland class correlation matrix

800m Wetland Class Spearman Rank Order Correlation Matrix									
	NP	LSI	SHAPE MN	CLUMPY	PLADJ	AI			
NP	1.000	0.772	-0.238	-0.445	0.036	-0.354			
LSI	0.772	1.000	0.347	-0.247	0.373	-0.112			
SHAPE MN	-0.238	0.347	1.000	0.450	0.699	0.514			
CLUMPY	-0.445	-0.247	0.450	1.000	0.719	0.971			
PLADJ	0.036	0.373	0.699	0.719	1.000	0.804			
AI	-0.354	-0.112	0.514	0.971	0.804	1.000			

Table A-19. 800m agriculture/forest class correlation matrix

800m Agriculture/Forest Class Spearman Rank Order Correlation Matrix									
	NP	LSI	SHAPE MN	CLUMPY	PLADJ	AI			
NP	1.000	0.880	0.075	-0.426	0.188	-0.379			
LSI	0.880	1.000	0.472	-0.170	0.525	-0.110			
SHAPE MN	0.075	0.472	1.000	0.456	0.851	0.482			
CLUMPY	-0.426	-0.170	0.456	1.000	0.614	0.992			
PLADJ	0.188	0.525	0.851	0.614	1.000	0.648			
AI	-0.379	-0.110	0.482	0.992	0.648	1.000			

Table A-20. 1\_2k forest class correlation matrix

1_2k Forest Class Spearman Rank Order Correlation Matrix									
	NP	LSI	SHAPE MN	CLUMPY	PLADJ	AI			
NP	1.000	0.946	0.182	-0.441	0.232	-0.409			
LSI	0.946	1.000	0.433	-0.396	0.328	-0.363			
SHAPE MN	0.182	0.433	1.000	0.253	0.660	0.275			
CLUMPY	-0.441	-0.396	0.253	1.000	0.630	0.998			
PLADJ	0.232	0.328	0.660	0.630	1.000	0.650			
AI	-0.409	-0.363	0.275	0.998	0.650	1.000			

Table A-21. 1\_2k wetland class correlation matrix

1_2k Wetland Class Spearman Rank Order Correlation Matrix									
	NP	LSI	SHAPE MN	CLUMPY	PLADJ	AI			
NP	1.000	0.842	-0.095	-0.287	0.267	-0.166			
LSI	0.842	1.000	0.374	-0.122	0.496	0.026			
SHAPE MN	-0.095	0.374	1.000	0.413	0.623	0.465			
CLUMPY	-0.287	-0.122	0.413	1.000	0.705	0.967			
PLADJ	0.267	0.496	0.623	0.705	1.000	0.786			
AI	-0.166	0.026	0.465	0.967	0.786	1.000			

Table A-22. 1\_2k agriculture/forest class correlation matrix

1_2k Agriculture/Forest Class Spearman Rank Order Correlation Matrix									
	NP	LSI	SHAPE MN	CLUMPY	PLADJ	AI			
NP	1.000	0.955	0.322	-0.433	0.374	-0.395			
LSI	0.955	1.000	0.535	-0.364	0.490	-0.323			
SHAPE MN	0.322	0.535	1.000	0.160	0.728	0.184			
CLUMPY	-0.433	-0.364	0.160	1.000	0.479	0.997			
PLADJ	0.374	0.490	0.728	0.479	1.000	0.505			
AI	-0.395	-0.323	0.184	0.997	0.505	1.000			

Table A-23. 1\_6k forest class correlation matrix

1_6k Forest Class Spearman Rank Order Correlation Matrix								
	NP	LSI	SHAPE MN	CLUMPY	PLADJ	AI		
NP	1.000	0.954	0.158	-0.196	0.311	-0.160		
LSI SHAPE	0.954	1.000	0.364	-0.178	0.351	-0.142		
MN	0.158	0.364	1.000	0.390	0.604	0.407		
CLUMPY	-0.196	-0.178	0.390	1.000	0.779	0.998		
PLADJ	0.311	0.351	0.604	0.779	1.000	0.799		
AI	-0.160	-0.142	0.407	0.998	0.799	1.000		

Table A-24. 1\_6k wetland class correlation matrix

1_6k Wetland Class Spearman Rank Order Correlation Matrix									
	NP	LSI	SHAPE MN	CLUMPY	PLADJ	AI			
NP	1.000	0.901	0.137	-0.289	0.348	-0.159			
LSI	0.901	1.000	0.471	-0.177	0.507	-0.023			
SHAPE MN	0.137	0.471	1.000	0.346	0.666	0.395			
CLUMPY	-0.289	-0.177	0.346	1.000	0.635	0.963			
PLADJ	0.348	0.507	0.666	0.635	1.000	0.717			
AI	-0.159	-0.023	0.395	0.963	0.717	1.000			

Table A-25. 1\_6k agriculture/forest class correlation matrix

1_6k Agriculture/Forest Class Spearman Rank Order Correlation Matrix									
	NP	LSI	SHAPE MN	CLUMPY	PLADJ	AI			
NP	1.000	0.956	0.415	-0.321	0.389	-0.284			
LSI	0.956	1.000	0.600	-0.238	0.492	-0.198			
SHAPE MN	0.415	0.600	1.000	0.298	0.799	0.325			
CLUMPY	-0.321	-0.238	0.298	1.000	0.537	0.997			
PLADJ	0.389	0.492	0.799	0.537	1.000	0.557			
AI	-0.284	-0.198	0.325	0.997	0.557	1.000			

Table A-26. 2k forest class correlation matrix

2k Forest Class Spearman Rank Order Correlation Matrix								
	NP	LSI	SHAPE MN	CLUMPY	PLADJ	AI		
NP	1.000	0.945	0.143	-0.226	0.449	-0.186		
LSI	0.945	1.000	0.342	-0.268	0.432	-0.228		
SHAPE MN	0.143	0.342	1.000	0.225	0.514	0.239		
CLUMPY	-0.226	-0.268	0.225	1.000	0.617	0.998		
PLADJ	0.449	0.432	0.514	0.617	1.000	0.639		
AI	-0.186	-0.228	0.239	0.998	0.639	1.000		

Table A-27. 2k wetland class correlation matrix

2k Wetland Class Spearman Rank Order Correlation Matrix									
	NP	LSI	SHAPE MN	CLUMPY	PLADJ	AI			
NP	1.000	0.923	0.170	-0.255	0.344	-0.143			
LSI	0.923	1.000	0.457	-0.185	0.452	-0.053			
SHAPE MN	0.170	0.457	1.000	0.306	0.643	0.352			
CLUMPY	-0.255	-0.185	0.306	1.000	0.655	0.968			
PLADJ	0.344	0.452	0.643	0.655	1.000	0.718			
AI	-0.143	-0.053	0.352	0.968	0.718	1.000			

Table A-28. 2k agriculture/forest class correlation matrix

2k Agriculture/Forest Class Spearman Rank Order Correlation Matrix									
	NP	LSI	SHAPE MN	CLUMPY	PLADJ	AI			
NP	1.000	0.969	0.425	-0.165	0.457	-0.134			
LSI	0.969	1.000	0.575	-0.114	0.515	-0.079			
SHAPE MN	0.425	0.575	1.000	0.405	0.765	0.429			
CLUMPY	-0.165	-0.114	0.405	1.000	0.638	0.997			
PLADJ	0.457	0.515	0.765	0.638	1.000	0.653			
AI	-0.134	-0.079	0.429	0.997	0.653	1.000			

#### Appendix B

Non-Spatial Binomial Model Scatterplots

WIAVGG

SHAPE\_MN

NP

Ogt 000

50

100

150

Figure B-1. Landscape-level "best model" variable scatterplots

6 8 10 12 14 16

### 800m Forest Class

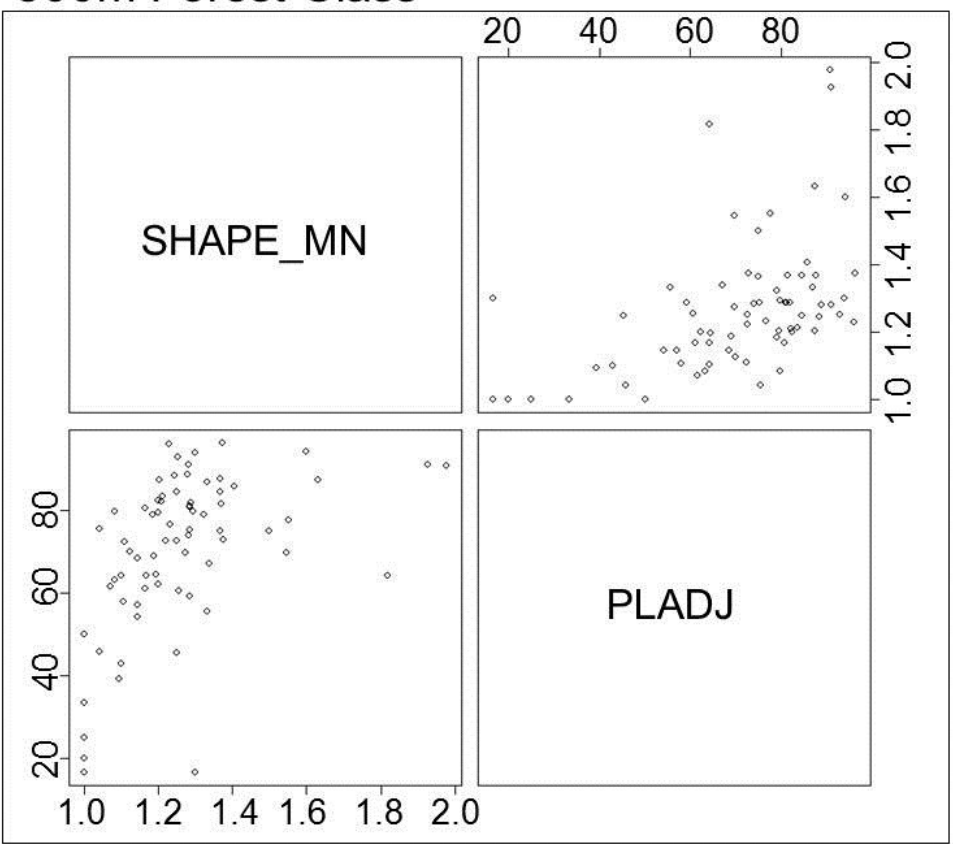


Figure B-2. 800m "best model" variable scatterplot

## 800m Wetland Class

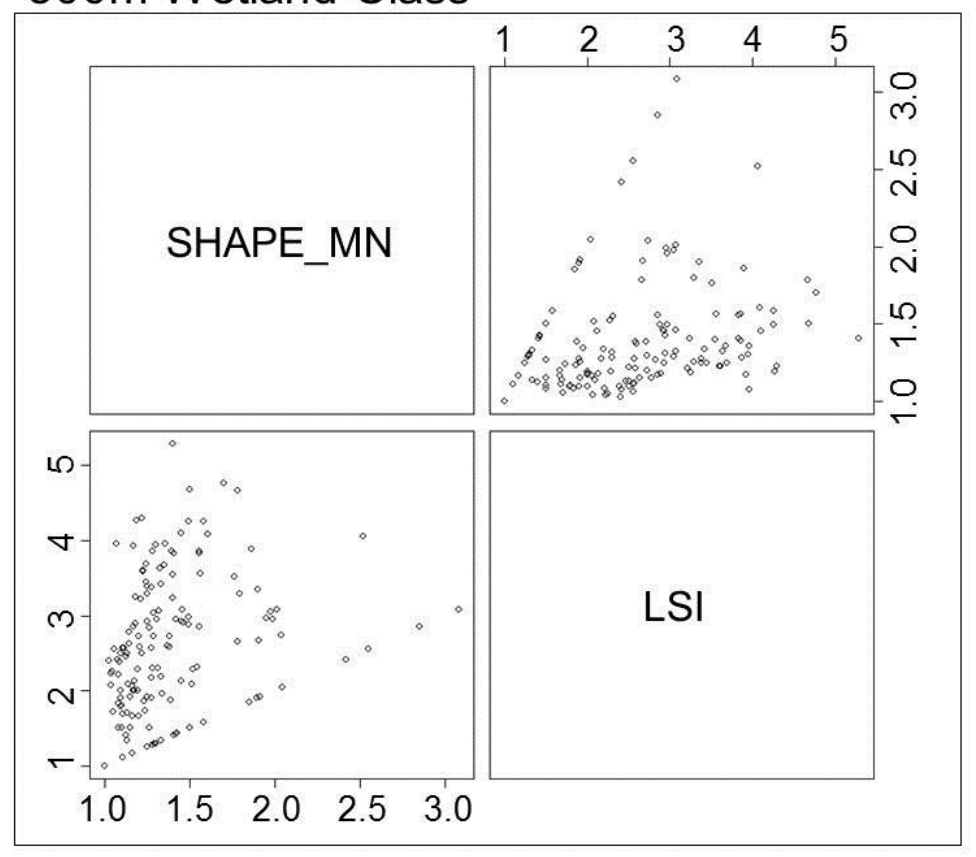


Figure B-3. 800m wetland "best model" variable scatterplot

# 800m Agriculture/Forest Class

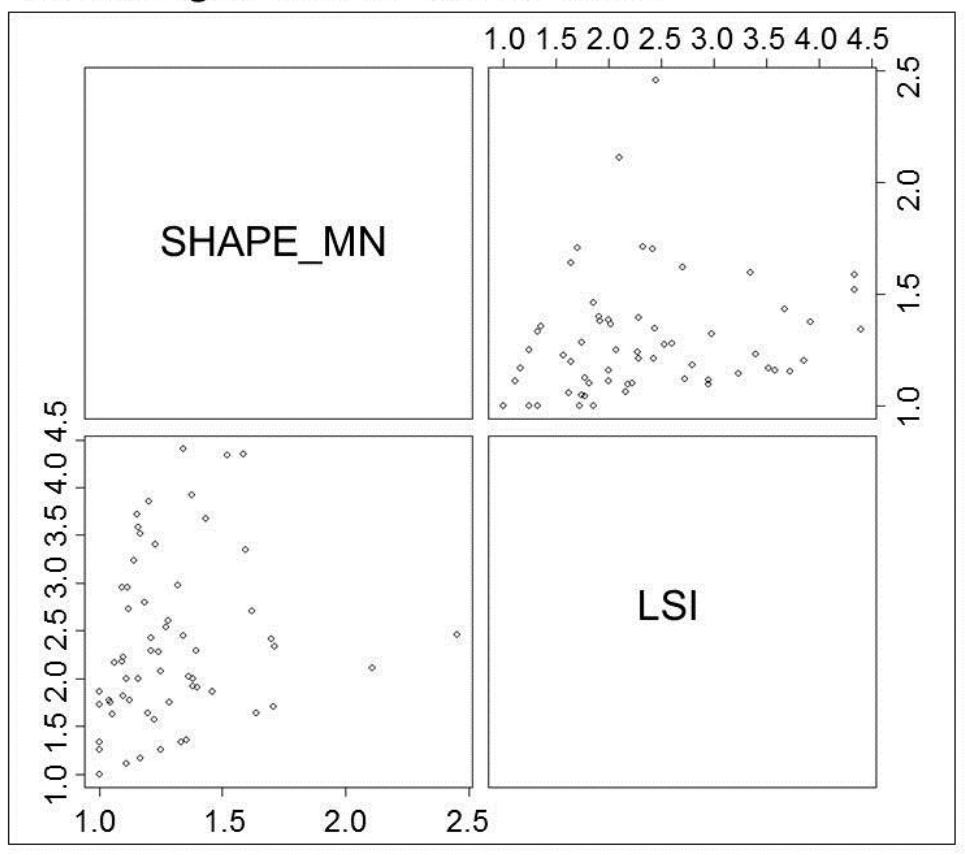


Figure B-4. 800m agriculture/forest class "best model" variable scatterplot

# 1\_2k Forest Class

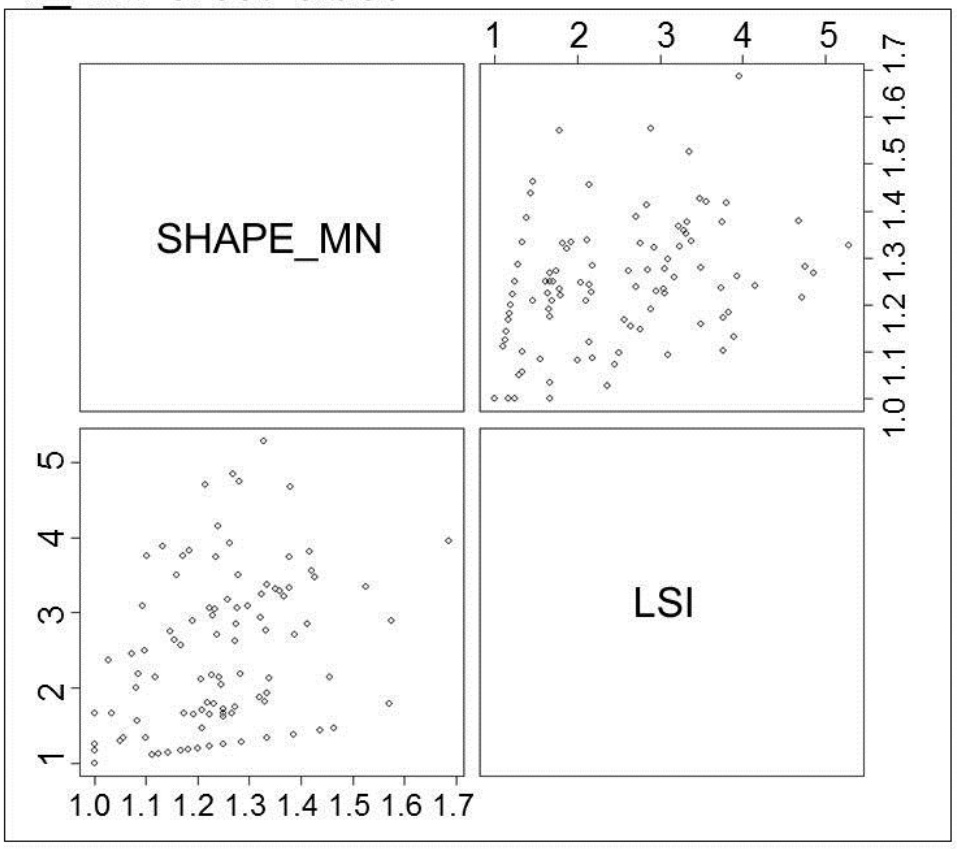


Figure B-5. 1\_2k forest class "best model" variable scatterplot

## 1\_2k Wetland Class

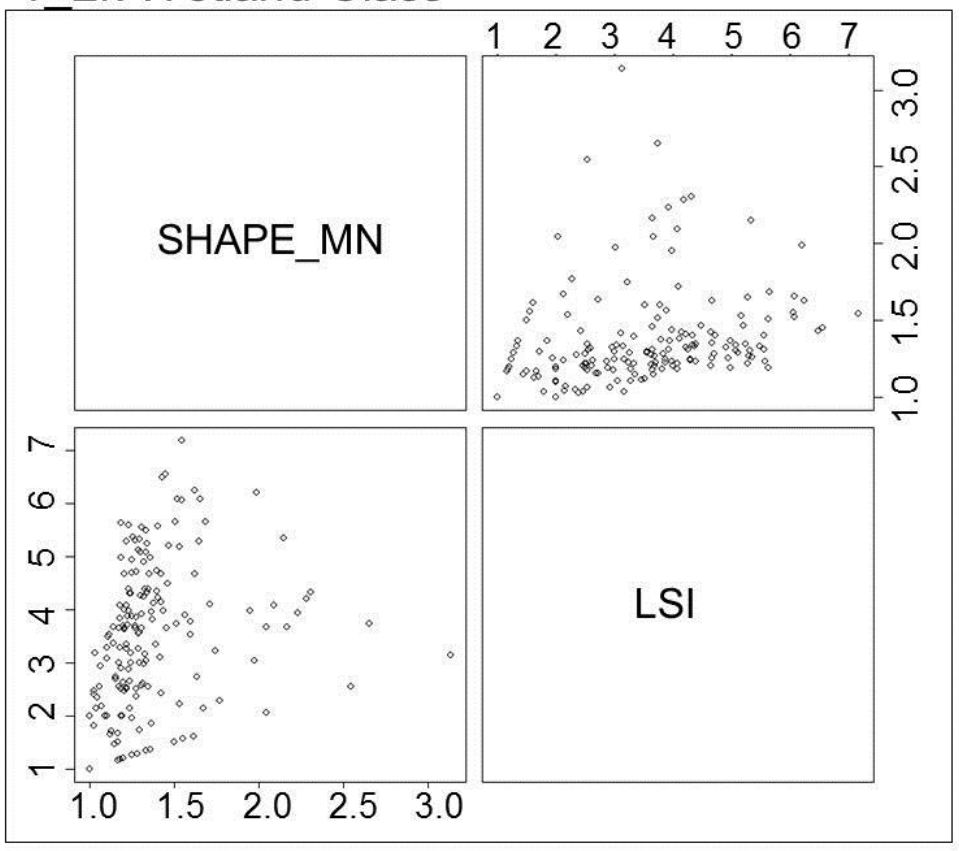


Figure B-6. 1\_2k wetland class "best model" variable scatterplot

# 

Figure B-7. 1\_2k agriculture/forest class "best model" variable scatterplot

1.8

1.2

1.4

1.6

# 1\_6k Forest Class

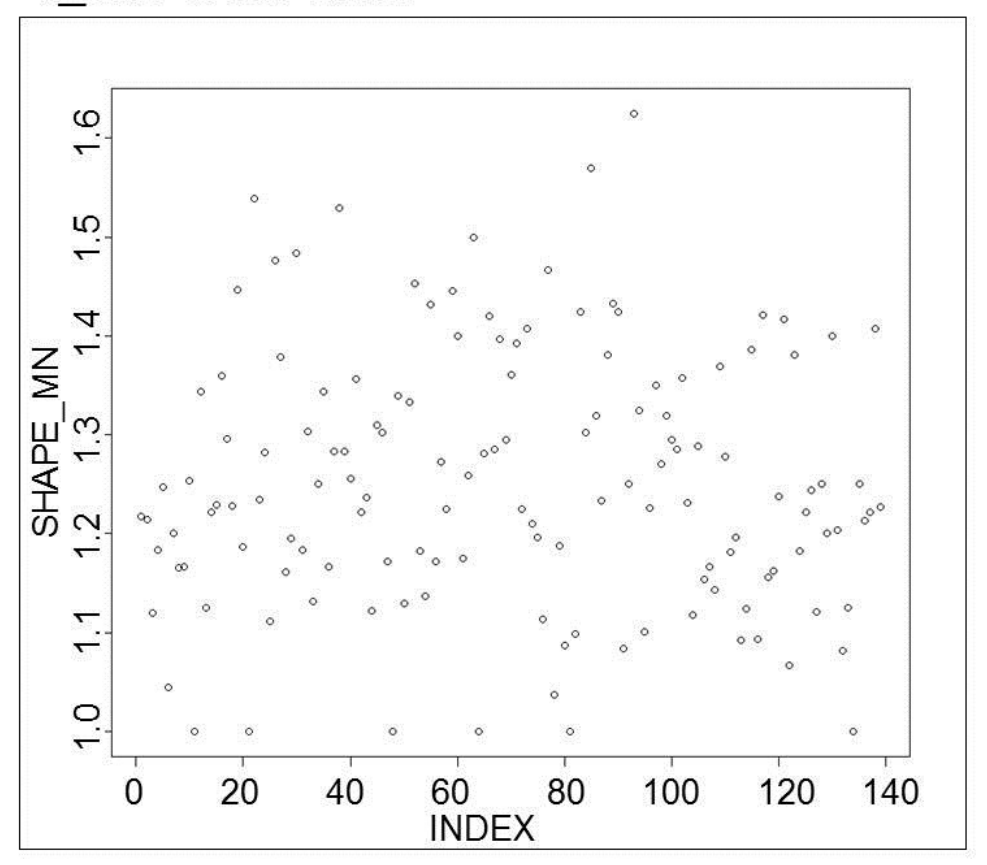


Figure B-8. 1\_6k forest class "best model" variable scatterplot

# 1\_6k Wetland Class

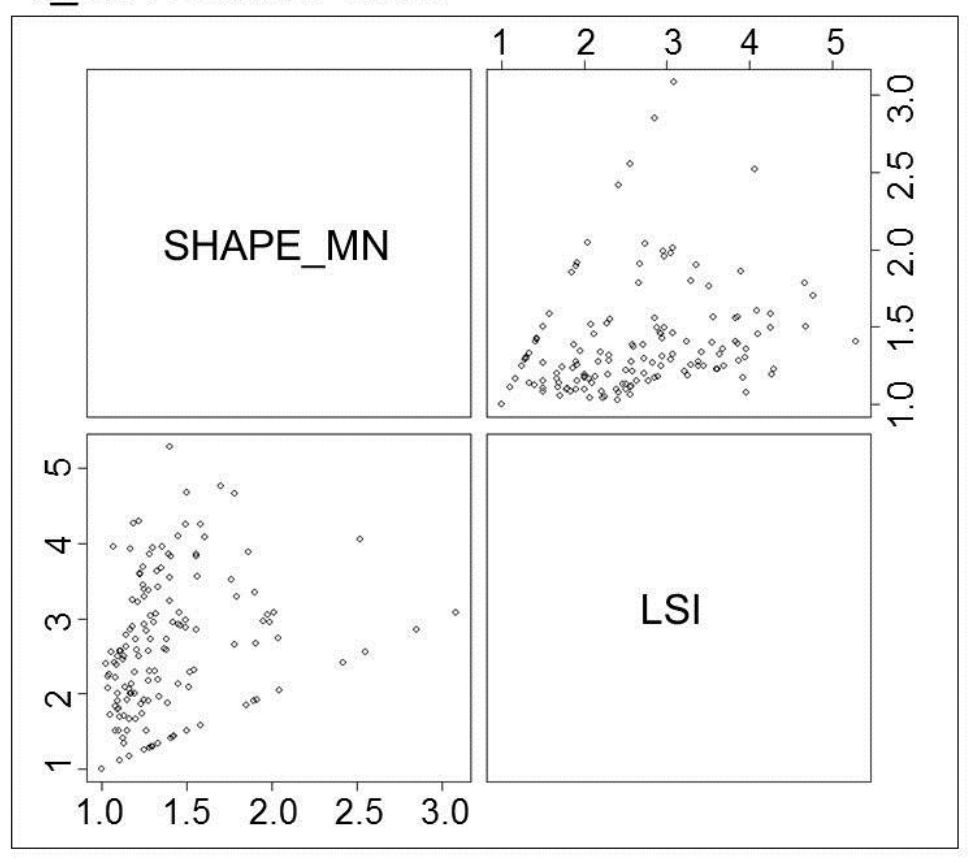


Figure B-9. 1\_6k wetland class "best model" variable scatterplot

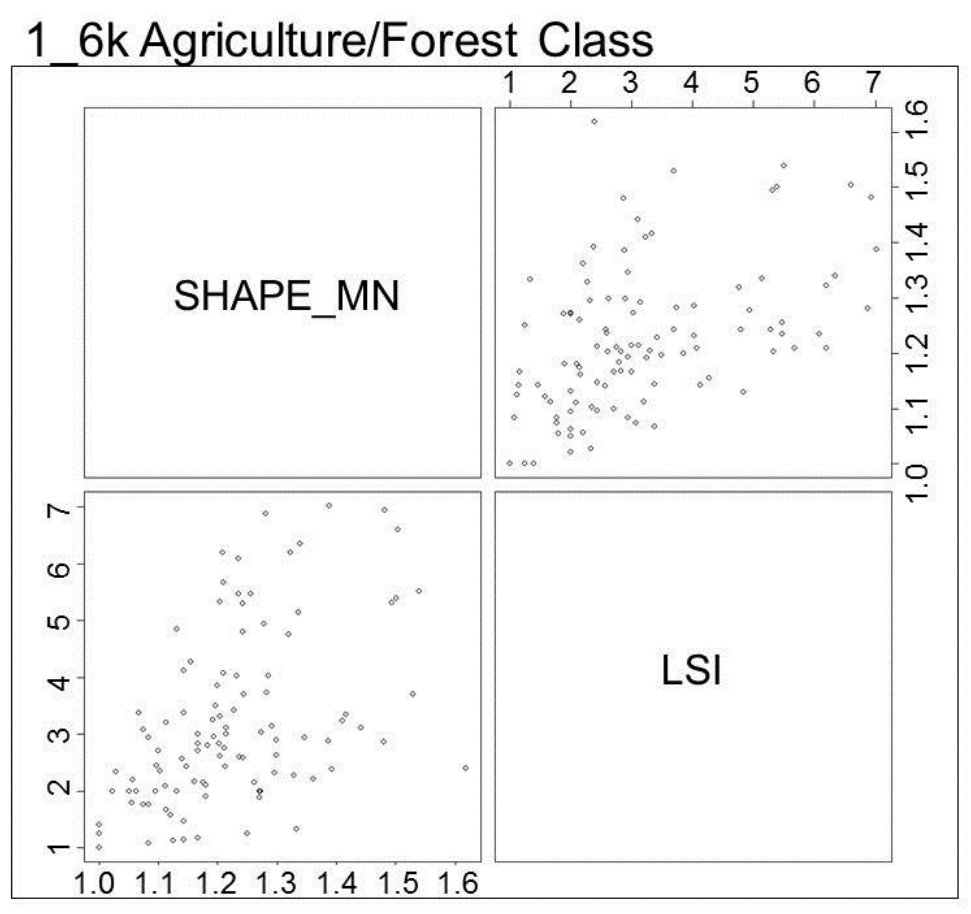


Figure B-10. 1\_6k agriculture/forest class "best model" variable scatterplot

# 2k Forest Class

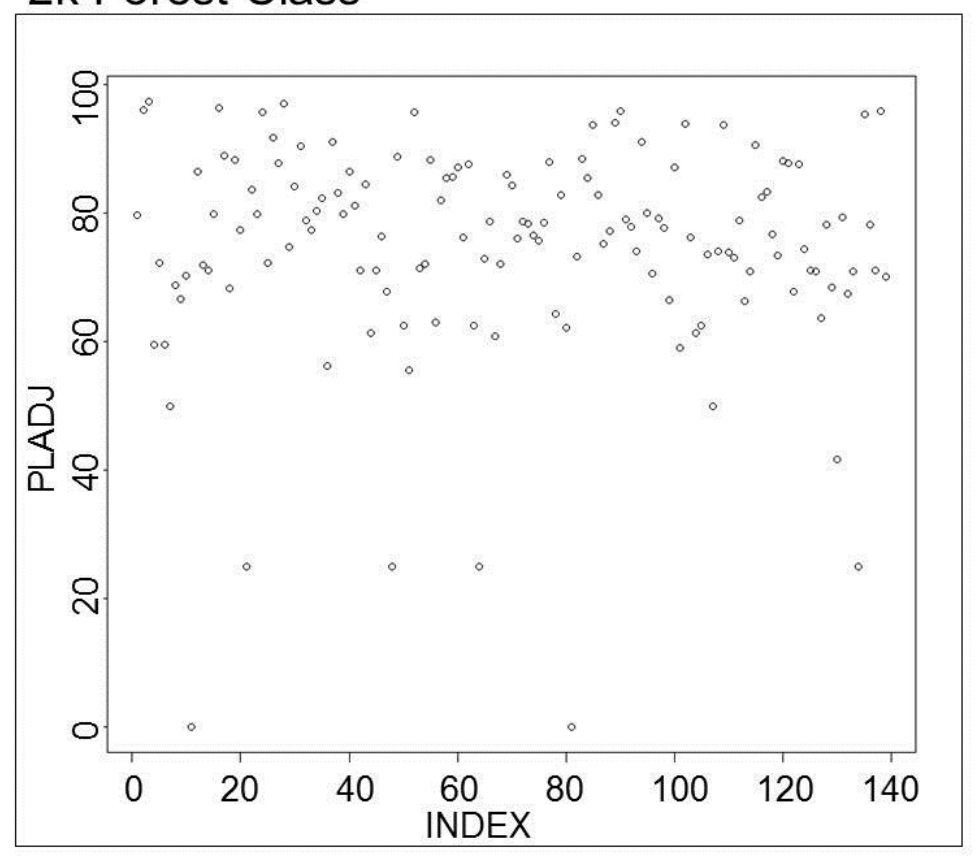


Figure B-11. 2k forest class "best model" variable scatterplot

## 2k Wetland Class

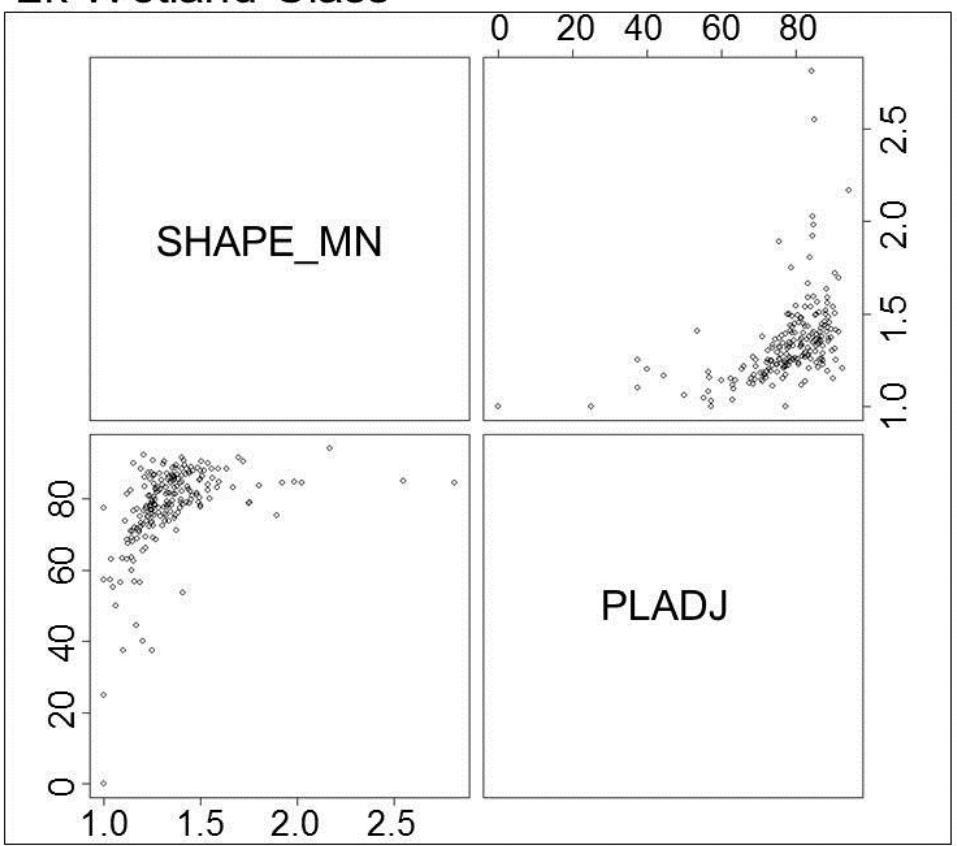


Figure B-12. 2k wetland class "best model" variable scatterplot

2k Agriculture/Forest Class

SHAPE\_MN

SHAPE\_MN

LSI

1.0 1.2 1.4 1.6

Figure B-13. 2k agriculture/forest class "best model" variable scatterplot

### Appendix C

Non-Spatial Binomial Models

Table C-1. Landscape-level non-spatial binomial GLMs

Non-Spatial Landscape-level Models												
	INTERCEPT			WIAVGG			SHAPE_MN					
Buffer		Std.				Std.				Std.		
Distance	Est.	Error	z-value	Pr(> z )	Est.	Error	z-value	Pr(> z )	Est.	Error	z-value	Pr(> z )
400m	-10.178	0.593	-17.163	< 2e-16	0.080	0.013	6.062	0.000	1.327	0.461	2.882	0.004
500m	-10.900	0.653	-16.694	< 2e-16	0.097	0.013	7.261	0.000	1.904	0.501	3.796	0.000
600m	-9.931	0.663	-14.971	< 2e-16	0.108	0.014	7.948	0.000	1.083	0.539	2.010	0.045
700m	-10.739	0.711	-15.111	< 2e-16	0.121	0.014	8.810	< 2e-16	1.603	0.564	2.844	0.004
800m	-12.630	0.770	-16.409	< 2e-16	0.127	0.014	9.267	< 2e-16	3.061	0.593	5.164	0.000
900m	-13.317	0.823	-16.182	< 2e-16	0.131	0.014	9.311	< 2e-16	3.597	0.631	5.700	0.000
1k	-12.374	0.818	-15.120	< 2e-16	0.131	0.015	8.817	< 2e-16	2.797	0.634	4.410	0.000
1_1k	-12.125	0.930	-13.040	< 2e-16	0.141	0.015	9.529	< 2e-16	2.522	0.728	3.466	0.001
1_2k	-10.845	0.933	-11.628	< 2e-16	0.151	0.015	10.079	< 2e-16	1.422	0.730	1.949	0.051
1_3k	-12.529	0.973	-12.880	< 2e-16	0.150	0.015	9.904	< 2e-16	2.724	0.761	3.577	0.000
1_4k	-11.218	1.025	-10.949	< 2e-16	0.161	0.015	10.371	< 2e-16	1.616	0.802	2.015	0.044
1_5k	-11.316	1.128	-10.032	< 2e-16	0.163	0.016	10.137	< 2e-16	1.704	0.891	1.911	0.056
1_6k	-10.841	1.214	-8.927	< 2e-16	0.168	0.016	10.219	< 2e-16	1.303	0.965	1.350	0.177
1_7k	-9.654	1.210	-7.982	0.000	0.176	0.017	10.381	< 2e-16	0.324	0.966	0.336	0.737
1_8k	-11.802	1.248	-9.454	< 2e-16	0.171	0.017	10.029	< 2e-16	2.014	0.990	2.034	0.042
1_9k	-9.983	1.300	-7.680	0.000	0.182	0.017	10.469	< 2e-16	0.538	1.040	0.517	0.605
2k	-11.231	1.347	-8.339	< 2e-16	0.181	0.018	10.346	< 2e-16	1.520	1.071	1.419	0.156

Non-Spatial Landscape-level Models										
	AIC									
		AIC								
Buffer		Std.								
Distance	Est.	Error	z-value	Pr(> z )						
400m	0.202	0.085	2.371	0.018	1872.800					
500m	0.110	0.073	1.501	0.133	1856.100					
600m	0.116	0.065	1.796	0.073	1853.400					
700m	0.109	0.057	1.900	0.057	1833.800					
800m	0.070	0.051	1.394	0.163	1805.200					
900m	0.049	0.046	1.049	0.294	1798.100					
1k	0.078	0.043	1.828	0.068	1809.300					
1_1k	0.088	0.041	2.138	0.033	1811.000					
1_2k	0.108	0.038	2.812	0.005	1812.500					
1_3k	0.093	0.037	2.535	0.011	1796.300					
1_4k	0.104	0.034	3.026	0.002	1801.600					
1_5k	0.093	0.033	2.822	0.005	1802.800					
1_6k	0.093	0.032	2.928	0.003	1806.100					
1_7k	0.097	0.030	3.209	0.001	1808.700					
1_8k	0.084	0.029	2.879	0.004	1803.500					
_ 1_9k	0.089	0.028	3.179	0.001	1806.700					
2k	0.079	0.027	2.941	0.003	1803.000					

Table C-2. Landscape-level non-spatial binomial GLMs

Non-Spatial Landscape-level Models												
	INTERCEPT				WIAVGG			SHAPE MN				
Buffer		Std.				Std.				Std.		
Distance	Est.	Error	z-value	Pr(> z )	Est.	Error	z-value	Pr(> z )	Est.	Error	z-value	Pr(> z )
400m	-10.564	0.612	-17.271	< 2e-16	0.080	0.013	5.996	0.000	1.758	0.441	3.989	0.000
500m	-11.158	0.673	-16.574	< 2e-16	0.096	0.013	7.211	0.000	2.194	0.484	4.531	0.000
600m	-10.284	0.667	-15.424	< 2e-16	0.108	0.014	7.904	0.000	1.434	0.498	2.879	0.004
700m	-11.232	0.728	-15.427	< 2e-16	0.119	0.014	8.641	8.641	2.032	0.535	3.796	0.000
800m	-13.003	0.801	-16.234	< 2e-16	0.126	0.014	9.146	9.146	3.396	0.583	5.824	0.000
900m	-13.612	0.853	-15.957	< 2e-16	0.130	0.014	9.236	9.236	3.855	0.622	6.197	0.000
1k	-12.879	0.855	-15.070	< 2e-16	0.129	0.015	8.678	8.678	3.244	0.631	5.143	0.000
1_1k	-12.735	0.952	-13.384	< 2e-16	0.140	0.015	9.430	9.430	3.093	0.708	4.371	0.000
1_2k	-11.555	0.954	-12.117	< 2e-16	0.150	0.015	9.997	9.997	2.144	0.710	3.018	0.003
1_3k	-13.263	0.999	-13.282	< 2e-16	0.149	0.015	9.811	9.811	3.409	0.746	4.570	0.000
1_4k	-12.048	1.050	-11.478	< 2e-16	0.159	0.016	10.282	10.282	2.433	0.787	3.090	0.002
1_5k	-12.166	1.138	-10.688	< 2e-16	0.161	0.016	9.994	9.994	2.535	0.863	2.936	0.003
1_6k	-11.820	1.211	-9.759	<2e-16	0.166	0.016	10.077	10.077	2.247	0.923	2.433	0.015
_ 1_7k	-10.790	1.204	-8.963	< 2e-16	0.174	0.017	10.226	10.226	1.392	0.920	1.513	0.130
1_8k	-12.940	1.256	-10.307	< 2e-16	0.169	0.017	9.899	9.899	3.035	0.954	3.182	0.001
_ 1_9k	-11.270	1.282	-8.791	< 2e-16	0.180	0.017	10.378	10.378	1.716	0.980	1.751	0.080
2k	-12.440	1.342	-9.273	< 2e-16	0.179	0.018	10.232	10.232	2.617	1.023	2.557	0.011

Non-Spatial Landscape-level Models										
	AIC									
		AIC								
Buffer		Std.								
Distance	Est.	Error	z-value	Pr(> z )						
400m	0.023	0.008	2.959	0.003	1869.800					
500m	0.010	0.006	1.619	0.105	1855.700					
600m	0.010	0.005	2.250	0.024	1851.700					
700m	0.010	0.004	2.693	0.007	1830.200					
800m	0.005	0.003	1.733	0.083	1804.100					
900m	0.003	0.003	1.300	0.194	1797.500					
1k	0.005	0.002	2.234	0.026	1807.700					
1_1k	0.004	0.002	2.260	0.024	1810.500					
1_2k	0.004	0.002	2.464	0.014	1814.500					
1_3k	0.004	0.001	2.665	0.008	1795.700					
1_4k	0.003	0.001	2.777	0.005	1803.100					
1_5k	0.003	0.001	2.548	0.011	1804.400					
1_6k	0.003	0.001	2.605	0.009	1808.000					
1_7k	0.003	0.001	3.001	0.003	1810.100					
1 8k	0.002	0.001	3.039	0.002	1802.700					
_ 1_9k	0.002	0.001	2.992	0.003	1807.900					
$\overline{2k}$	0.002	0.001	2.861	0.004	1803.500					
	1				ı					

Table C-3. Landscape-level non-spatial binomial GLMs

				Non-S <sub>1</sub>	patial Lai	ndscape-	level Mod	lels				
		INTE	RCEPT			WL	AVGG			SHA	PE_MN	
Buffer		Std.				Std.				Std.		
Distance	Est.	Error	z-value	Pr(> z )	Est.	Error	z-value	Pr(> z )	Est.	Error	z-value	Pr(> z )
400m	-7.749	1.143	-6.780	0.000	0.080	0.013	6.061	0.000	1.313	0.461	2.847	0.004
500m	-9.313	1.237	-7.529	0.000	0.097	0.013	7.272	0.000	1.892	0.503	3.759	0.000
600m	-7.821	1.363	-5.738	0.000	0.109	0.014	7.959	0.000	1.052	0.541	1.944	0.052
700m	-8.578	1.394	-6.152	0.000	0.121	0.014	8.818	< 2e-16	1.597	0.564	2.830	0.005
800m	-11.026	1.382	-7.978	0.000	0.127	0.014	9.269	< 2e-16	3.058	0.593	5.158	0.000
900m	-12.082	1.437	-8.406	< 2e-16	0.131	0.014	9.314	< 2e-16	3.596	0.631	5.696	0.000
1k	-10.212	1.439	-7.095	0.000	0.131	0.015	8.822	< 2e-16	2.800	0.634	4.416	0.000
1_1k	-9.434	1.619	-5.828	0.000	0.141	0.015	9.536	< 2e-16	2.521	0.728	3.463	0.001
1_2k	-7.307	1.627	-4.492	0.000	0.151	0.015	10.087	< 2e-16	1.427	0.730	1.955	0.051
1_3k	-9.222	1.683	-5.479	0.000	0.150	0.015	9.909	< 2e-16	2.731	0.761	3.588	0.000
1_4k	-7.270	1.716	-4.236	0.000	0.161	0.015	10.374	< 2e-16	1.632	0.801	2.038	0.042
1_5k	-7.540	1.844	-4.089	0.000	0.163	0.016	10.134	< 2e-16	1.728	0.889	1.944	0.052
1_6k	-6.904	1.963	-3.517	0.000	0.168	0.016	10.214	< 2e-16	1.346	0.962	1.400	0.161
1_7k	-5.251	1.993	-2.635	0.008	0.176	0.017	10.376	< 2e-16	0.371	0.962	0.386	0.699
1_8k	-7.762	2.035	-3.813	0.000	0.171	0.017	10.026	< 2e-16	2.051	0.988	2.076	0.038
_ 1_9k	-5.450	2.134	-2.554	0.011	0.182	0.017	10.464	< 2e-16	0.589	1.036	0.569	0.570
2k	-7.038	2.146	-3.279	0.001	0.181	0.018	10.340	< 2e-16	1.567	1.067	1.468	0.142

	Non-Spat	ial Lands	scape-leve	l Models	
		PLA	ADJ		AIC
Buffer		Std.			
Distance	Est.	Error	z-value	Pr(> z )	
400m	-0.023	0.009	-2.484	0.013	1872.300
500m	-0.015	0.010	-1.510	0.131	1856.000
600m	-0.020	0.011	-1.899	0.058	1853.000
700m	-0.021	0.011	-1.913	0.056	1833.800
800m	-0.016	0.011	-1.412	0.158	1805.100
900m	-0.012	0.011	-1.057	0.290	1798.000
1k	-0.021	0.012	-1.806	0.071	1809.400
1_1k	-0.026	0.012	-2.134	0.033	1811.000
1_2k	-0.035	0.013	-2.757	0.006	1812.800
1_3k	-0.033	0.013	-2.483	0.013	1796.600
1_4k	-0.039	0.013	-2.944	0.003	1802.000
1_5k	-0.038	0.014	-2.766	0.006	1803.100
1_6k	-0.039	0.014	-2.830	0.005	1806.700
1_7k	-0.044	0.014	-3.119	0.002	1809.300
1_8k	-0.040	0.014	-2.787	0.005	1804.100
1_9k	-0.045	0.015	-3.102	0.002	1807.200
2k	-0.042	0.015	-2.852	0.004	1803.500

Table C-4. Landscape-level non-spatial binomial GLMs

				Non-Sp	atial La	ndscape-	level Mod	lels				
		INTE	RCEPT			WI	AVGG			SHA	PE_MN	
Buffer		Std.				Std.				Std.		
Distance	Est.	Error	z-value	Pr(> z )	Est.	Error	z-value	Pr(> z )	Est.	Error	z-value	Pr(> z )
400m	-10.124	0.586	-17.269	< 2e-16	0.081	0.014	5.963	0.000	1.570	0.449	3.499	0.000
500m	-10.818	0.653	-16.575	< 2e-16	0.094	0.014	6.897	0.000	1.936	0.495	3.914	0.000
600m	-9.764	0.676	-14.441	< 2e-16	0.103	0.014	7.479	0.000	1.002	0.535	1.874	0.061
700m	-10.619	0.716	-14.822	< 2e-16	0.114	0.014	8.186	0.000	1.542	0.555	2.778	0.005
800m	-12.503	0.783	-15.974	< 2e-16	0.121	0.014	8.621	< 2e-16	2.953	0.600	4.925	0.000
900m	-13.228	0.844	-15.670	< 2e-16	0.124	0.015	8.551	< 2e-16	3.457	0.643	5.377	0.000
1k	-12.197	0.833	-14.643	< 2e-16	0.123	0.015	8.076	0.000	2.627	0.646	4.067	0.000
1_1k	-11.894	0.954	-12.461	< 2e-16	0.131	0.015	8.560	< 2e-16	2.316	0.742	3.120	0.002
1_2k	-10.612	0.953	-11.132	< 2e-16	0.140	0.015	9.030	< 2e-16	1.267	0.743	1.705	0.088
1_3k	-12.381	0.986	-12.562	< 2e-16	0.141	0.016	9.016	< 2e-16	2.654	0.768	3.455	0.001
1_4k	-10.970	1.033	-10.618	<2e-16	0.150	0.016	9.387	<2e-16	1.494	0.809	1.848	0.065
1_5k	-11.042	1.137	-9.707	< 2e-16	0.153	0.017	9.234	< 2e-16	1.541	0.897	1.719	0.086
1_6k	-10.634	1.232	-8.630	< 2e-16	0.156	0.017	9.202	< 2e-16	1.192	0.972	1.226	0.220
1_7k	-9.443	1.227	-7.697	0.000	0.161	0.017	9.230	< 2e-16	0.203	0.970	0.209	0.834
1_8k	-11.497	1.267	-9.073	< 2e-16	0.157	0.018	8.979	< 2e-16	1.815	1.001	1.814	0.070
1_9k	-9.576	1.327	-7.219	0.000	0.166	0.018	9.238	< 2e-16	0.252	1.054	0.239	0.811
2k	-10.797	1.370	-7.879	0.000	0.166	0.018	9.143	< 2e-16	1.206	1.086	1.110	0.267

	Non-Spat	ial I ands	scape-leve	l Models	
	rvon-spat	SH		1 1/104615	AIC
		эп	DI		AIC
Buffer		Std.			
Distance	Est.	Error	z-value	Pr(> z )	
400m	0.105	0.135	0.776	0.437	1877.900
500m	0.197	0.136	1.450	0.147	1856.200
600m	0.333	0.140	2.381	0.017	1850.900
700m	0.368	0.142	2.594	0.009	1830.600
800m	0.309	0.143	2.161	0.031	1802.400
900m	0.329	0.145	2.271	0.023	1793.900
1k	0.421	0.147	2.858	0.004	1804.300
1_1k	0.488	0.150	3.249	0.001	1804.800
1_2k	0.538	0.150	3.590	0.000	1807.300
1_3k	0.456	0.152	3.003	0.003	1793.600
1_4k	0.514	0.152	3.389	0.001	1799.100
1_5k	0.502	0.155	3.250	0.001	1800.100
1_6k	0.533	0.157	3.399	0.001	1802.900
1_7k	0.605	0.159	3.801	0.000	1804.200
1_8k	0.548	0.164	3.343	0.001	1800.500
1_9k	0.632	0.167	3.779	0.000	1802.200
2k	0.589	0.169	3.496	0.000	1799.200

Table C-5. Landscape-level non-spatial binomial GLMs

				Non-Sp	oatial La	ndscape-	level Mod	dels				
		INTE	RCEPT			WI	AVGG			SHA	PE_MN	
Buffer		Std.				Std.				Std.		
Distance	Est.	Error	z-value	Pr(> z )	Est.	Error	z-value	Pr(> z )	Est.	Error	z-value	Pr(> z )
400m	-9.975	0.595	-16.762	< 2e-16	0.084	0.013	6.358	0.000	1.663	0.421	3.953	0.000
500m	-10.624	0.650	-16.353	< 2e-16	0.100	0.013	7.517	0.000	2.091	0.462	4.522	0.000
600m	-10.024	0.663	-15.109	< 2e-16	0.108	0.014	7.859	0.000	1.453	0.480	3.026	0.002
700m	-10.919	0.734	-14.885	< 2e-16	0.120	0.014	8.579	< 2e-16	1.982	0.516	3.837	0.000
800m	-12.617	0.801	-15.748	< 2e-16	0.128	0.014	8.958	< 2e-16	3.252	0.569	5.715	0.000
900m	-13.495	0.890	-15.161	< 2e-16	0.129	0.015	8.731	< 2e-16	3.812	0.624	6.105	0.000
1k	-13.211	0.865	-15.280	< 2e-16	0.117	0.016	7.355	0.000	3.326	0.625	5.323	0.000
1_1k	-13.431	0.985	-13.629	< 2e-16	0.119	0.016	7.388	0.000	3.317	0.717	4.624	0.000
1_2k	-12.599	0.988	-12.748	< 2e-16	0.120	0.017	7.275	0.000	2.486	0.721	3.450	0.001
1_3k	-13.995	1.009	-13.871	< 2e-16	0.116	0.017	6.756	0.000	3.584	0.743	4.824	0.000
1_4k	-12.449	1.051	-11.848	< 2e-16	0.134	0.017	7.727	0.000	2.457	0.779	3.157	0.002
1_5k	-13.048	1.162	-11.227	< 2e-16	0.122	0.019	6.561	0.000	2.720	0.869	3.130	0.002
1_6k	-12.760	1.238	-10.307	< 2e-16	0.121	0.019	6.415	0.000	2.343	0.933	2.510	0.012
1_7k	-11.471	1.224	-9.371	< 2e-16	0.129	0.020	6.542	0.000	1.379	0.926	1.489	0.137
1_8k	-13.687	1.272	-10.759	< 2e-16	0.118	0.020	5.911	0.000	2.984	0.958	3.113	0.002
1_9k	-11.825	1.287	-9.188	< 2e-16	0.137	0.020	6.858	0.000	1.663	0.977	1.703	0.089
2k	-12.979	1.349	<b>-</b> 9.619	< 2e-16	0.136	0.021	6.615	0.000	2.606	1.020	2.555	0.011

	Non-Spat	ial Lands	scape-leve	l Models	
		PR	2D		AIC
Buffer		Std.			
Distance	Est.	Error	z-value	Pr(> z )	
400m	-0.032	0.026	-1.247	0.212	1876.900
500m	-0.062	0.039	-1.587	0.113	1855.800
600m	-0.019	0.056	-0.337	0.736	1856.600
700m	0.013	0.080	0.160	0.873	1837.400
800m	-0.012	0.099	-0.120	0.905	1807.100
900m	0.059	0.128	0.458	0.647	1799.000
1k	0.424	0.151	2.801	0.005	1804.700
1_1k	0.706	0.190	3.714	0.000	1801.500
1_2k	1.109	0.225	4.926	0.000	1795.800
1_3k	1.244	0.272	4.573	0.000	1781.500
1_4k	1.181	0.322	3.669	0.000	1797.100
1_5k	1.853	0.389	4.763	0.000	1787.800
1_6k	2.464	0.456	5.409	0.000	1784.900
1_7k	2.608	0.525	4.966	0.000	1793.900
1_8k	3.252	0.595	5.471	0.000	1781.700
1_9k	3.019	0.644	4.688	0.000	1794.900
2k	3.082	0.715	4.313	0.000	1793.200

Table C-6. 800m forest class non-spatial binomial GLMs

					80	00m Forest	Class					
				High	Leverage	e Points: 1,	3,5,6,31,34,6	64,76				
	INTE	RCEPT			SHA	APE MN			CLU	MPY		
	Std.				Std.	<u></u>			Std.			
Est.	Error	z-value	Pr(> z )	Est.	Error	z-value	Pr(> z )	Est.	Error	z-value	Pr(> z )	AIC
-11.736	0.733	-16.010	< 2e-16	2.157	0.384	5.626	0.000	2.302	0.806	2.857	0.004	421.46
							1					
	INTE	RCEPT			SHA	APE_MN			L	SI		
	Std.				Std.				Std.			
Est.	Error	z-value	Pr(> z )	Est.	Error	z-value	Pr(> z )	Est.	Error	z-value	Pr(> z )	AIC
-10.078	0.489	-20.612	< 2e-16	2.687	0.355	7.565	0.000	-0.199	0.123	-1.613	0.107	427.66
	INTE	RCEPT			SHA	APE_MN			A	I		
	Std.				Std.				Std.			
Est.	Error	z-value	Pr(> z )	Est.	Error	z-value	Pr(> z )	Est.	Error	z-value	Pr(> z )	AIC
-11.644	0.721	-16.157	< 2e-16	2.137	0.388	5.501	0.000	0.022	0.008	2.746	0.006	422.14
	INTE	RCEPT			SHA	APE_MN			PLA	ADJ		
	Std.				Std.				Std.			
Est.	Error	z-value	Pr(> z )	Est.	Error	z-value	Pr(> z )	Est.	Error	z-value	Pr(> z )	AIC
-												
10.803	0.562	-19.228	< 2e-16	1.533	0.470	3.261	0.001	0.025	0.007	3.831	0.000	413.67

Table C-7. 800m wetland class non-spatial binomial GLMs

					800r	n Wetland	Class					
			High	Leverag	ge Points: 9	9,36,47,52,7	71,112,114	4,123,128,	,152			
	INTER	СЕРТ			SHA	PE_MN			CLU	MPY		
	Std.				Std.				Std.			
Est.	Error	z-value	<b>Pr(&gt;</b>  z )	Est.	Error	z-value	Pr(> z )	Est.	Error	z-value	Pr(> z )	AIC
-9.524	0.551	-17.302	< 2e-16	0.885	0.185	4.800	0.000	1.204	0.671	1.793	0.073	1049.1
	INTER	CEPT			SHA	PE_MN			L	SI		
	Std.				Std.				Std.			
Est.	Error	z-value	<b>Pr(&gt;</b>  z )	Est.	Error	z-value	Pr(> z )	Est.	Error	z-value	Pr(> z )	AIC
-8.382	0.258	-32.467	< 2e-16	1.158	0.177	6.557	0.000	-0.213	0.071	-2.997	0.003	1044.5
	INTER	CEPT			SHA	PE_MN			A	ΑI		
	Std.				Std.				Std.			
Est.	Error	z-value	<b>Pr(&gt;</b>  z )	Est.	Error	z-value	Pr(> z )	Est.	Error	z-value	Pr(> z )	AIC
-9.211	0.533	-17.279	< 2e-16	0.908	0.187	4.843	0.000	0.008	0.007	1.171	0.241	1052.3
	INTER	CEPT			SHA	PE_MN			PL	ADJ		
	Std.				Std.				Std.			
Est.	Error	z-value	Pr(> z )	Est.	Error	z-value	Pr(> z )	Est.	Error	z-value	Pr(> z )	AIC
-8.866	0.336	-26.359	< 2e-16	0.894	0.202	4.435	0.000	0.004	0.005	0.914	0.361	1053

Table C-8. 800m agriculture/forest class non-spatial binomial GLMs

					800m Agri	culture/Fo	rest Class					
				I	High Lever	age Points	s: 19,59,62	2				
	INTER	СЕРТ			SHAP	E_MN			CLUI	MPY		
	Std.				Std.				Std.			
Est.	Error	z-value	Pr(> z )	Est.	Error	z-value	Pr(> z )	Est.	Error	z-value	Pr(> z )	AIC
-8.889	0.490	-18.133	< 2e-16	1.456	0.378	3.856	0.000	-0.127	0.381	-0.333	0.739	460.12
	INTER	CEPT			SHAP	E_MN			LS	SI		
	Std.				Std.				Std.			
Est.	Error	z-value	Pr(> z )	Est.	Error	z-value	Pr(> z )	Est.	Error	z-value	Pr(> z )	AIC
-7.750	0.453	-17.096	< 2e-16	1.826	0.320	5.703	0.000	-0.760	0.133	-5.717	0.000	423.04
	INTER	CEPT			SHAP	E_MN			A	I		
	Std.				Std.				Std.			
Est.	Error	z-value	Pr(> z )	Est.	Error	z-value	Pr(> z )	Est.	Error	z-value	Pr(> z )	AIC
-8.713	0.519	-16.790	< 2e-16	1.568	0.393	3.992	0.000	-0.005	0.006	-0.892	0.372	459.5
	INTER	CEPT			SHAP	E_MN			PLA	ΔDJ		
	Std.				Std.	<del></del>			Std.			
Est.	Error	z-value	Pr(> z )	Est.	Error	z-value	Pr(> z )	Est.	Error	z-value	Pr(> z )	AIC
-8.740	0.421	-20.752	< 2e-16	2.143	0.397	5.403	0.000	-0.016	0.005	-3.164	0.002	451.87

Table C-9. 1\_2k forest class non-spatial binomial GLMs

					1_2k	Forest Cl	ass					
				High	Leverag	ge Points: 6	6,26,45,10	)2				
	INTER	RCEPT			SHAP	E_MN			CLU	MPY		
	Std.				Std.				Std.			
Est.	Error	z-value	Pr(> z )	Est.	Error	z-value	Pr(> z )	Est.	Error	z-value	Pr(> z )	AIC
-9.734	0.720	-13.527	< 2e-16	0.787	0.544	1.447	0.148	2.139	0.662	3.230	0.001	796.43
				Hig	h Levera	ge Points:	26,45,102	2				
	INTER	RCEPT			SHAP	E_MN			L	SI		
	Std.				Std.				Std.			
Est.	Error	z-value	Pr(> z )	Est.	Error	z-value	Pr(> z )	Est.	Error	z-value	Pr(> z )	AIC
-10.022	0.595	-16.836	< 2e-16	3.258	0.506	6.442	0.000	-0.452	0.070	-6.480	0.000	773.27
				High	Leverag	ge Points: 6	5,26,45,10	2				
	INTER	RCEPT			SHAP	E_MN			A	ΑI		
	Std.				Std.				Std.			
Est.	Error	z-value	Pr(> z )	Est.	Error	z-value	Pr(> z )	Est.	Error	z-value	Pr(> z )	AIC
-9.586	0.706	-13.569	< 2e-16	0.798	0.551	1.448	0.148	0.019	0.007	2.937	0.003	798.3
				High l	Leverage	Points: 6,	26,45,85,1	102				
	INTER	RCEPT			SHAP	E_MN			PL	ADJ		
	Std.				Std.				Std.			
Est.	Error	z-value	Pr(> z )	Est.	Error	z-value	Pr(> z )	Est.	Error	z-value	Pr(> z )	AIC
-9.413	0.668	-14.082	< 2e-16	2.126	0.655	3.248	0.001	-0.004	0.005	-0.851	0.395	777.71

Table C-10. 1\_2k wetland class non-spatial binomial GLMs

					1_2k	Wetland (	Class					
	INTER	CEPT			SHAP	E_MN			CLUI	MPY		
	Std.				Std.				Std.			
Est.	Error	z-value	Pr(> z )	Est.	Error	z-value	Pr(> z )	Est.	Error	z-value	Pr(> z )	AIC
-8.485	0.429	-19.772	< 2e-16	0.498	0.180	2.775	0.006	0.642	0.514	1.251	0.211	1240.8
	INTER	CEPT			SHAP	E_MN			LS	SI		
	Std.				Std.				Std.			
Est.	Error	z-value	Pr(> z )	Est.	Error	z-value	Pr(> z )	Est.	Error	z-value	Pr(> z )	AIC
-7.386	0.236	-31.359	< 2e-16	0.852	0.159	5.351	0.000	-0.311	0.044	-7.040	0.000	1190.4
	INTER	CEPT			SHAP	E MN			PLA	DJ		
	Std.				Std.	_			Std.			
Est.	Error	z-value	Pr(> z )	Est.	Error	z-value	Pr(> z )	Est.	Error	z-value	Pr(> z )	AIC
-7.532	0.298	-25.245	< 2e-16	0.761	0.181	4.204	0.000	-0.011	0.004	-2.692	0.007	1236.1

Table C-11. 1\_2k agriculture/forest class non-spatial binomial GLMs

				1	2k Agric	culture/For	ect Clace					
				_		ge Points: 2		13				
	INTER	CEDT		11151		PE MN	21,27,73,0	,,,	CLU	MDV		
	Std.	CEFI			Std.	LL_IVIIN			Std.	IVII I		
Est.	Error	z-value	Pr(> z )	Est.	Error	z-value	Pr(> z )	Est.	Error	z-value	Pr(> z )	AIC
-11.687	0.757	-15.450	< 2e-16	1.305	0.458	2.847	0.004	3.929	0.638	6.163	0.000	672.61
11.007	0.707	1000	20 10			age Points			0.020	0.102	0.000	0,2.01
	INTER	СЕРТ		1112		PE MN	. 21,75,05		1 (	SI		
	Std.	CLII			Std.	L_IVIIN			Std.	31		
Est.	Error	z-value	Pr(> z )	Est.	Error	z-value	Pr(> z )	Est.	Error	z-value	Pr(> z )	AIC
-9.196	0.555	-16.576	< 2e-16	2.651	0.457	5.806	0.000	-0.374	0.055	-6.848	0.000	691.12
7.170	0.000	10.070	20 10			ge Points: 2			0.022	0.010	0.000	071.12
	INTER	CEDT		11151		PE MN	21,27,73,0	,,	A	Ţ		
	Std.	CLII			Std.	L_IVIIN			Std.	11		
Est.	Error	z-value	Pr(> z )	Est.	Error	z-value	Pr(> z )	Est.	Error	z-value	Pr(> z )	AIC
-11.561	0.735	-15.720	< 2e-16	1.208	0.460	2.626	0.009	0.039	0.006	6.186	0.000	675.41
						Points: 21						
	INTER	CFPT		1118111		PE MN	,_,,,,,,,,,,,,,,,,,,,,,,,,,,,,,,,,,,,,,	,02	PLA	ADI		
	Std.	CLI I			Std.	L_IVIIV			Std.	1103		
Est.	Error	z-value	Pr(> z )	Est.	Error	z-value	Pr(> z )	Est.	Error	z-value	Pr(> z )	AIC
-9.146	0.593	-15.425	<2e-16	1.564	0.573	2.732	0.006	0.006	0.004	1.445	0.149	688.36

Table C-12. 1\_6k forest class non-spatial binomial GLMs

					1_61	Forest C	lass					
				High I	Leverage	Points: 29	,36,50,97	,101				
	INTER	CEPT			SHAP	E_MN			CLUI	MPY		
	Std.				Std.				Std.			
Est.	Error	z-value	Pr(> z )	Est.	Error	z-value	Pr(> z )	Est.	Error	z-value	Pr(> z )	AIC
-9.228	0.580	-15.919	< 2e-16	1.335	0.499	2.677	0.007	0.428	0.369	1.159	0.247	949.23
	INTERCEPT				SHAP	E_MN			LS	SI		
Std.					Std.				Std.			
Est.	Error	z-value	Pr(> z )	Est.	Error	z-value	Pr(> z )	Est.	Error	z-value	Pr(> z )	AIC
-9.161	0.557	-16.436	< 2e-16	1.702	0.443	3.840	0.000	-0.068	0.046	-1.478	0.140	948.4
	INTER	CEPT		SHAPE_MN			AI					
	Std.				Std.				Std.			
Est.	Error	z-value	Pr(> z )	Est.	Error	z-value	Pr(> z )	Est.	Error	z-value	Pr(> z )	AIC
-9.220	0.579	-15.930	< 2e-16	1.348	0.500	2.695	0.007	0.004	0.004	1.081	0.280	949.42
	INTER	CEPT			SHAP	E_MN			PLA	ADJ		
	Std.				Std.				Std.			
Est.	Error	z-value	Pr(> z )	Est.	Error	z-value	Pr(> z )	Est.	Error	z-value	Pr(> z )	AIC
-9.142	0.583	-15.684	< 2e-16	1.351	0.513	2.633	0.008	0.003	0.003	0.990	0.322	949.62
	INTER	CEPT			SHAP	E_MN						
	Std.				Std.							
Est.	Error	z-value	Pr(> z )	Est.	Error	z-value	Pr(> z )					AIC
-9.142	0.583	-15.684	< 2e-16	1.351	0.513	2.633	0.008					949.62

Table C-13. 1\_6k wetland class non-spatial binomial GLMs

					1_6k W	Vetland Cl	ass					
	INTER	CEPT			SHAPE	E_MN			CLUN	MPY		
	Std.				Std.	_		Std.				
Est.	Error	z-value	Pr(> z )	Est.	Error	z-value	Pr(> z )	Est.	Error	z-value	Pr(> z )	AIC
-7.784	0.331	-23.524	< 2e-16	0.463	0.160	2.889	0.004	-0.218	0.351	-0.620	0.535	1412.8
	INTER	CEPT			SHAPE	E_MN			LS	SI		
	Std.				Std.				Std.			
Est.	Error	z-value	Pr(> z )	Est.	Error	z-value	Pr(> z )	Est.	Error	z-value	Pr(> z )	AIC
-7.697	0.208	-36.957	< 2e-16	0.681	0.151	4.500	0.000	-0.140	0.029	-4.852	0.000	1388.9
	INTER	CEPT			SHAPE	E_MN			A	I		
	Std.				Std.				Std.			
Est.	Error	z-value	Pr(> z )	Est.	Error	z-value	Pr(> z )	Est.	Error	z-value	Pr(> z )	AIC
-7.421	0.392	-18.955	< 2e-16	0.505	0.161	3.142	0.002	-0.007	0.005	-1.556	0.120	1410.9
	INTER	CEPT			SHAPE	E_MN			PLA	DJ		
	Std.	Z-			Std.				Std.			
Est.	Error	value	Pr(> z )	Est.	Error	z-value	Pr(> z )	Est.	Error	z-value	Pr(> z )	AIC
-7.004	0.266	-26.288	< 2e-16	0.738	0.157	4.689	0.000	-0.018	0.004	-5.008	0.000	1392.3

Table C-14. 1\_6k agriculture/forest class non-spatial binomial GLMs

				1	l_6k Agri	culture/Fo	rest Class					
				High L	everage P	oints: 24,3	32,68,85,9	4,101				
	INTER	CEPT			SHAP	E_MN			CLUI	MPY		
	Std.				Std.				Std.			
Est.	Error	z-value	Pr(> z )	Est.	Error	z-value	Pr(> z )	Est.	Error	z-value	Pr(> z )	AIC
-8.669	0.690	-12.563	<2e-16	0.854	0.532	1.605	0.108	0.878	0.495	1.775	0.076	821.61
				High	Leverage	Points: 24	,32,85,94	,101				
	INTERCEPT SHAPE MN LSI											
	Std.				Std.				Std.			
Est.	Error	z-value	Pr(> z )	Est.	Error	z-value	Pr(> z )	Est.	Error	z-value	Pr(> z )	AIC
-9.128	0.581	-15.716	< 2e-16	2.681	0.511	5.244	0.000	-0.328	0.044	-7.478	0.000	787.29
				High L	everage P	oints: 24,3	32,68,85,9	4,101				
	INTER	CEPT			SHAP	E_MN			A	I		
	Std.				Std.				Std.			
Est.	Error	z-value	Pr(> z )	Est.	Error	z-value	Pr(> z )	Est.	Error	z-value	Pr(> z )	AIC
-8.601	0.680	-12.640	<2e-16	0.842	0.537	1.567	0.117	0.008	0.005	1.642	0.101	822.1
			-	High Leve	erage Poin	its: 24,32,4	17,68,85,9	4,98,101				
	INTER	CEPT			SHAP	E_MN			PLA	ΔDJ		
	Std.				Std.				Std.			
Est.	Error	z-value	Pr(> z )	Est.	Error	z-value	Pr(> z )	Est.	Error	z-value	Pr(> z )	AIC
-8.769	0.690	-12.711	<2e-16	1.590	0.752	2.114	0.035	-0.001	0.006	-0.170	0.865	766.23

Table C-15. 2k forest class non-spatial binomial GLMs

					2k	Forest Cla	.SS					
				High	Leverage	Points: 1,2	2,33,57,73	,109				
	INTER	RCEPT		SHAPE_MN					CLU	MPY		
	Std.				Std.			Std.				
Est.	Error	z-value	Pr(> z )	Est.	Error	z-value	Pr(> z )	Est.	Error	z-value	Pr(> z )	AIC
-9.379	0.714	-13.140	< 2e-16	0.022	0.456	0.049	0.961	2.508	0.666	3.766	0.000	1062.4
	INTER	RCEPT			SHAP	E_MN			LS	SI		
	Std.				Std.			Std.				
Est.	Error	z-value	Pr(> z )	Est.	Error	z-value	Pr(> z )	Est.	Error	z-value	Pr(> z )	AIC
-8.017	0.530	-15.124	<2e-16	0.672	0.428	1.572	0.116	-0.015	0.037	-0.414	0.679	1080.6
	INTER	RCEPT			SHAP	E_MN			A	I		
	Std.				Std.				Std.			
Est.	Error	z-value	Pr(> z )	Est.	Error	z-value	Pr(> z )	Est.	Error	z-value	Pr(> z )	AIC
-9.300	0.704	-13.210	< 2e-16	0.007	0.459	0.015	0.988	0.024	0.007	3.691	0.000	1063.2
	INTER	RCEPT			SHAP	E_MN			PLADJ			
	Std.				Std.				Std.			
Est.	Error	z-value	Pr(> z )	Est.	Error	z-value	Pr(> z )	Est.	Error	z-value	Pr(> z )	AIC
-8.464	0.597	-14.187	< 2e-16	-0.407	0.504	-0.808	0.419	0.023	0.005	4.686	0.000	1054.7

Table C-16. 2k wetland class non-spatial binomial GLMs

					2k V	Vetland Cl	ass					
				High L	everage P	oints: 2,3,	39,54,75,9	96,203				
	INTER	CEPT			SHAP	E_MN			CLUI	MPY		
	Std.				Std.				Std.			
Est.	Error	z-value	Pr(> z )	Est.	Error	z-value	Pr(> z )	Est.	Error	z-value	Pr(> z )	AIC
-5.895	0.476	-12.394	<2e-16	-0.693	0.270	-2.565	0.010	-0.674	0.493	-1.367	0.172	1552.5
	INTER	CEPT			SHAP	E_MN			LS	SI		
	Std.				Std.				Std.			
Est.	Error	z-value	Pr(> z )	Est.	Error	z-value	Pr(> z )	Est.	Error	z-value	Pr(> z )	AIC
-6.406	0.340	-18.821	<2e-16	-0.583	0.274	-2.126	0.034	-0.039	0.023	-1.734	0.083	1551.2
	INTER	CEPT			SHAP	E_MN			A	I		
	Std.				Std.				Std.			
Est.	Error	z-value	Pr(> z )	Est.	Error	z-value	Pr(> z )	Est.	Error	z-value	Pr(> z )	AIC
-5.838	0.459	-12.731	<2e-16	-0.662	0.271	-2.442	0.015	-0.008	0.005	-1.640	0.101	1551.7
				High Lev	erage Poi	nts: 2,3,39	,54,75,96,	177,203				
	INTER	CEPT			SHAP	E_MN			PLA	ADJ		
	Std.				Std.				Std.			
Est.	Error	z-value	Pr(> z )	Est.	Error	z-value	Pr(> z )	Est.	Error	z-value	Pr(> z )	AIC
-5.837	0.376	-15.512	<2e-16	-0.635	0.302	-2.102	0.036	-0.009	0.004	-2.000	0.046	1537.1

Table C-17. 2k agriculture/forest class non-spatial binomial GLMs

					2k Agricu	ulture/Fore	est Class					
				High		Points: 25		,104				
	INTER	CEPT			SHAP				CLUI	MPY		
	Std.				Std.	_		Std.				
Est.	Error	z-value	Pr(> z )	Est.	Error	z-value	Pr(> z )	Est.	Error	z-value	Pr(> z )	AIC
-9.431	0.608	-15.520	< 2e-16	0.607	0.466	1.304	0.192	2.247	0.466	4.821	0.000	900.78
				Hig	h Leverag	e Points: 2	25,34,93,1	04				
	INTER	CEPT			SHAP	E_MN			LS	SI		
Std. Std.					Std.							
Est.	Error	z-value	Pr(> z )	Est.	Error	z-value	Pr(> z )	Est.	Error	z-value	Pr(> z )	AIC
-9.382	0.496	-18.911	< 2e-16	2.633	0.430	6.128	0.000	-0.227	0.033	-6.858	0.000	918.08
				High	Leverage	Points: 25	,34,52,93	,104				
	INTER	CEPT			SHAP	E_MN			A	I		
	Std.				Std.				Std.			
Est.	Error	z-value	Pr(> z )	Est.	Error	z-value	Pr(> z )	Est.	Error	z-value	Pr(> z )	AIC
-9.350	0.600	-15.570	< 2e-16	0.550	0.469	1.175	0.200	0.022	0.005	4.765	0.000	901.54
	INTER	CEPT			SHAP	E_MN			PLA	ADJ		
	Std.				Std.				Std.			
Est.	Error	z-value	Pr(> z )	Est.	Error	z-value	Pr(> z )	Est.	Error	z-value	Pr(> z )	AIC
-7.833	0.614	-12.750	< 2e-16	-0.738	0.624	-1.182	0.237	0.026	0.005	5.244	0.000	897.88

## Appendix D

Spatial Binomial Models

Table D-1. 800m forest class spatial binomial GLM

Summary 800m Forest	3 Chains a	t 100,000	)
Parameters	50.0%	2.5%	97.5%
		-	
Intercept	-8.621	11.906	-8.192
Shape Index Mean	0.703	-1.772	1.903
Percent Land Cover			
Adjacency	0.034	0.009	0.045
sigma.sq	2.628	1.853	4.305
Phi	350.850	26.887	387.372
effective range 3/phi	0.009	0.008	0.185
max intersite distance = $1.174$			

Table D-2. 800m wetland class spatial binomial GLM

Summary 800m Wetlan	Summary 800m Wetland 3 Chains at 50,000									
Parameters	50.0%	2.5%	97.5%							
	-	-								
Intercept	10.022	10.095	-8.918							
Shape Index Mean	0.986	0.722	1.096							
sigma.sq	3.503	3.158	3.869							
Phi	15.224	12.006	21.354							
effective range 3/phi	0.197	0.141	0.251							
max intersite distance = $1.260$										

Table D-3. 800m agriculture/forest class spatial binomial GLM

Summary 800m Agriculture/Forest 3 Chains at 50,000									
Parameters	50.0%	2.5%	97.5%						
Intercept	-8.868	-9.844	-8.245						
Shape Index Mean	2.319	1.774	2.500						
Landscape Shape Index	-0.549	-0.776	-0.192						
sigma.sq	1.345	1.142	2.309						
Phi	283.921	234.639	551.114						
effective range 3/phi	0.011	0.006	0.013						

Table D-4. 1\_2k forest class spatial binomial GLM

Summary 1_2k Forest	3 Chains a	t 100,000	
Parameters	50.0%	2.5%	97.5%
	-	-	
Intercept	11.411	15.723	-8.792
Shape Index Mean	3.439	1.076	6.52
Landscape Shape Index	-0.31	-0.45	-0.07
sigma.sq	4.392	4.304	4.449
Phi	75.14	18.076	189.105
effective range 3/phi	0.04	0.017	0.191
Max intersite distance = $1.260$	•		

Table D-5. 1\_2k wetland class spatial binomial GLM

Summary 1_2k Wetland	l 3 Chains	at 100,000	)
Parameters	50.0%	2.5%	97.5%
Intercept	-7.448	-8.688	-7.447
Shape Index Mean	0.368	-0.401	1.16
Landscape Shape Index	-0.184	-0.295	0.011
sigma.sq	2.495	2.194	2.897
Phi	22.312	16.076	33.448
effective range 3/phi	0.134	0.09	0.188
max intersite distance = $1.277$			

Table D-6. 1\_2k agriculture/forest class spatial binomial GLM

Summary 1_2k Agriculture/	Summary 1_2k Agriculture/Forest 3 Chains at 100,000									
Parameters	50.0%	2.5%	97.5%							
Intercept	-9.096	-10.403	-6.957							
Shape Index Mean	2.240	0.555	3.582							
Landscape Shape Index	-0.255	-0.424	-0.242							
sigma.sq	1.547	1.112	1.733							
Phi	449.736	319.780	592.320							
effective range 3/phi	0.007	0.005	0.009							
max intersite distance = $1.230$										

Table D-7. 1\_6k forest class spatial binomial GLM

Summary 1_6k Forest 3 Chains at 50,000			
Parameters	50.0%	2.5%	97.5%
Intercept	-9.490	-9.759	-6.676
Shape Index Mean	-0.111	-2.042	0.629
sigma.sq	6.166	4.735	6.917
Phi	9.049	6.944	13.169
effective range 3/phi	0.332	0.229	0.434
max intersite distance = $1.260$			

Table D-8. 1\_6k wetland class spatial binomial GLM

Summary 1_6k Wetland 3 Chains at 100,000			
Parameters	50.0%	2.5%	97.5%
Intercept	-9.375	-9.485	-8.770
Shape Index Mean	0.870	-0.060	1.127
Landscape Shape Index	0.051	-0.028	0.080
sigma.sq	3.969	3.623	6.301
Phi	17.402	11.701	20.866
effective range 3/phi	0.172	0.144	0.259
max intersite distance = $1.250$			

Table D-9. 1\_6k agriculture/forest spatial binomial GLM

Summary 1_6k Agriculture/Forest 3 Chains at 50,000			
Parameters	50.0%	2.5%	97.5%
	-	-	-
Intercept	10.739	11.111	10.168
Shape Index Mean	3.635	3.004	3.741
Landscape Shape Index	-0.248	-0.319	-0.208
sigma.sq	1.921	1.334	2.199
Phi	16.864	10.402	33.195
effective range 3/phi	0.178	0.093	0.292
max intersite distance = $1.224$			

Table D-10. 2k forest class spatial binomial GLM

Summary 2k Forest 3 Chains at 50,000			
Parameters	50.0%	2.5%	97.5%
	-	-	
Intercept	10.811	11.266	-9.358
Percent Land Cover			
Adjacency	0.024	0.014	0.029
sigma.sq	5.164	4.708	5.165
Phi	18.343	15.803	23.018
effective range 3/phi	0.164	0.131	0.190
max intersite distance = $1.174$			

Table D-11. 2k wetland class spatial binomial GLM

Summary 2k Wetland 3 Chains at 50,000			
Parameters	50.0%	2.5%	97.5%
Intercept	-7.522	-8.621	-6.267
Percent Land Cover			
Adjacency	-0.004	-0.020	0.002
sigma.sq	3.376	2.859	4.107
Phi	25.083	21.627	63.926
effective range 3/phi	0.120	0.049	0.139
max intersite distance =	·		

Table D-12. 2k agriculture/forest class spatial binomial GLM

Summary 2k Agriculture/Forest 3 Chains at 50,000			
Parameters	50.0%	2.5%	97.5%
Intercept	-9.434	-11.430	-8.954
Shape Index Mean	2.448	1.700	4.771
Landscape Shape Index	-0.253	-0.492	-0.120
sigma.sq	2.232	1.873	2.707
Phi	366.493	334.177	489.995
effective range 3/phi	0.008	0.006	0.009
max intersite distance = $1.256$			

## LITERATURE CITED

- Aiga H, Amano T, Cairncross S, Domako JA, Nanas O, and Colemen S (2004). Assessing Water-Related Risk Factors for Buruli Ulcer: A Case-Control Study in Ghana. *American Journal of Tropical Medicine and Hygiene*, 71(4), 387-392.
- Abrahams EW, Tonge JI (1964). *Mycobacterium ulcerans* infection in Queensland. *Medical Journal of Australia i: 334.s*
- Akaike H. A New Look at the Statistical Model Identification (1974). *IEEE Transactions on Automatic Control*, AC-19(6).
- Amofah G, Bonsu F, Tetteh C, Okrah J, Asamoa K, Asiedu K, Addy J (2002). Buruli Ulcer in Ghana: Results of a National Case Search. *Emerging Infectious Diseases*.
- Amofah GK, Sagoe-Moses C, Adjei-Acquah C, Frimpong EH (1993). Epidemiology of Buruli ulcer in Amansie West district, Ghana. *Transactions of the Royal Society of Tropical Medicine and Hygiene*, 87, 644-645.
- Anderson JR, Hardy EE, Roach JT, and Witmer RE (1976). A Land Use and Land Cover Classification System for Use with Remote Sensor Data. *Geological Survey Professional Paper 964*.
- Aujoulat I, Johnson C, Zinsou C, Guedenon A, Portaels F (2003). Psychosocial aspects of health seeking behaviours of patients with Buruli ulcer in southern Benin. *Tropical Medicine and International Health* 8, 750-759.
- Beck LR, Lobitz BM, Wood BL (2000). Remote Sensing and Human Health: New Sensors and New Opportunities. *Emerging Infectious Diseases*, 6(3).
- Benbow ME, Williamson H, Kimbirauskas R, McIntosh MD, Kolar R, Quaye C, Akpabey F, Boakye D, Small P, and Merritt RW (2008). Aquatic Invertebrates as Unlikely Vectors of Buruli Ulcer Disease. *Emerging Infectious Diseases*, 14(8) <www.cdc.gov/eid>
- Beven KJ, and Kirkby MJ (1979). A physically based, variable contributing area model of basin hydrology. *Hydrological Sciences, Bulletin 24(1)*.
- Blackburn JK, McNyset KM, Curtis A, Hugh-Jones ME(2007). Modeling the Geographic Distribution of *Bacillus anthracis*, the Causative Agent of Anthrax Disease, for the Contiguous United States using Predictive Ecologic Niche Modeling. *American Journal of Tropical Medicine and Hygiene*, 77(6):1103-1110.
- Bland JM, Altman DG (1998). Bayesians and Frequentists. Statistics Notes. *British Medical Journal*, 317.
- Bolstad P. GIS Fundamentals: A First Text on Geographic Information Systems, Second Ed. 2005. Eider Press, White Bear Lake, MN 55110.

- Boyd HA, Flanders WD, Addiss DG, and Waller LA (2005). Residual Spatial Correlation Between Geographically Referenced Observations *A Bayesian Hierarchical Modeling Approach*. *Epidemiology*, 16(4).
- Brooks SP, and Gelman A (1998). General Methods for monitoring Convergence of Iterative Simulations. *Journal of Computational and Graphical Statistics*, *7(4)*, 434-455.
- Brou T, Broutin H, Elguero E, Asse H, Guegan J (2008). Landscape Diversity Related to Buruli Ulcer Disease in Côte d'Ivoire. *PLOS Neglected Tropical Diseases*, *2*(7), e271.
- Brownstein JS, Skelly DK, Holford TR, Fish D (2005). Forest fragmentation predicts local scale heterogeneity of Lyme disease risk. *Oecologia*, *146*, 469-475.
- Condeso TE and Meentemeyer RK (2007). Effects of landscape heterogeneity on the emerging forest disease sudden oak death. *Journal of Ecology*, *95*, 364-375.
- Confalonieri UEC (2005). The Millennium Assessment: Tropical Ecosystems and Infectious Diseases. *EcoHealth 2*, 231-233.
- Centers for Disease Control (2005). Burul Ulcer. National Center for Immunization and Respiratory Disease: Division of Bacterial Diseases. Last Accessed Online 22 Nov 2010 <a href="http://www.cdc.gov/ncidod/dbmd/diseaseinfo/buruliculer\_t.htm">http://www.cdc.gov/ncidod/dbmd/diseaseinfo/buruliculer\_t.htm</a>
- Central Intelligence Agency. The World Factbook: Africa: Benin. Last Accessed Online 22 Nov 2010 <a href="https://www.cia.gov/library/publications/the-world-factbook/geos/bn.html">https://www.cia.gov/library/publications/the-world-factbook/geos/bn.html</a>
- Chauty A, Ardant MF, Adeye A, Euverte H, Guedenon A, Johnson C, Aubry J, Nuermberger E, Grosset J (2007). Promising Clinical Efficacy of Streptomycin-Rifampin Combination for Treatment of Buruli Ulcer (*Mycobacterium ulcerans* Disease). *Antimicrobial Agents and Chemotherapy*, 4029-4035.
- Clancey JK, Dodge OG, Lunn HF (1962). Study of a mycobacterium causing skin ulceration in Uganda. *Ann. Soc. Belge Med. Trop, 4*, 585-590.
- Clark WC, Kates RW, et al. editors. The Earth as transformed by Human Action. Cambridge: Cambridge University Press; 1990.
- Clarke KC Ed. *Getting Started with Geographic Information Systems*. Fourth Edition. Chapter 3: Maps as Numbers, pp 67 70. Prentice Hall Series in Geographic Information Systems. Pearson Education Inc.Upper Saddle River, New Jersey.
- Coetzee M, Craig M, le Sueur D (2000). Distribution of African Malaria Mosquitoes Belonging to the *Anopheles gambiae* Complex. *Parasitology Today*, 16(2).
- Cook A, Jardine, A, Weinstein P (2004). Using Human Disease Outbreaks as a Guide to Multilevel Ecosystem Interventions. *Environmental Health Perspectives*, 112(11).

- Cook RD (1977). Detection of Influential Observations in Linear Regression. *Technometrics*, 19(1).
- Danson FM, Craig PS, Man W, Shi D, and Giraudoux P (2004). Landscape Dynamics and Risk Modeling of Human Alveolar Echinococcosis. *Photogrammetric Engineering & Remote Sensing*, 70(3), 359-366.
- de Knegt HJ, van Langevelde F, Coughenour MB, Skidmore AK, de Boer WF, Heitkönig IMA, Knox NM, Slotow R, van der Waal C, and Prins HHT (2010). Spatial autocorrelation and the scaling of species-environment relationships. *Ecology*, *91*(8), 2455-2465.
- Debacker M, Aguiar J, Steunou C, Zinsou C, Meyers WM, Guedenon A, Scott J, Dramaix M, Portaels F (2004a). *Mycobacterium ulcerans* Disease (Buruli Ulcer) in Rural Hospital, Southern Benin, 1997-2001. *Emerging Infectious Diseases*, 10(8), <www.cdc.gov/eid>
- Debacker M, Aguiar J, Steunou C, Zinsou C, Meyers WM, Scott JT, Dramaix M, Portaels F (2004b). *Mycobacterium ulcerans* disease: role of age and gender in incidence and morbidity. *Tropical Medicine and International Health*, *9*, 1297-1304.
- Debacker M, Zinsou C, Aguiar J, Meyers WM, Portaels F (2003). First case of *Mycobacterium ulcerans* disease (Buruli ulcer) following a human bite. *Clinical Infectious Disease*. 1;36(5).
- Debacker M, Aguiar J, Steunou C, Zinsou C, Meyers WM, Portaels F (2005). Buruli Ulcer Recurrence, Benin. *Emerging Infectious Diseases* 11(4).
- Dobos, Karen M, Quinn, Frederick D, Ashford, David A, Horsburgh, Robert C, King, C Harold. Emergence of a Unique Group of Necrotizing Mycobacterial Diseases (1999). *Emerging Infectious Diseases*, *5*(*3*).
- Dossou KM and Gléhouenou-Dossou (2007). The vulnerability to climate change of Cotonou (Benin): the rise in sea level. *Environment and Urbanization 19(65)*.
- Duker AA, Carranza EJM, Hale M. (2004). Spatial dependency of Buruli ulcer prevalence on arsenic-enriched domains in Amansie West District, Ghana: implications for arsenic mediation in *Mycobacterium ulcerans* infection. *International Journal of Health Geographics*, *3*(19).
- Duker AA, Stein A, Hale M. A statistical model for spatial patterns of Buruli ulcer in the Amansie West district, Ghana (2006). *International Journal of Applied Earth Observation and Geoinformation*, 8, 126-136.
- Durnez L, Suykerbuyk P, Nicolas V, Barrière, Verheyen E, Johnson CR, Leirs H, Portaels F (2010). Terrestrial Small Mammals as Reservoirs of *Mycobacterium ulcerans* in Benin. *Applied and Environmental Microbiology, July*, 4574-4577.

- Eddyani M, Portaels F (2007). Survival of *Mycobacterium ulcerans* at 37°C. *European Society of Clinical Microbiology and Infectious Diseases, CMI 13*, 1023-1035.
- Eddyani M, Ofori-Adjei D, Teugels G, De Weirdt D, Boakye D, Meyers WM, Portaels F (2004). Potential role for fish in transmission of Mycobacterium ulcerans disease (Buruli ulcer): an environmental study. *Applied Environmental Microbiology*, 70(9), 5679-81.
- Elsner L, Wayne J, O'Brien CR, McCowan C, Malik R, Hayman JA, Globan M, Lavender CJ, Fyfe JA (2008). Localized Mycobacterium ulcerans infection in a cat in Australia. *Journal of Feline Med Surg*, 10, 407-12.
- Epstein PR. Biodiversity, Climate Change, and Emerging Infectious Diseases. Chapter 4. pg 27. *Conservation Medicine: Ecological Health in Practice*. Ed. Aguirre AA, Ostfeld RS, Tabor GM, House C, Pearl MC. Oxford University Press. New York, New York. 2002.
- Foley JA, DeFries R, Asner GP, Barfoard C, Bonan G, Carpenter SR, Chapin FS, Coe MT, Daily GC, Gibbs HK, Helkowski JH, Holloway T, Howard EA, Kucharik CJ, Monfreda C, Patz JA, Prentice IC, Ramankutty N, Snyder PK (2005). Review: Global Consequences of Land Use. *Science*. 22 July (309).
- Fyfe JA, Lavender CJ, Johnson PD, Globan M, Sievers A, Azuolas J and Stinear TP (2007). Development and application of two multiplex real-time PCR assays for the detection of Mycobacterium ulcerans in clinical and environmental samples. *Applied Environmental Microbiology*, 73, 4733–4740.
- Fyfe JAM, Lavender CJ, Handasyde KA, Legione AR, O'Brien CR, Stinear TP, Pidot SJ, Seemann T, enbow ME, Wallace JR, McCowan C, Johnson PDR (2010). A Major Role for Mammals in the Ecology of *Mycobacterium ulcerans*. *PLoS Neglected Tropical Diseases*, *4*(8), e791.
- George, KM, Chatterjee, D, Gunawardana, G. (1999). Mycolactone: a polyketide toxin from *Mycobacterium ulcerans* required for virulence. *Science*, *283*, 854-857.
- Gergel S. E., Turner M.G. Ed. (2002). Learning Landscape Ecology: A Practical Guide to Concepts and Techniques. Springer, New York, NY.
- Godwin E. (2010 Nov 2). Floods waters from Dam carry away Traditional Ruler. *Ghana News Link*. Accessed Online 22 Nov 2010. <a href="http://www.ghananewslink.com">http://www.ghananewslink.com</a>
- Goldberg TL, T.R. Gillespie, I.B. Rwego, E.L. Estoff., and C.A. Chapman (2008). Forest fragmentation as cause of bacterial trasmission among nonhuman primates, humans, and livestock, Uganda. *Emerging Infectious Diseases*. 14(9),1375-1382.

- Graham AJ, Danson FM, Giraudoux P, Craig PS (2004). Ecological epidemiology: landscape metrics and human alveolar echinococossis. *Acta Tropica*, *91*, 267-278.
- Haase, Peter (1995). Spatial pattern analysis in ecology based on Ripley's *K*-function: Introduction and methods of edge correction. *Journal of Vegegation Science*, *6*, 575-582.
- Hansen MC, Stehman SV, Potapov PV, Loveland TR, Townshend JRG, DeFries RS, Pittman KW, Arunarwatil B, Stolle F, Steininger MK, Carroll M, DiMiceli C (2008). Humid tropical forest clearing from 2000 to 2005 quantified by using multiptemporal and mutiresolution remotely sensed data. *PNAS*, 105(27), 9941.
- Hayman J (1991). Postulated Epidemiology of *Mycobacterium ulcerans* Infection. *International Journal of Epidemiology*, 20(4).
- Helbert C, Dupuy D, Carraro L (2009). Assessment of uncertainty in computer experiments from Universal to Bayesian Kriging. *Applied Stochastic Models in Business and Industry*, 25(2), 99-113.
- Horsburgh Jr CR and Meyers WM. Buruli ulcer. In: Horsburgh Jr CR and Nelson AM (ed). Pathology of emerging infections. Washington DC: American Society for Microbiology. P 119-126.
- Hughes RH and Hughes, JS. *A Directory of African Wetlands*. IUCN, Gland, Switzerland & Cambridge, UK/UNEP, Nairobi, Kenya, WCMC, Cambridge, UK.
- Huygen K, Adjei O, Affolabi D, Bretzel G, Demangel C, Fleischer B, Johnson RC, Pedrosa J, Phanzu DM, Phillips RO, Pluschke G, Siegmund V, Singh M, van der Werf TS, Wansbrough-Jones M, and Portaels F (2009). Buruli ulcer disease: prospects for a vaccine. *Medical Microbiology and Immunology*, 198, 6-77.
- Iverson LR (1988). Land-use changes in Illinois, USA: The influence of landscape attributes on current and historic land use. *Landscape Ecology*, *2*(*1*), 45-61.
- Jenkin JA, Smith M, Fairley M, Johnson PDR (2002). Acute, oedematous *Mycobacterium ulcerans* infection in a farmer from far north Queensland. *Medical Journal of Australia*, 176,180-182.
- Jensen J.R. Introductory digital image processing: a remote sensing perspective, 2nd ed. 1996. Simon & Schuster, Upper Saddle River, NJ.
- Johnson PDR, Stinear TP, and Hayman JA (1999). *Mycobacterium ulcerans* -- a mini-review. *Journal of Medical Microbiology*, 48, 511-13.
- Johnson PDR, Stinear T, Small PLC, Plushke G, Merritt RW, Portaels F, Huygen K, Hayman JA, Asiedu K (2005). Buruli Ulcer (*M. ulcerans* Infection): New Insights, New Hope for Disease Control. *PLoS Med*, *2*(4), e108.

- Johnson PDR, Azuolas J, Lavender CJ, Wishart E, Stinear TP, Hayman JA, Brown L, Jenkin GA, and Fyfe JAM (2007). *Mycobacterium ulcerans* in Mosquitoes Captured during Outbreak of Buruli Ulcer, Southeastern Australia. *Emerging Infectious Diseases*, 13(11). <www.cdc.gov/eid>
- Johnson PDR, Lavender CJ (2009). Correlation between Buruli Ulcer and Bector-borne Notifiable Diseases, Victoria, Australia. *Emerging Infectious Diseases*, 15(4). <www.cdc.gov/eid>
- Keitt TH, Bjørnstad ON, Dixon PM, Citron-Pousty S (2002). Accounting for spatial pattern when modeling organism-environment interactions. *Ecography*, *25*, 616-625.
- Kitron U (1998). Landscape Ecology and Epidemiology of Vector-Borne Diseases: Tools for Spatial Analysis. *Journal of Medical Entomology*, *35(4)*, 435-445.
- Krummel JR, Gardner RH, Sugihara G, O'Neill RV, Coleman PR (1987). Landscape Patterns in a Disturbed Environment. *Oikos*, 48(3), 321-324.
- Legendre P and Fortin MJ. Spatial pattern and ecological analysis. *Vegetation*, 80, 107-138.
- Lennon JL (2000). Red-shifts and red herrings in geographical ecology. *Ecography*, 23(1), 101-113.
- Lillesand and Kiefer. *Remote Sensing and Image Interpretation*. 4<sup>th</sup> ed. New York: John Wiley & Sons.
- MacCallum P, Tolhurst JC, Buckle G, Sissons HA (1948). A new mycobaterial infection in man. *Journal of Pathologic Bacteriology*, 60, 93-122.
- Malone JB, Nieto P, Tadesse A (2006). Biology-based mapping of vector-borne parasites by geographic information systems and remote sensing. *Parassitologia*, 48, 77-79.
- Marion E, Eyangoh S, Yeramian E, Doannio J, Landier J, Aubry J, Fontanet A, Rogier C, Cassisa V, Cottin J, Marot A, Eveillard M, Kamdem Y, Legras P, Deshayes C, Saint-André J, and Marsollier L (2010). Seasonal and Regional Dynamics of *M. ulcerans* Transmission in Environmental Context: Deciphering the Role of Water Bugs as Hosts and Vectors. *PLoS Neglected Tropical Diseases*. *4*(7): e731.
- Marsollier L, Robert R, Aubry J, Saint Andre J, Kouakou H, Legras P, Manceau A, Mahaza C, and Carbonnelle B (2002). Aquatic Insects as a Vector for *mycobacterium ulcerans*. *Applied and Environmental Microbiology*, *68*(9), 4623-4628.
- Marsollier L, Aubry J, Saint-Andre P, Robert R, Legras P, Manceau AL, Bourdon S, Audrain C, and Carbonnelle B (2003). Ecology and transmission of Mycobacterium ulcerans. *Pathologie Biologie* 51,490-495

- Marsollier L, Severin T, Bubry J, Merritt RW, Saint-Andre JP, Legras P, Manceau A, Chauty A, Carbonnelle B, and Cole ST. (2004a). Aquatic snails, passive hosts of *Mycobacterium ulcerans*. *Applied and Environmental Microbiology*, 70, 6296-6298.
- Marsollier L, Stinear T, Aubry J, Saint Andre JP, Robert R, Legras P, Manceau A, Audrain C, Bourdon S, Kouakou H, and Carbonnelle B (2004b). Aquatic Plants Stimulate the Growth of and Biofilm Formation by *Mycobacterium ulerans* in Axenic Culture and Harbor These Bacteria in the Environment. *Applied Environmental Microbiology*, 70, 1097-1103.
- Marston BJ, Diallo MO, Horsburgh CR Jr, Diomande I, Saki MZ, Kanga JM, Patrice G, Lipman HB, Ostroff SM, Good RC (1995). Emergence of Buruli ulcer disease in the Daloa region of Côte d'Ivoire. *American Journal of Tropical Medicine and Hygiene*, *52*(3), 219-24.
- Mather PM (2004). Computer processing of remotely sensed images: an introduction 3rd Edition. John Wiley & Sons Ltd. West Sussex, England.
- Matson PA, Parton WJ, Power AG, and Swift MJ. Agricultural Intensification and Ecosystem Properties (1997). *Science* 277, 504.
- McGarigal K, Marks B. FRAGSTATS: spatial pattern analysis program for quantifying landscape structure. Gen. Tech. Rep. PNW-GTR-351. Portland, OR: U.S. Department of Agriculture, Forest Service, Pacific Northwest Research Station. 122 p.
- Merrit RW, Benbow ME, Small PLC (2005). Unraveling an emerging disease associated with disturbed aquatic environments: the case of Buruli ulcer. Reivew. *Frontiers in Ecology and the Environment*, *3*(6), 323-331.
- Merritt RW, Walker ED, Small PLC, Wallace JR, Johnson PDR, Benbow ME, Boakye DA (2010). Buruli Ulcer Disease: A Systematic Review of Ecology and Transmission. *PLoS Neglected Tropical Diseases*, *4*(12), e911.
- Meyers, Derek H (2007). Letters: *Mycobacterium ulcerans* infection: an eponymous ulcer. *Medical Journal of Australia, 187(1),* 63.
- Meyers WM, Shelly WM, Connor DH, Meyers EK. Human Mycobacterium ulcerans infections developing at sites of trauma to skin (1974). *American Journal of Tropical Medicine and Hygiene*, 23, 919.
- Meyers WM, Tignokpa N, Priuli GB, and Portaels F. *Mycobacterium ulcerans* infection (Buruli ulcer): first reported patients in Togo (1996). *British Journal of Dermatology*, *134*, 1116-1121.
- Mitchell, PJ, Jerrett, IV, Slee, KJ (1984). Skin ulcers caused by *Mycobacterium ulcerans* in koalas near Bairnsdale, Australia. *Pathology 16*, 256-260.

- Morse S (1995). Factors in the Emergence of Infectious Diseases. *Emerging Infectious Diseases*, *1*(1).
- Mosi L, Williamson H, Wallace JR, Merritt RW, Small PLC (2008). Persistent Association of *Mycobacterium ulcerans* with West African Predaceous Insects of the Family Belostomatidae. *Applied Envrionmental Microbiology*, 74(22) 7036-7042.
- Moyeed RA and Papritz A (2002). An Empirical Comparison of Kriging Methods for Nonlinear Spatial Point Prediction. *Mathematical Geology*, 34(4).
- Nackers F, Johnson RC, Glynn JR, Zinsou C, Tonglet R, and Portaels F (2007). Environmental and Health-related Risk Factors for *Mycobacterium ulcerans* Disease (Buruli Ulcer) in Benin. *American Journal of Tropical Medicine and Hygiene*. 77(5), 834-836.
- Narumalani S, Mishra DR, and Rothwell RG (2004). Change detection and landscape metrics for inferring anthropogenic processes in the greater EFMO area. *Remote Sensing of the Environment*, 91(3-4), 478-489.
- Noeske J, Kuaban C, Rondini S, Sorlin P, Ciaffi L, Mbuagbaw J, Portaels F, and Pluschke G (2004). Buruli Ulcer Disease in Cameroon Rediscovered. *American Journal of Tropical Medicine and Hygiene*, 70(5), 520-526.
- O'Callaghan JF and Mark DM (1984). The Extraction of Drainage Networks from Digital Elevation Data. *Computer Vision, Graphics, and Image Processing.* 28, 323-344.
- Oluwasanmi JO, Solanke TF, Olurin EO, Itayemi SO, Alabi GO, and Lucas AO (1976). Mycobacterium Ulcerans (Buruli) Skin Ulceration in Nigeria. *The American Journal of Tropical Medicine and Hygiene*, 25(1).
- Ostfeld RS, Glass GE, Keesing F (2005). Spatial epidemiology: an emerging (or re-emerging) discipline. *TRENDS in Ecology and Evolution*, 20(6).
- Patz JA and Confalonieri UEC, coord. eds. Human Health: Ecosystem Regulation of Infectious Diseases. In Hassan RM, Scholes R, and Ash N *Ecosystems and Human Well-being: Current State and Trends: Findings of the Condition and Trends Working Group.* Pp 393-415. Millenium Ecosystem Assessment (2005). Island Press, Washington D.C., USA.
- Patz JA, Graczyk TK, Geller N, Vittor AY (2000). Effects of environmental change on emerging parasitic diseases. *International Journal for Parasitology*, 30, 1395-1405.
- Patz JA, Olson SH, Uejio CK, Gibbs HK (2008). Disease Emergence from Global Climate and Land Use Change. *Medical Clinics of North America*, *92*, 1473-1491.
- Pavlovsky, EN (1966). The natural nidality of transmissible disease. University of Illinois Press, Urbana.

- Pickett STA and Cadenasso ML (1995). Landscape Ecology: Spatial Heterogeneity in Ecological Systems. *Science*, *269*(*5222*), 331-334.
- Pickett STA and White PS, eds. *The Ecology of Natural Disturbance and Patch Dynamics*. NewYork: Academic. 472 pp. 1985.
- Plowright RK, Sokolow SH, Gorman ME, Daszak P, Foley JE (2008). Causal inference in disease ecology: investigating ecological drivers of disease emergence. *Frontiers in Ecology and the Environment*, 6(8), 420-429.
- Pongsiri MJ, Roman J, Ezenwa VO, Goldberg TL, Koren HS, Newbold SC, Ostfeld RS, Pattanayak SK, and Salkeld DJ (2009). Biodiversity Loss Affects Global Disease Ecology. *BioScience*, *59*(11).
- Pouillot R, Matias G, Wondje CM, Portaels F, Valin N, Ngos F, Njikap A, Marsollier L, Fontanet A, Eyangoh S (2007). Risk Factors for Buruli Ulcer: A Case Control Study in Cameroon. *PLOS Neglected Tropical Diseases*, *1*(3), e101.
- Portaels F, Elsen P, Guimaraes-Peres A, Fonteyne P-A, Meyers WM (1999). Insects in the transmission of Mycobacterium ulcerans infection. *Lancet*, *353*(9157), 986.
- Portaels F, Aguiar J, Debacker M, Steunou C, Zinsou C, Guédénon A, Meyers WM (2002). Prophylactic effects of Mycobacterium bovis BCG vaccination against osteomyelitis in children with Mycobacterium ulcerans disease (Buruli Ulcer). *Clininical Diagnostics and Laboratory Immunology*, *9*, 1389–1391.
- Portaels F, Meyers WM, Ablordey An, Castro AG, Chemlal K, de Rijk P, Elsen P, Fissette K, Fraga AG, Lee R, Mahrous E, Small PLC, Stragier P, Torrado E, Aerde AV, Silva MT, Pedrosa J (2008). First Cultivation and Characterization of *Mycobacterium ulcerans* from the Environment. *PLOS Neglected Tropical Diseases*, *2*(3), e178.
- Quek TY, Athan E, Henry MJ, Pasco JA, Redden-Hoare J, Hughes A, Johnson PDR (2007). Risk factors for *Mycobacterium ulcerans* infection, southeastern Australia. *Emerging Infectious Diseases*, 13(11), 1661–6.
- Raghunathan, PL, Whitney, EA, Asamoa, S, Stienstra, Y, Taylor Jr, TH, Amofah GK, Ofori-Adjei, David, Dobos, Karen, Guarner, Jeannette, Martin, Stacey, Pathak, Sonal, Klutse, Erasmus, Etuaful, Samuel, van der Fraaf, Winette TA, van der Werf, Tjip S, King, CH (2005). Risk Factors for Buruli ulcer disease (Mycobacterium ulcerans infection): Results from a Case-Control study in Ghana. *Clinical Infectious Diseases*, 40(10), 1445-53.
- Riitters KH, O'Neill RV, Hunsaker CT, Wickham JD, Yankee DH, Timmins SP, Jones KB, and Jackson BL (1995). A factor analysis of landscape pattern and structure metrics. *Landscape Ecology*, 10(1) 23-39.
- RESPOND Health Mapping Activity Ivory Coast. Document No: S-18106-DLR-I1.00-P1\_Health\_Mapping. Verson 1.00. ESA/ESRIN contract No: 18106 05/09/06.

- Ross BC, Honson PD, Oppedisano F, Marino L, Sievers A, Stinear T, Hayman JA, Veitch MG, Robins-Browne RM (1997). Detection of *Mycobacterium ulcerans* in environmental samples during an outbreak of ulcerative disease. *Applied Environmental Microbiology*, 63(10), 4135-4138.
- SAS/STAT(R) 9.2 User's Guide, Second Edition. http://support.sas.com/documentation/cdl/en/statug/63033/HTML/default/viewer.htm#/documentation/cdl/en/statug/63033/HTML/default/statug\_mcmc\_sect045.htm Accessed 27 June 2010.
- Schabenberger O, and Gotway CA. *Statistical Methods for Spatial Data Analysis*. 2005. Chapman & Hall/CRC, Boca Raton, FL.
- Schmidt F and Persson A. Comparison of DEM Data Capture and Topographic Wetness Indices (2003). *Precision Agriculture*, *4*, 179-192.
- Schunk M, Thompson W, Klutse E, Nitschke Jorg, Opare-Asamoah K, Thompson R, Fleischmann E, Siegmund V, Herbinger Kh, Adjei O, Fleischer B, Loscher T, and Bretzel G (2009). Outcome of Patients with Buruli Ulcer after Surgical Treatment with or without Antimycobacterial Treatment in Ghana. *American Journal of Tropical Medicine and Hygiene*, 81(1), 75-81.
- Sizaire V, Nackers F, Comte E, Poratels F (2006). *Mycobacterium ulcerans* infection: control, diagnosis, and treatment. *The Lancet Infectious Diseases*, 6(5), 288-296.
- Sopah GE, Johnson RC, Chauty A, Dossou AD, Aguiar J, Salmon O, Portaels F, Asiedu K (2007). Buruli ulcer surveillance, Benin, 2003-2005. *Emerging Infectious Diseases*, 13(9), 1374-1376.
- Spiegelhalter DJ, Best NG, Carlin BP, and van der Linde A (2002). Bayesian measures of model complexity and fit. *Journal of the Royal Statistical Society: Series B (Statistical Methodology)*, 64(4).
- Spies TA, Ripple WJ, Bradshaw GA. Dynamics and Pattern of a Managed Coniferous Forest Landsape in Oregon (1994). *Ecological Applications*, *4*(3), 555-568.
- Stinear TP, Seemann T, Pidot S, Wafa F, Yeysset G, Garnier T, Meurice G, Simon D, Bouchier C, Ma L, Tichit M, Porter JL, Ryan J, Johnson PDR, Davies JK, Jenkin GA, Small PLC, Jones LM, Tekaia F, Laval F, Daffé, Parkhill J, Cole ST (2007). Reductive evolution and niche adaptation inferred from the genome of *Mycobacterium ulcerans*, the causative agent of Buruli ulcer. *Genome Research*, 17(2), 192-200.
- Stienstra Y, van der Graaf WTA, Asamoa K, and van der Werf TS. Beliefs and Attitudes Toward Buruli Ulcer in Ghana (2002). *American Journal of Tropical Medicine and Hygiene*, 67(2), 207-213.

- Stragier P, Ablordey A, Durnez L, Portaels F (2007). VNTR analysis differentiates *Mycobacterium ulcerans* and IS2404 positive mycobacteria. *Systematic and Applied Microbiology*, 30(7), 252-530.
- Tobias NJ, Seemann T, Pidot S, Porter JL, Marsollier L, Marion E, Letournel F, Zakir T, Azuolas J, Wallace JR, Hong H, Davies JK, Howden BP, Hohnson PDR, Jenkin GA, and Stinear TP (2009). Mycolactone Gene Expression is Controlled by Strong SigA-Like Promoters with Utility in Studies of *Mycobacterium ulcerans* and Buruli Ulcer. *PLoS Neglected Tropical Diseases*, *3*(11).
- Tobler WR (1970). A Computer Movie Simulating Urban Growth in the Detroit Region. *Economic Geography*, *46*, Supplement: Proceedings. International Geographical Union. Commission on Quantitative Methods, 234-240.
- Turner MG and Gardner RH. Quantitative Methods in Landscape Ecology: An Introduction. Chapter 1. *Quantitative Methods in Landscape Ecology*. pp 3-14. Springer-Verlag New York Inc. New York, New York. USA. 1991.
- Turner MG, Gardner RH, O'Neill RV. Landscape Ecology In Theory and Practice: Pattern and Process. Springer-Verlag New Yrok, Inc. 2001.
- Turner MG (2005). Landscape Ecology: What is the State of the Science? *Annual Review of Ecology and Evolutionary Systems*, *36*, 319-44.
- Turner W., Spector S., Gardiner N., Fladeland M., Sterling E., and Steininger M (2003). Remote sensing for biodiversity science and conservation. *TRENDS in Ecology and Evolution*, 18(6).
- U.S. Agency for International Development (USAID), Bureau for Africa, Office of Sustainable Development (AFR/SD). 118/119 Biodiversity and Tropical Forest Assessment for Benin. EPIZ IQC: EPP-1-00-03-00014-00, Task Order 02. Accessed online 20 Oct 2010 <a href="http://www.encapafrica.org/documents/biofor/Benin%20118%20119%20FINAL%20October%202007.pdf">http://www.encapafrica.org/documents/biofor/Benin%20118%20119%20FINAL%20October%202007.pdf</a>
- United Nations, Permanent Mission of the Republic of Benin to the United Nations. Country Facts. Access online 20 Oct 2010 < http://www.un.int/wcm/content/site/benin/>
- United Nations Statistical Division. World Statistics Pocketbook. Benin. Last Accessed Online 22 Nov 2010 < http://data.un.org/Search.aspx?q=benin>
- Veitch MGK, Johnson PDR, Flood PE, Leslie DE, Street AC, and Hayman JA (1997). A large localized outbreak of *Mycobacterium ulcerans* infection on a temperate southern Australian island. *Epidemiology and Infection*, 119(3), 313-318.

- van Ravensway J, Tsonis AA, Benbow ME, Campbell LP, Johnson PDR, Qi J. Regional-scale Climate, Landscape, and Social Risk Factors Identified as Potential Drivers of the Network of Buruli Ulcer Cases in Victoria, Australia. (IN PREP, 2010).
- van Zyl A, Daniel J, Wayne J, McCowan C, Malik R, Jelfs P, Lavender CJ, and Fyfe JA (2010). *Mycobacterium ulcerans* infections in two horses in south-eastern Australia. *Australian Veterinary Journal*, 88,(3),101-106.
- Yang K, Wang XH, Yang GJ, Wu XH, Qi YL, Li HJ, and Zhou XN (2008). An integrated approach to identify distribution of *Oncomelania hupensis*, the intermediate host of *Schistosoma japonicum*, in a mountainous region in China. *International Journal for Parasitology*, 38(8-9), 1007-1016.
- Wagner HH and Fortin MJ (2005). Spatial analysis of landscapes: concepts and statistics. *Ecology*, 86(8), 1975-1987.
- Wagner T, Benbow ME, Brenden TO, Qi J, Johnson RC (2008a). Buruli ulcer disease prevalence in Benin, West Africa: associations with land use/cover and the identification of disease clusters. *International Journal of Health Geographics*, 7, 25.
- Wagner, Tyler, Benbow, M Eric, Burns, Meghan, Johnson, R Christian, Merritt, Richard W, Qi, Jiaguo, Small, Pamela LC (2008b). A Landscape-based Model for Prediction *Mycobacterium ulcerans* Infection (Buruli Ulcer Disease) Presence in Benin, West Africa. *EcoHealth*, *5*(1), 69-79.
- Walsh DS, Portaels F, Meyers WM (2008). Buruli ulcer (*Mycobacterium ulcerans* infection). *Transactions of the Royal Society of Tropical Medicine and Hygiene*, 102(10), 969-78.
- Waller LA and Gotway CA. *Applied Spatial Statistics for Public Health Data*. 2004. John Wiley & Sons, Inc. Hoboken, NJ.
- Wansbrough-Jones M, Phillips R (2006). Buruli ulcer: emerging from obscurity. *Lancet*, *367(9525)*, 1849-1858.
- Wilcox BA, Gubler DJ (2005). Disease Ecology and the Global Emergence of Zoonotic Pathogens. *Environmental Health and Preventive*, 10(5), 263-272.
- Williamson HR, Benbow ME, Nguyen KD, Beachboard DC, Kimbirauskas RK, McIntosh MD, Quaye C, Ampadu EO, Boakye D, Merritt RW, Small PLC (2008). Distribution of *Mycobacterium ulcerans* in Buruli Ulcer Endemic and Non-Endemic Aquatic Sites in Ghana. *PLOS Neglected Tropical Diseases*, 2(3), e205.
- Wilcove DS, McLellan CH, Dobson AP (1986). Habitat fragmentation in the temperate zone. *Conservation Biology*, ed. ME Soul'e, pp. 237–56. Sunderland, MA: Sinauer

- With KA, Gardner RH, Turner MG (1997). Landscape connectivity and population distributions in heterogeneous environments. *Oikos*, 78(1),151–69
- World Health Organization (2000). Buruli ulcer-*Mycobacterium ulcerans* infection. Asiedu K, Scherpbier R, Raviglione M., editors. Geneva: The Organization.
- World Health Organization (2007). Fact Sheet: Buruli ulcer disease (Mycobacterium ulcerans infection). <a href="http://www.who.int/mediacentre/factsheets/fs199/en/print.html">http://www.who.int/mediacentre/factsheets/fs199/en/print.html</a>
- World Health Organization (2009). Weekly epidemiological record, *6(84)*, 41-48. <a href="http://www.who.int/wer">http://www.who.int/wer</a>